THE APPLICATION OF ESTIMATION AND CONTROL TECHNIQUES IN TWO MODES OF EXERCISE FOR THE SPINAL CORD INJURED

Andrew Pennycott

A thesis submitted for the degree of Doctor of Philosophy (PhD)

Department of Mechanical Engineering
Faculty of Engineering
University of Glasgow
May 2008

Abstract

A spinal cord injury (SCI) can result in a loss of sensory and motor capacity, dysfunction of the autonomic nervous system and also in a number of secondary health conditions including muscular atrophy, cardiovascular disease and osteoporosis.

The impact of these secondary health conditions may be reduced through exercise which loads the muscles, skeleton and central cardiovascular system. A number of new exercise methods are emerging in the field of rehabilitation.

Functional electrical stimulation (FES) is a technique for inducing artificial muscular contractions that has been applied to facilitate cycling amongst adults with a spinal cord injury. Preliminary data has demonstrated the feasibility of FES cycling in the paediatric SCI population. The use of an electric motor to provide torque assistance where required allows the exercise to continue for longer periods and over a wider range of cadences. In this thesis, a feedback control system is devised whereby the cadence can be automatically controlled to reference levels using such a motor, and tested during FES cycling of children with an SCI.

The use of robot-assisted body weight supported devices is gaining popularity in the rehabilitation world. Their application has thus far been focused on rehabilitation of gait via neural re-learning. However, robot-assisted gait can also elicit a significant cardiovascular response and thus has potential as a tool for exercise training and testing. In this thesis, a method for estimating the work rate contributed by an exercising subject is developed and then incorporated into a feedback control scheme where the objective is to

regulate the work rate to reference values. This enables specific work rate profiles to be performed during robot-assisted gait as is often required for standard exercise tests and training.

In addition to controlling the mechanical variables during exercise, it is also possible to control some of the physiological variables. A feedback system whose goal is to control the rate of oxygen uptake rate is developed which also incorporates the work rate control method. This allows a predetermined level of physiological response to be achieved so that the training is of sufficient intensity to promote improvements in physical capacity and fitness.

This thesis examines the application of estimation and control techniques in two exercise modes for the spinal cord injured. The ultimate aim of the exercise is to reduce the severity of the secondary health conditions that spinal cord injured people face. The estimation and control algorithms allow the exercise to be regulated with respect to speed and intensity and therefore have utility in both training and testing applications.

Acknowledgements

I would like to thank my supervisors Ken Hunt and Henrik Gollee for their help and encouragement throughout my PhD.

Secondly, thanks go to my colleagues both in Glasgow and in Nottwil, and all the subjects who kindly agreed to participate in my experiments. I am grateful to Ben for being my MATLAB and FES cycling guru during the early days of the PhD.

To Jan, I appreciate all your advice and tuition on PhDs, life and barbecueing, and for the very generous offer of using Nottwil H.Q. to write a large part of this thesis.

To all the Friends of the Lokomat and in particular Tanja, I am very grateful for your help and patience during the experiments and paper writing.

Finally, to my parents and grandparents: thanks for the tremendous amount of help and support that you have given me over the years.

Thesis Outline

- **Chapter 1:** A background of spinal cord injury and its secondary effects is presented. The influence of exercise and the role of estimation and control therein are described.

- **Chapter 2:** The basic methods of identification and control used in later chapters are detailed. The techniques of determining empirical dynamic models and design of feedback control systems that are employed throughout the study are described with examples.

- **Chapter 3:** A feedback control system is developed which regulates the cadence during paediatric functional electrical stimulation cycling. The resulting system is tested using a variety of reference inputs and also in a cycling trial where a child with a spinal cord injury was the subject.

- **Chapter 4:** The application of treadmill walking in rehabilitation is reviewed and the concept of robot-assisted treadmill walking introduced. Following this, a method for estimating the work rate contributed by an exercising subject during robot-assisted walking is developed and incorporated into a feedback system where the subject's work rate is controlled in real time. This control method is tested during robot-assisted gait of 3 spinal cord injured subjects.

- **Chapter 5:** A technique for controlling the oxygen uptake during robot-assisted gait is developed, incorporating the previously described work rate controller of Chapter 4. Following system identification

tests and calculation of the control parameters, the resulting feedback-controlled system is tested during robot-assisted ambulation of 5 able bodied subjects.

- **Chapter 6:** The conclusions of the thesis are presented, and open areas of research relevant to functional electrical stimulation cycling and robot-assisted gait are discussed. These have the potential to improve the methodology of the exercise formats in this project and also to prove their clinical efficacy with respect to developing fitness and reducing the impact of the secondary health conditions of spinal cord injury.

Thesis Contributions

- A feedback control system for cadence control during functional electrical stimulation cycling of children with a spinal cord injury is developed. This enables the practical implementation of an electric motor during cycling to support the subject where necessary, initiating the cycling motion by overcoming inertia and sustaining the cycling as fatigue develops and the subject's own torque contribution diminishes. The system may be used in training programmes and also in exercising testing designed to determine the cardiovascular parameters of subjects, and also to assess the efficacy of the training in longitudinal studies.

- A method for estimating the active subject work rate during robot-assisted body weight supported treadmill walking is developed. Previously, no direct measurement of subject power was available. This estimate can be used to encourage and assess the level of work rate contribution of a subject during ambulation.

- A feedback control system is developed using the work rate estimate during robot-assisted walking where the subject adjusts his effort level in order to produce a work rate in accordance with a reference value. This approach was validated through experiments with 3 spinal cord injured subjects. The system may be used in exercise testing where specific profiles of work rate are required, and also to ensure a sufficient level of work rate contribution during training programmes.

- A system to control the level of oxygen uptake during robot-assisted walking is developed using empirical models of the oxygen uptake dynamics, and validated using 5 able-bodied subjects. This may be used in exercise training utilising the robot-assisted technology to ensure that the exercise is sufficiently intense to induce improvements in the cardiovascular system and to produce required, predetermined levels of oxygen uptake during exercise testing protocols.

Publications

- A. Pennycott, K.J. Hunt, L.P. Jack, C. Perret and T.H. Kakebeeke, 'Estimation and volitional feedback control of active work rate during robotic-assisted gait', submitted to *IEEE Transactions on Control Systems Technology*.

- K.J. Hunt, L.P. Jack, A. Pennycott, C. Perret, M. Baumberger and T.H. Kakebeeke, 'Control of work-rate-driven exercise facilitates cardiopulmonary training and assessment during robot-assisted gait in incomplete spinal cord injury', *Biomedical Signal Processing and Control*, to appear.

- K.J. Hunt, L.P. Jack, A. Pennycott, T.H. Kakebeeke, C. Perret and M. Baumberger, 'Cardiopulmonary assessment protocols for robot-assisted gait in incomplete spinal cord injury', *Robotics in Rehabilitation Symposium*, Zürich, Switzerland, 2006.

- A. Pennycott, K.J. Hunt, S. Coupaud, D.A.B. Allan, T.H. Kakebeeke, 'Feedback control of oxygen uptake rate during robot-assisted gait', submitted to *Control Engineering Practice*.

- A. Pennycott and K.J. Hunt, 'Cadence Control System for Paediatric Functional Electrical Stimulation Cycling', submitted to *Control Engineering Practice*.

Nomenclature

$\beta_\mathbf{1}$, $\beta_\mathbf{1}$, $\mathbf{l_1}$, $\mathbf{l_2}$ Constant lengths of upper Lokomat geometry.

$\dot{\mathbf{W}}_\mathbf{L}$ Work rate contributed by the Lokomat.

$\dot{\mathbf{W}}_\mathbf{S}$ Work rate contributed by the subject.

$\gamma_\mathbf{1}$, $\gamma_\mathbf{1}$, $\mathbf{d_1}$, $\mathbf{d_2}$ Constant lengths of lower Lokomat geometry.

$\omega_\mathbf{n}$ Natural Frequency.

ω Cadence/frequency.

τ Time constant.

$\theta_\mathbf{1}$, $\theta_\mathbf{2}$ Angles of upper and lower Lokomat limb segments.

$\theta_\mathbf{h}$, $\theta_\mathbf{k}$ Alternative measures of the angles of upper and lower Lokomat limb segments.

ξ Damping factor.

$\mathbf{A_m}$, $\mathbf{A_o}$ Control and observer and polynomials.

$\mathbf{A}$ Denominator polynomial of a model.

$\mathbf{B}^+$, $\mathbf{B}^-$ Factors of polynomial B.

$\mathbf{B}$ Numerator polynomial of a model.

$\mathbf{d(t)}$ Disturbance signal.

$\mathbf{e(t)}$ Tracking error.

$\mathbf{e_{LS}}$ Least squares error.

$\mathbf{F}$, $\hat{\mathbf{F}}$ Measured and modelled forces.

$\mathbf{H(s)}$ Transfer function of a dynamic system.

$\mathbf{j}$ Imaginary number i.e. $\sqrt{-1}$.

$\mathbf{k}$ The delay order of a model.

$\mathbf{n(t)}$ Noise signal.

$\mathbf{N}$ The number of samples in a data set.

$\mathbf{n}$ The order of a model.

$\mathbf{q^{-1}}$ The delay operator.

$\mathbf{r(t)}$ Reference/desired signal.

$\mathbf{R}$, $\mathbf{S}$, $\mathbf{T}$, $\mathbf{R_o}$, $\mathbf{F}$ Closed loop control polynomials.

$\mathbf{s}$ Laplace operator.

$\mathbf{T}$ Period.

$\mathbf{t}$ Time.

$\mathbf{u(t)}$ System input.

$\mathbf{X^P}$, $\mathbf{X^A}$ The variable X during passive and active walking.

$\mathbf{x_1}$, $\mathbf{x_2}$ Lengths of the upper and lower Lokomat actuators.

$\mathbf{X_{upper}}$, $\mathbf{X_{lower}}$ The variable X at the upper and lower limb segments.

$\mathbf{y'(t)}$ System output after corruption by noise.

$\mathbf{y(t)}$ System output.

fit Variable quantifying the quality of a model.

$\dot{V}_{O_2}$ Rate of oxygen uptake.

AB Able bodied

ACE Arm cranking ergometry.

ARX Autoregressive model with exogenous input.

ATP Adenosine triphosphate.

BWSTT Body weight supported treadmill training.

BWS Body weight support.

CNS Central nervous system.

DAQ Card Data acquisition card.

FES Functional electrical stimulation.

HR Heart rate.

IET Incremental exercise test.

MLSS Maximum lactate steady state.

MRT Mean response time.

PRBS Pseudorandom binary sequence.

SCIWORA Spinal cord injury without radiological abnormality.

SCI Spinal cord injury

SET Step exercise test.

SWEET Square-wave endurance exercise test.

$\mathbf{S}_1$, $\mathbf{S}_2$, $\mathbf{S}_3$ Subjects of the work rate control tests.

$\mathbf{S}_A$, $\mathbf{S}_B$, $\mathbf{S}_C$, $\mathbf{S}_D$, $\mathbf{S}_E$ Subjects of the $\dot{V}_{O_2}$ control tests.

ZOH Zero order hold.

Contents

List of Tables

List of Figures

Chapter 1

Introduction

1.1 Introduction to Spinal Cord Injury

Spinal cord injury (SCI) represents a devastating event in a person's life. The most common causes of injury are traffic accidents, sports and recreational activities, falls, violence and work-related accidents [22, 29, 104]. Common mechanisms include fracture and dislocation of vertebral segments.

The annual incidence of SCI in the UK is between 10 and 15 per million of the population [42]. The likelihood of initial survival is strongly influenced by age and the neurological characteristics of the injury [104].

Spinal cord injury can occur at different levels of the cord, consequently producing varying degrees of impairment [42, 56]. Injuries are normally classified according to the vertebral section corresponding to the injury level as shown in figure 1.1. People with an injury to the upper (cervical) regions of the spine normally have impairments in all four limbs, trunk and pelvic organs and are called tetraplegics, whilst lower injuries in the thoracic and lumbar regions spare function and sensation in the arms, and such patients are called paraplegics [42].

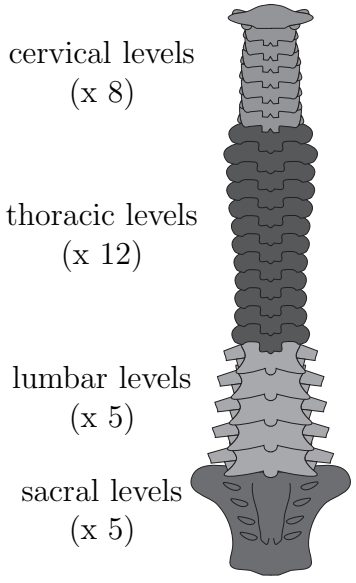

Figure 1.1: Anterior view of vertebral levels.

Aside from the initial mechanical impact, further, secondary damage to the cord may be incurred through a series of biochemical and cellular processes internal to the body [104].

The spinal cord is organised into different pathways called tracts. As a result, there are many patterns of motorisensory impairment - often called SCI symptoms - which can ensue following the injury [56].

Neural transmission below the injury level can be affected to varying degrees. In some cases, some motor or sensory facility is preserved below the lesion level; such an injury is termed incomplete, whilst the converse case of no sensory or motor ability being spared is called a compete injury [42, 56]. The completeness of the injury may be classified by the American Spinal Cord Injury Association (ASIA) impairment scale [14]. This scheme is summarised in table 1.1.

Class	Completeness	Description
A	Complete	No motor or sensory function is preserved in the sacral segments S4-S5.
B	Incomplete	Sensory but not motor function is preserved below the neurological level and extends throughout the sacral segments S4-S5.
C	Incomplete	Motor function is preserved below the neurological level, and the majority of key muscles below the neurological level have a muscle grade less than 3.
D	Incomplete	Motor function is preserved below the neurological level, and the majority of key muscles below the neurological level have a muscle grade greater than or equal to 3.
E	N/A	Motor and sensory function is normal.

Table 1.1: ASIA Classification Scale.

In addition to the loss of sensory and motor ability, spinal cord injury adversely affects urinary and bowel processes, autonomic control and sexual function [42].

1.2 Overview of the Spinal Cord

Figure 1.2 provides simplified illustrations of the spinal cord. The spinal cord is not simply the body's pipeline for neural transmission but is also involved in integration and processing of neural signals. The white matter of the cord is divided into tracts which primarily transmit the signals from the periphery nervous system to the brain whilst the grey matter is responsible for signal processing.

1.3 Health Complications of SCI

The loss of sensation and motor ability coupled with autonomic dysfunction are the most obvious results of spinal cord injury. However, SCI patients also have to cope with a number of secondary conditions. In spite of improvements in care and technology, the mortality rate of SCI persons is higher, and their life expectancy is lower than members of the general population [33]. The following section reviews the main complications afflicting SCI persons. The central idea motivating this thesis is that that the severity of some of these conditions may be alleviated via appropriate treatment and therapy, of which exercise forms an important part.

Respiratory problems are common amongst the spinal cord injured, particulary for those with a high lesion and are thus reliant on the diaphragm for breathing, lacking the support of the intercostal muscles. The dysfunction can also prevent effective coughing to remove secretions and pneumonia can often develop [44, 81, 106].

Pressure sores result from prolonged pressure and a poor blood supply to an area of skin caused by the sedentary nature of an SCI person's life and the reduced ability to change posture. The most common sites are ischial tuberosities, trochanter and sacral regions which can result e.g. in cellulitis, abscesses and joint infections. Other forms of infection faced by SCI persons include urinary tract infections, infected pressure ulcers, pneumonia, bacteremia (bacteria in the blood, often secondary to urinary infection) and

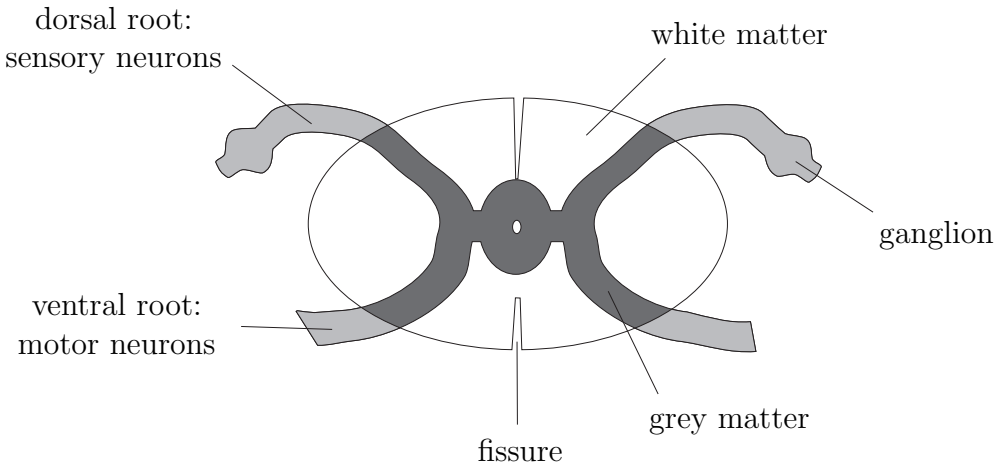

(a) Transverse Section of the Spinal Cord.

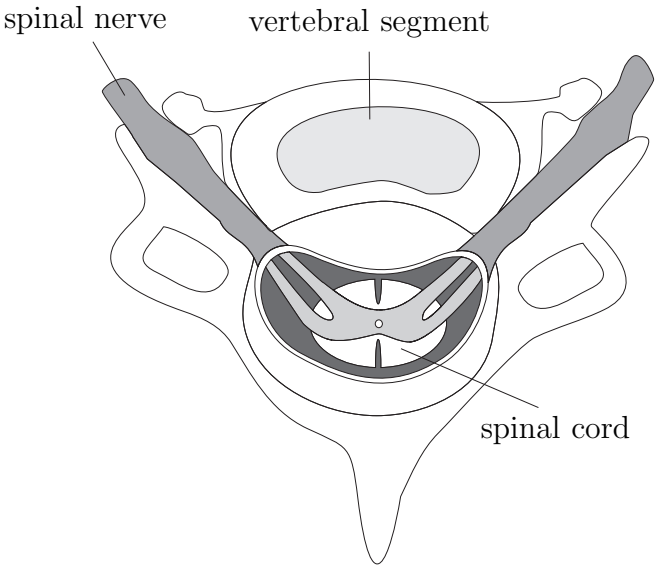

(b) Exit of the spinal nerves from the vertebrae.

Figure 1.2: Diagrams of the spinal cord.

MRSA [81].

At around the time of the Second World War, the main cause of death of the SCI patients who survived the initial post-injury period was urinary complication. Improvements in urinary care and technology have produced a shift away from urinary causes of death [33]; nevertheless, urinary infections remain a problem for SCI persons. The infections result partly from increased pressure in the bladder and greater volumes of residual urine [21]. These infections can also be caused by the use of indwelling catheters, bladder thickening and fibrosis, fistulae and abscesses [81]. Early detection may be impeded by the loss of sensation accompanying the SCI. Bladder complications have been correlated with a lower quality of life and a greater level of 'overall disability' amongst SCI patients [45], and risk factors include high lesion levels and reliance on chronic catheterisation [21].

SCI persons are thought to be at risk from cardiovascular disease owing to their sedentary lifestyles and autonomic impairment. Ischaemic and non-ischaemic heart disease were the second leading cause of death between 1973 - 1990 in the SCI population of Britain, with the leading cause being pulmonary complication [33]. Underlying factors include insulin resistance [97], and depressed levels of high-density lipoprotein cholesterol [5], a factor which is recognised as a risk factor for cardiovascular disease [12]. Despite this, other investigations have failed to statistically demonstrate that people with an SCI are more at risk from heart disease than the general population [44, 106].

Pain in the upper extremities - including shoulder, elbow and wrist pain - is a common occurrence amongst spinal cord injured persons due to an increased stress in and usage of the upper limbs in everyday living. At the same time, the dependency on the upper extremities for daily living makes such an injury even more consequential for the SCI person [18].

As a result of disuse, the paralysed muscles of an SCI patient demonstrate a rapid atrophy [13]. Moreover, an injury can affect the distribution of the different fibre types present in the muscle tissue [41].

Spinal cord injury leads to a reduction in loading of the skeletal system and a change in the balance between bone resorption and formation. As a result, decreases in bone mineral density (BMD) in the epiphyses and a thinning of the cortical walls in the diaphyses can occur, increasing the risk of fracture [28].

1.4 Reducing Health Complications through Exercise

SCI patients therefore suffer not only from the primary outcomes of the injury - i.e. paralysis and loss of sensation - but also from a number of secondary issues. However, the impact of some of these - e.g. muscular and skeletal degradation, pressure sores and cardiovascular disease - may be reduced through appropriate exercise.

1.4.1 Benefits of SCI Exercise in the Literature

Although the level [11, 62, 114] and completeness [8] of injury have been shown to be important factors in determining the physical work capacity of SCI persons[1], the level of involvement in exercise has also been shown to be highly correlated with capacity [62, 84]. This is important not only because of the health implications of the increased capacity afforded, but also because it is likely to have a positive influence on the person's functionality for daily living [62].

Arm cranking is an accessible exercise format where the subject uses the remaining upper body motor capacity. Increases in peak oxygen uptake [110] and arm strength [109] have been noted following this training which could facilitate the activities of daily living in addition to reducing the risk of cardiovascular disease and muscular atrophy.

[1]The level and completeness of injury are influential because they directly determine the quantity of available muscle and also govern the effectiveness of autonomic response e.g. in cardiac and temperature regulation.

It has been noted that active SCI individuals can have a higher peak oxygen uptake and lower heart rate than their more sedentary (SCI) counterparts [11, 48, 133].

Some authors hypothesise that the relationship between physical capacity and exercise participation could form the basis of the vicious circle depicted in figure 1.3: a low physical capacity limits exercise rate which itself lowers the subject's capacity due to lack of use, and the cycle continues in this fashion [43, 48]. Hoffman argues for the additional role of decreased incentive from decreased capacity in this cycle [47].

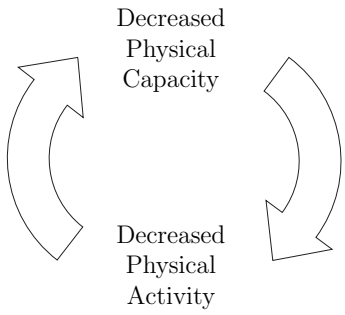

Figure 1.3: Vicious circle of SCI exercise decline.

Square-wave endurance exercise test (SWEET) training successfully elicited increases in maximal power, oxygen uptake rate and maximum tolerable power in paraplegic participants, with lower heart rates during 'base-loads' also being noted [10].

Increases in muscle fibre cross-sectional area, a change in the muscle morphology (i.e. distribution of fibre types), an increase in capillary density and increased enzymic activity were noted following a 10 week exercise programme with a frequency of 3 times per week, demonstrating the utility of exercise training in reversing the morphological and biochemical degeneration of the muscle fibres following SCI [17].

1.4.2 General Concepts and Structuring of SCI Exercise Training

Most of the guidelines for effective exercise participation have been developed for able bodied (AB) persons. Nevertheless, much of the advice is also applicable to spinal cord injured people wishing to undertake an exercise programme.

The concept of overloading the various systems of the body is central in provoking adaptations and therefore changes in fitness [1]. In order to train the cardiovascular system, for example, it is necessary to use a large muscle mass. The activity, however, need not be exhaustive: for instance, the American College of Sports Medicine recommends training at intensities corresponding to 50-85% of maximal oxygen uptake reserve[2] [91].

Changes occur at the central, cardiovascular system level. However, adaptations will also occur in the local muscles being activated in the activity. Consequently, improvements gained from training are in general activity-specific, meaning that training in one activity/sport may not lead to improvements in performance in another [1].

Furthermore, the adaptations are not limited to changes in the delivery mechanisms and muscle actuators but can also occur in the neurological control of the exercise, with changes in the neurological systems occurring to improve efficiency in some activities. However, adaptations of this sort are less applicable to certain SCI activities where voluntary neural control is largely absent e.g. in functional electrical stimulation exercise.

The frequency of training is also important. Whilst an insufficient intensity or duration of training will clearly not yield the desired improvements, training above the optimal level would lead to little benefit at the cost of increased risk of injury. This may have harmful effects on motivation and thus the likelihood of continuing the training. The American College of Sports Medicine recommends training at a frequency of around 3 times per week

[2]Maximal oxygen uptake reserve is defined as the difference between the maximum and resting rates of oxygen uptake.

[91].

Stretching prior to exercise may help to increase the range of motion of the joints and to alter tendon properties leading to a reduced chance of injury [91]. It is important in SCI exercise programmes because it can also reduce the magnitude of muscular spasms which interrupt exercise and place excessive loads on the skeletal structures. Stretching can therefore potentially decrease the likelihood of fracture and joint damage.

1.4.3 Exercise Testing

The effectiveness of a particular programme can be assessed by means of exercise testing, with different aspects of the exercise response being studied using different test structures. For example, a step test where the subject performs exercise at a constant intensity after being previously inactive or at a lower intensity can be used to assess the parameters of the kinetic response, e.g. the rise time of the oxygen uptake dynamics. The rise time can be used as a guide to fitness, since more unfit individuals tend to have a longer rise time. On the other hand, an incremental exercise test can be used to determine the maximal levels of capacity, e.g. the highest attainable rate of oxygen uptake during exercise.

Although both aerobic and anaerobic systems (see section 5.2.1) can be trained, it may be more difficult and even psychologically more stressful to assess the status of the anaerobic system due to the higher intensities required [1]. Moreover, unlike the aerobic system where gas measurements are indicative of metabolic contribution [119], it is difficult to non-invasively determine the contribution of the anaerobic component during exercise. Consequently, it can be difficult to assess the effectiveness of programmes designed to develop anaerobic power.

The various determinants of fitness and response to exercise of SCI subjects can make evaluation and comparison under experimental protocols difficult. Effective comparison depends on the grouping of the SCI subjects to allow variables to be controlled between cases [11].

Ergometry work is popular amongst exercise physiologists partly because the skill levels required for the activity are low due to the simple mechanics and thus skill will be approximately the same across subjects. Consequently, differences in response to the exercise should not be due to differences in technique but rather result from differences in the physiological status across the subjects. However, this may not be true for tetraplegics during arm ergometry since, due to the impairment of the upper extremities, some compensatory learning may take place which would represent a confounding effect [11].

The results of a test are not only dependent on the subject group's characteristics but also on specific protocols used for the testing as discussed in the literature review of Haisma [43]. Clearly, inconsistencies in methodology can make it difficult to draw general conclusions from the various studies in the literature. For example, a poorly designed maximal test can cause the development of local fatigue in the muscles before the cardiovascular system is maximally strained, and thus the true level of maximal oxygen uptake would not be found [114].

1.4.4 Limitations of SCI Exercise

As already stated, exercise in the spinal cord population may be restricted in scope by a reduced available muscle mass. Moreover, the subjects' cardiovascular responses to the exercise may be irregular. For example, due to reduced local control, there may be hypokinesis[3] and reduced efficiency of heart pumping as a result of the organ's altered structural properties. Heart rate responses of tetraplegics rely on vagal withdrawal and therefore are normally blunted in magnitude. Due to abnormal adrenergic activity, the exercise itself is often inefficient and therefore work rates may be limited [56].

Due in part to the secondary conditions that SCI people suffer from, exercise participation incurs a higher risk of interrupting the activities of

[3] A diminished or abnormally slow movement.

daily living via injury than is the case for able bodied exercisers. For example, bone fracture, autonomic dysreflexia, hypotension and thermal dysregulation are risks faced by SCI persons undertaking exercise [56].

The various forms of competitive sport available to SCI people can be limited by ethical issues relating to competitors 'holding back' during testing designed to categorise the athletes according to degree of disability [8].

1.5 Modelling, Estimation and Control Methods in Rehabilitation

In addition to the design and realisation of new technology, engineering methods find application in the modelling, estimation and control of exercise for rehabilitation. The following section introduces these concepts and provides some examples of their application in the rehabilitation world.

Modelling methods aiming to mathematically represent the behaviour of a system can be used in order to design or improve the performance of a control system for a particular application [38, 103]. Alternatively, they may be used to explore the underlying mechanics or processes of some aspects of exercise, e.g. locomotion [25, 93]. The models may attempt to follow the real physical and biological processes (biophysical models) [26, 99] or be derived purely by empirical means [40].

Estimation techniques are used to determine the state of a system (e.g. a position or velocity variable) or to estimate the parameters of a dynamic model. For example, a biofeedback variable used to assess the performance of a subject's walking may be estimated from force and position data [72]. Knowledge of the dynamics of a system may be used to provide an estimate of system states e.g. angular position from noisy measurement data using an extended Kalman filter [101]. Parameter estimation is also a necessary step for many types of empirical model, where the values of the model's parameters are to be calculated from experimental data [107].

Many applications require a means to drive certain variables to desired

values, a task which can be achieved via a suitably designed control system. Obstacles to control can include changes in the dynamic system. In the case of rehabilitation engineering where the dynamic systems have a human subject as an element, system changes can result in the short term due to subject fatigue or in the longer term from changes induced by training. For example the forces that a subject is able to produce (using the muscle 'actuators') may increase and the subject may change mass as a result of the training. Feedback control constitutes an effective means of regulating certain variables online which would be difficult to realise using manual control or an inverse-model type approach. Moreover, the control methods allow effective control of a system even where the model representing the system is inaccurate or is only a simplified or partial model of the underlying dynamics.

Examples of control application in rehabilitation are diverse. For instance, control systems have been used to enable paraplegics to perform standing for short periods [57]. The body is an inherently unstable dynamic system in the standing position and subject to disturbances but this system may be stabilised by feedback control. Standing work may help to regain functionality and also prevent secondary conditions resulting from immobilisation such as pressure sores and bladder infection. Other areas of control in rehabilitation include control of artificial muscle contractions: this work can either focus on a specific application such as cycling aimed at improving the physical capacity of subjects [15, 53], or control of more basic movements which form an integral part of more complex applications e.g. prostheses [65, 96].

Moreover, there are many methods of implementing online control in research. Many applications are based on linear control e.g. [53], others on more complex nonlinear methods [102] whilst some research has used a non-physically based modelling and control approach [15, 40].

New forms of exercise available for the SCI population are emerging. In this thesis, paediatric functional electrical stimulation cycling and robot-assisted treadmill walking are the exercise platforms investigated and are

reviewed in Chapters 3 and 4, respectively. In the case of cycling, the cadence (angular velocity) is controlled to take on reference values using an electric motor. Estimation techniques are necessary to determine the parameters of the dynamic model central to the control system design. For the robot-assisted walking, the work rate produced by a subject is estimated online using an empirical approach, and this estimate is later harnessed in a feedback scheme to control the subject's active work rate. Following on from the control of this mechanical variable, a control system for regulation of oxygen uptake is developed. In common with the other applications discussed above, obstacles to effective control include changes in the system, disturbances and modelling errors.

1.6 Summary

Spinal cord injury can cause a wide spectrum of motor and sensory dysfunction. Additionally, the injury can lead to a number of secondary health issues. However, it has been demonstrated that exercise can bring about changes in the physical capacity of SCI people and therefore can potentially reduce the impact of some of the secondary conditions. The remainder of this thesis examines engineering methods applied to realise and improve two specific modes of exercise for the spinal cord injured population.

Chapter 2

Basic Methods: System Identification and Control

2.1 Introduction

This chapter describes the system identification and control system design methods used in the later chapters of the thesis. The basic techniques are outlined and worked examples are included to further clarify the concepts where applicable.

2.2 System Identification

2.2.1 Overview

In order to design a control system, it is usually necessary to have a mathematical model of the plant to be controlled. Using such a model in subsequent calculation schemes, the behaviour of the overall closed-loop system can be assigned certain properties as desired.

It is possible to use an analytical model based on the physics of the system. For example, free body diagrams may be drawn for a mechanical system and the corresponding differential equations determined. This will then give a continuous time model in Laplace transform form.

However, such an analytical model will have inherent physical parameters such as mass and inertia; some of these may be unknown or difficult to measure or determine through empirical means. Moreover, if the system is to be controlled using a computer, the continuous time model must normally be discretised (i.e. converted to an equivalent discrete time model) so that the control signal can be calculated at discrete intervals during realisation of computer-based control.

A more direct approach is to empirically identify a dynamic model using data collected when the system is in open loop operation. In this way, a fully parameterised, discrete time model can be developed and subsequently used for control design. The empirical modelling approach is employed in the work of this thesis.

2.2.2 System Identification Methods

The objective of the system identification procedure is to determine a model that represents the dynamic system, relating the output to the applied input as in figure 2.1. The model would allow the output at time t, $y(t)$, to be predicted or simulated based on past values of the output and the input signal, $u(t)$.

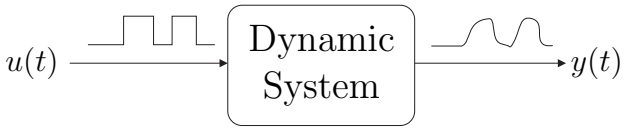

Figure 2.1: A dynamic system. The input signal $u(t)$ excites the system, yielding the output $y(t)$. Using these two recorded signals, a model representing the dynamic system can be calculated.

In this thesis, the inputs and outputs as discussed in a system identification context are not absolute levels of these variables but instead represent deviations from a steady-state operating point where their values are u_0 and y_0 . This is illustrated in figure 2.2. Moreover, experimental results relating to system identification are presented in this form throughout this thesis.

$$u(t) = u_{measured}(t) - u_0 \tag{2.1}$$

$$y(t) = y_{measured}(t) - y_0 \tag{2.2}$$

A pseudo random binary sequence (PRBS) can be used as a driving input signal in order to excite the various modes of the system and thereby elicit a response. This type of signal varies between two levels and switches between them at 'random' time instants, leading to a rich frequency content. The generated input-output data can be used to calculate a model of the underlying dynamics [68, 69].

An autoregressive with exogenous input (ARX) model as depicted in figure 2.3 was selected as a model structure since this could be directly applied

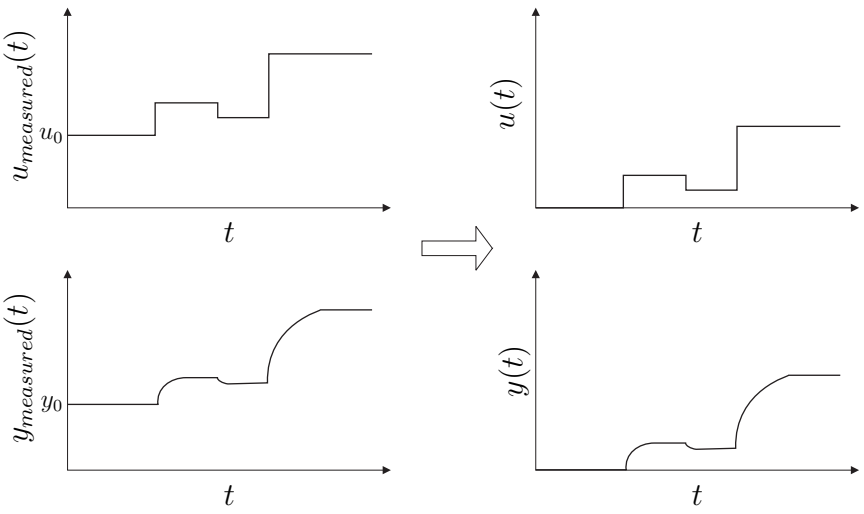

Figure 2.2: $u(t)$ and $y(t)$ represent deviations from the operating points of the input and output signals.

to the design of a feedback control system by standard pole placement methods. The system is driven by the input $u(t)$ and also by a disturbance term, $d(t)$.

With reference to figure 2.3, the equation governing the response of the ARX model is

$$y(t) = \frac{q^{-k}B(q^{-1})}{A(q^{-1})}u(t) + \frac{1}{A(q^{-1})}d(t) \tag{2.3}$$

where

$$A(q^{-1}) = 1 + a_1 q^{-1} + a_2 q^{-2} + \ldots + a_{n_a} q^{-n_a} \tag{2.4}$$

$$B(q^{-1}) = b_0 + b_1 q^{-1} + \ldots + b_{n_b} q^{-n_b}. \tag{2.5}$$

Note that the equations have been written in terms of the delay operator, q^{-1}. For a sequence $f(t)$, the delay operator has the property [2]

$$q^{-1} f(t) = f(t-1). \tag{2.6}$$

Moreover, the following vectors are introduced for convenience of notation:

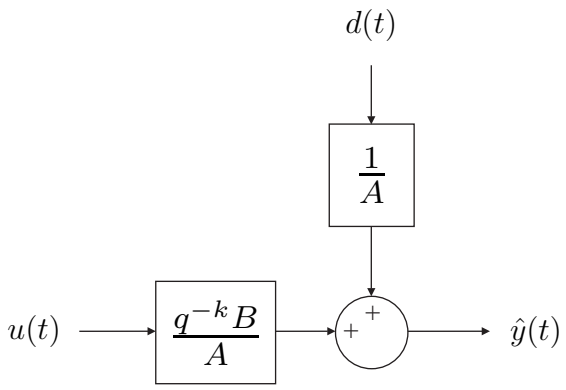

Figure 2.3: Block diagram of the basic ARX structure. The modelled output $\hat{y}(t)$ is driven by the input signal $u(t)$ and the stochastic disturbance signal $d(t)$.

$$\theta = \begin{bmatrix} b_0 \\ b_1 \\ \vdots \\ b_{n_b} \\ a_1 \\ a_2 \\ \vdots \\ a_{n_a} \end{bmatrix} \quad \varphi(t) = \begin{bmatrix} u(t-k) \\ u(t-1-k) \\ \vdots \\ u(t-n_b-k) \\ -y(t-1) \\ -y(t-2) \\ \vdots \\ -y(t-n_a) \end{bmatrix} \tag{2.7}$$

The model structure may be used to give a prediction of the output at time t, based on the inputs and measurements of the previous outputs up until time $t-1$. This prediction is dependent on the parameter set θ and is denoted $\hat{y}(t|\theta)$. Since $d(t)$ is a stochastic white-noise process, the best prediction at t is given by equation (2.8) [68].

$$\begin{aligned} \hat{y}(t|\theta) &= b_0 u(t-k) + b_1 u(t-1-k) + b_2 u(t-2-k) \\ &\quad + \ldots + b_{n_b} u(t-n_b-k) - a_1 \hat{y}(t-1) \end{aligned}$$

$$\begin{aligned} & -a_2\hat{y}(t-2) - a_3\hat{y}(t-3) - \ldots - a_{n_a}\hat{y}(t-n_a) \\ = \; & \varphi(t)^T\theta. \end{aligned} \tag{2.8}$$

In order to determine the parameter θ set that yields the optimal prediction of the output, it is necessary to have a criterion whose output reflects the quality of the model for a given parameter vector. The least squares criterion of equation (2.9) is used.

$$e_{LS}(\theta) = \sum_{i=1}^{N} [y(i) - \hat{y}(i|\theta)]^2 \tag{2.9}$$

The variable $e_{LS}(\theta)$ quantifies the difference between the actual output and that predicted by a given model. To solve for the optimal parameter vector, $e_{LS}(\theta)$ must be minimised with respect to θ. The following notation is used to simplify the form of the solution:

$$Y = \begin{bmatrix} y(1) & y(2) & \ldots & y(N) \end{bmatrix}^T \tag{2.10}$$

$$\Phi = \begin{bmatrix} \varphi^T(1) \\ \varphi^T(2) \\ \ldots \\ \varphi^T(N) \end{bmatrix} \tag{2.11}$$

The error can thus be written as

$$e_{LS}(\theta) = (Y - \Phi\theta)^T (Y - \Phi\theta) = Y^TY - \theta^T\Phi^TY - Y^T\Phi\theta + \theta^T\Phi^T\Phi\theta \tag{2.12}$$

which can be rewritten by completing the square [2]:

$$\begin{aligned} e_{LS}(\theta) = \; & \left[\theta - \left(\Phi^T\Phi\right)^{-1}\Phi^TY\right]^T \left(\Phi^T\Phi\right) \left[\theta - \left(\Phi^T\Phi\right)^{-1}\Phi^TY\right] \\ & -Y^T\Phi\left(\Phi^T\Phi\right)^{-1}\Phi^TY + Y^TY \end{aligned} \tag{2.13}$$

Since $\Phi^T\Phi$ is symmetric and positive definite, the minimum of the above equation is given by equation (2.14).

$$\theta = \left(\Phi^T\Phi\right)^{-1}\Phi^TY \tag{2.14}$$

2.2.3 Model Validation and the Fit Criterion

In order to assess the predictive power of a certain model and to compare models of different orders, the fit criterion as used in [51] was employed, i.e:

$$\text{fit} = 100\left[1 - \left(\frac{\sum_{i=1}^{N}\left(y(i) - \hat{y}(i)\right)^2}{\sum_{i=1}^{N}\left(y(i) - \bar{y}\right)^2}\right)^{0.5}\right] \tag{2.15}$$

In equation (2.15), $y(i)$ and $\hat{y}(i)$ are the measured and modelled outputs at time i, and $\bar{y}$ is the mean of the measured output signal. Therefore, the fit criterion uses N sample points to determine the percentage of the output variance that is accounted for by the model.

The data set from a system identification test is partitioned into 2 subsets. The first of these - the estimation data - is used to calculate the parameter vector θ for a given order of model. The second subset - the validation data - is used to calculate the fit for each model and thereby assess its relative quality.

It is appropriate to partition the data set in this way because if the model order is excessive (i.e. much higher than that of the real system it is trying to represent), the values of the estimated parameters will tend to be influenced by ('fit around') the spurious noise signal. Such overfitting would lead to a higher numerical fit if the working data were also used to validate the model. Using new data for validation shows how accurately the model predicts the response to the input signal since the 'noise fitting' effect during parameter calculation will not transfer to the new data.

The concept of overfitting is illustrated in figure 2.4 which shows an example of linear interpolation. The true function is a simple linear function, and polynomials of various orders were calculated to represent the relationship $y = f(x)$ from the data, where the measurement of y has been corrupted by white noise. When a high order polynomial is used, it tends to fit itself around the noise. Although this will increase the degree of fit for this set of data, it does not represent the relationship between x and y.

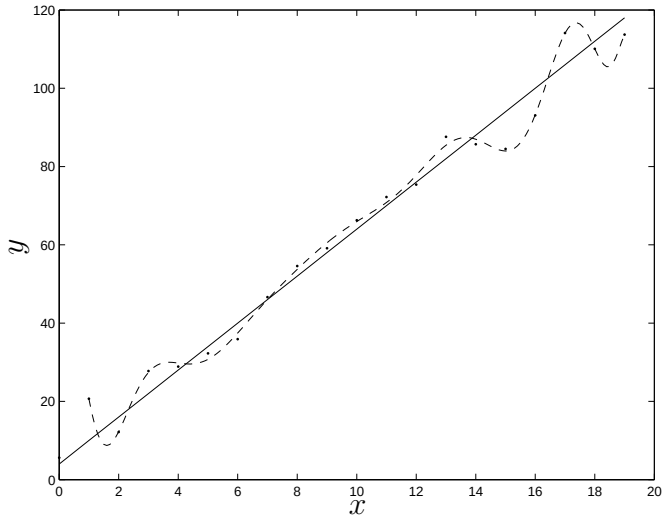

Figure 2.4: Example of overfitting: a function for the true output y (shown as a solid line) is represented by a high order polynomial, shown as a dashed line. This polynomial is calculated from input-output data, shown as individual data points.

2.3 Control Design by Pole Placement

2.3.1 Overview

Given a model of the system, the next stage is to decide on a control structure and then to calculate the various parameters of the closed loop system. The following sections provide an outline of closed loop control, the structure selected for this thesis and how a control system's parameters may then be set.

2.3.2 Motivation for Closed Loop Control

Control methods provide an effective means of eliciting a desired response from a dynamic system in the face of disturbances which perturb the system output. Effective feedback control design can also reduce the impact of modelling errors on the performance of a system since a system based on

closed loop control can have a lower sensitivity to modelling errors than one based on inverse open loop control [34]. These two configurations are shown in figure 2.5.

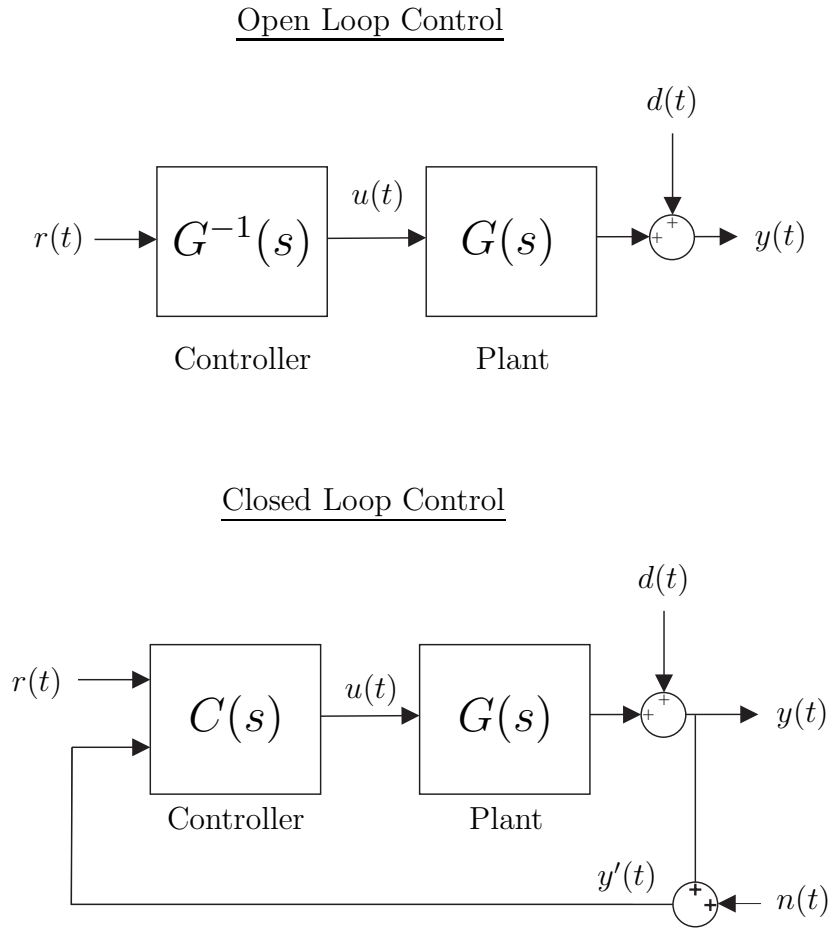

Figure 2.5: Open loop control contrasted with closed loop control.

Considering firstly the disturbances, the transfer function from $d(t)$ to $y(t)$ is simply 1 in the open loop case, whilst it is $\frac{1}{1+C(s)G(s)}$ in the closed loop configuration. The influences of the disturbances in the latter scenario can thus be made small by making the magnitude of $C(s)$ large in the appropriate frequency range.

Denoting the plant model by $G_o(s)$, let the actual plant be given by

$G_o\Delta_G$, that is, the plant has a multiplicative error. The ratio $\frac{\partial y/y}{\partial \Delta_G/\Delta_G}$ is the sensitivity of the plant with respect to the modelling error. In the case of the open loop strategy, the sensitivity is equal to

$$\frac{\partial y}{\partial \Delta_G} \cdot \frac{\Delta_G}{y} = G_o^{-1}G_o \cdot \frac{\Delta_G}{G_o^{-1}G_o\Delta_G} = 1 \tag{2.16}$$

and therefore a relative error (or change) in the plant causes a relative change in the output of equal magnitude.

However, for the closed loop case:

$$\frac{\partial y}{\partial \Delta_G} \cdot \frac{\Delta_G}{y} = \frac{CG_o}{(1+CG_o)^2} \cdot \frac{\Delta_G(1+CG_o\Delta_G)}{CG_o\Delta_G} = \frac{1}{1+CG} \tag{2.17}$$

Again, this may be made small by ensuring that $C(s)$ has a high gain in the frequency range where there is most uncertainty (or likelihood of change) in the model.

One disadvantage of closed loop control is that since a measurement of the system output is required, measurement noise is introduced into the system and the true output $y(t)$ is corrupted by the noise signal $n(t)$ to form $y'(t)$.

2.3.3 Overall Control Structure

Figure 2.6 depicts the structure chosen for the feedback loop. Its components are a reference signal $r(t)$, an output $y(t)$, a measurement noise signal $n(t)$ which corrupts the measurement of the output and a disturbance $d(t)$ which perturbs the output of the dynamic system. The various polynomials R, S and T have the backward shift operator q^{-1} as arguments and are the main elements to be calculated during control synthesis.

The system in figure 2.6 is the nominal structure - i.e. it is based on a model of the plant. The calculation of the control parameters is also based on this nominal structure but the real closed loop system will have different properties and response characteristics as the model can never represent the real plant with total accuracy.

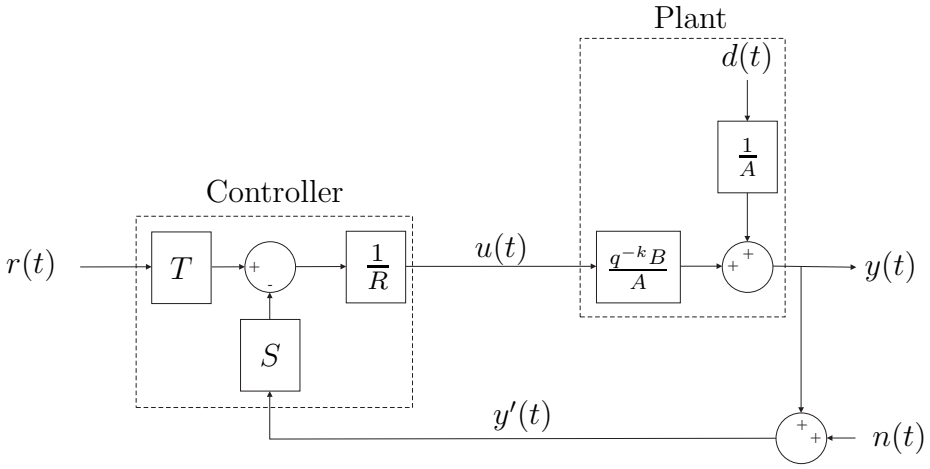

Figure 2.6: Schematic of the nominal closed-loop control structure. The control polynomials R, S and T are synthesised based on the properties of the plant model and according to pre-specified closed loop properties.

2.3.4 Calculation of the Control Polynomials by Pole Placement

In this project, the parameters inherent to blocks R, S and T are calculated by means of pole placement. The central principle behind this method is that the desired properties of the closed loop are specified in the form of polynomials which contain information about the response via the poles of the system.

Referring to figure 2.6, an expression for the output signal in terms of the reference input, disturbance and noise signals may be written; for brevity, the backward shift argument of the polynomials has been omitted.

$$y(t) = \frac{q^{-k}BT}{AR + q^{-k}BS}r(t) + \frac{R}{AR + q^{-k}BS}d(t) - \frac{q^{-k}BS}{AR + q^{-k}BS}n(t) \quad (2.18)$$

Notice that the term $AR + q^{-k}BS$ appears in the denominator of all the terms of the above equation. This is called the characteristic polynomial and it is specified in terms of two polynomials called the control and observer

polynomials, denoted A_m and A_o, respectively. These have as their roots the desired closed loop poles. Therefore, the following equation is set up:

$$AR + q^{-k}BS = A_oA_m \tag{2.19}$$

The above diophantine equation is soluble for R and S if and only if A_oA_m is a multiple of the greatest common factor of A and $q^{-k}B$ [2].

The response of $y(t)$ to $r(t)$ is partly governed by the model polynomial B. This influence can be reduced by factoring B into polynomials B^+ and B^-, where B^+ has zeros which all lie within the unit circle, to give $B = B^+B^-$. If B^+ is made a factor of R such that $R = B^+R'$, forced pole-zero cancellation results in the modified closed loop transfer function given in (2.20)[1].

$$y(t) = \frac{q^{-k}B^-T}{AR' + q^{-k}B^-S}r(t) + \frac{R'}{AR' + q^{-k}B^-S}d(t) - \frac{q^{-k}B^-S}{AR' + q^{-k}B^-S}n(t) \tag{2.20}$$

Since the response is to be governed by the observer and control polynomials, the denominator of each of the terms is equal to A_oA_m and the characteristic equation becomes

$$AR' + q^{-k}B^-S = A_oA_m. \tag{2.21}$$

If $T = \lambda A_o$ where λ is a constant, pole-zero cancellation results in the transfer function between the reference input and the output having the form

$$\frac{q^{-k}B^-\lambda}{A_m}. \tag{2.22}$$

Therefore, the response of the output to the reference input is set only by the control polynomial, whilst the responses of the output to the noise and disturbance signals are still governed by both control and observer polynomials.

[1]However, the influence of B on the response cannot be totally eliminated if B has unstable zeros. Including B^- as an additional factor of R would violate the internal stability of the closed loop system.

In order to ensure a unity gain from r to y and therefore zero error for a step input, the term λ must be set as in equation (2.23), which derives from the final value theorem [2].

$$\lambda = \frac{A_m(1)}{B^-(1)} \tag{2.23}$$

2.3.5 Interpretation of the Observer Polynomial

The observer poles (the roots of A_o) do not govern the command signal response. A_o is given the name observer polynomial because it is mathematically equivalent to the observer dynamics found in state estimation using a Luenberger Observer in a state-space design approach. The observer eigenvalues which govern the observer's dynamic response do not affect the response to a command reference [34] and are assigned a faster bandwidth than the control poles of the closed loop system. For a system whose dynamics can be described in state-space form as

$$\dot{x} = Ax + Bu \tag{2.24}$$

$$y = Cx \tag{2.25}$$

and where the control output u is given from the state estimate $\hat{x}$ by $u = r - K\hat{x}$, the system takes the form of figure 2.7.

Briefly, the speed at which the state estimate of the observer converges to the 'true' value (errors are caused by unknown initial states) is determined by setting the eigenvalues of the observer. However, these do not affect the response from the reference to output signals.

2.3.6 Pole Placement with Pole-Zero Cancellation: Example

Consider the plant in equation (2.26):

$$G(q^{-1}) = \frac{q^{-1}(1 - 0.1q^{-1})(1 - 0.3q^{-1})}{(1 - 0.4q^{-1})(1 - 0.5q^{-1})} \tag{2.26}$$

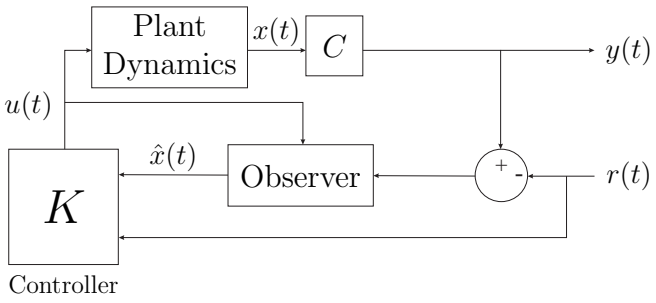

Figure 2.7: Luenberger Observer employed in state space design. The observer has eigenvalues which do not affect the response of the output $y(t)$ to the input $r(t)$, analogous to the observer polynomial used in the present work.

The desired closed loop control polynomial is set as

$$A_m = 1 - 0.8q^{-1} \tag{2.27}$$

while the desired closed loop observer polynomial is

$$A_o = 1 - 0.2q^{-1} \tag{2.28}$$

giving rise to the characteristic polynomial:

$$\begin{aligned} R(1 - 0.4qz^{-1})(1 - 0.5q^{-1}) + q^{-1}(1 - 0.1q^{-1})(1 - 0.3q^{-1})S \\ = (1 - 0.8q^{-1})(1 - 0.2q^{-1}). \end{aligned} \tag{2.29}$$

To eliminate the influence of the plant polynomial $(1-0.1q^{-1})(1-0.3q^{-1})$ on the output, the substitutions $B^+ = (1 - 0.1q^{-1})(1 - 0.3q^{-1})$, $B^- = 1$ and $R = B^+R'$ are made and the new diophantine equation becomes

$$R'(1 - 0.4q^{-1})(1 - 0.5q^{-1}) + q^{-1}S = (1 - 0.8q^{-1})(1 - 0.2q^{-1}). \tag{2.30}$$

The solution to the above equation of the lowest order is found by setting the order of R' to zero and that of S to one, giving

$$R'(q^{-1}) = a \tag{2.31}$$

$$S(q^{-1}) = b + cq^{-1}. \tag{2.32}$$

By expansion of the diophantine equation and equating the coefficients of the various powers of q, the solution is given by $a = 1$, $b = -0.1$ and $c = -0.04$ so that

$$R(q^{-1}) = (1 - 0.1q^{-1})(1 - 0.3q^{-1}) \quad (2.33)$$

$$S(q^{-1}) = -0.1 - 0.04q^{-1}. \quad (2.34)$$

The observer polynomial A_o is made a factor of T as discussed giving

$$T(q^{-1}) = (1 - 0.2q^{-1})\lambda. \quad (2.35)$$

Therefore, after cancellation, the new relationship between r and y is

$$\frac{q^{-1}\lambda}{A_m}. \quad (2.36)$$

It now remains to set λ such that the value of the response of y as $t \to \infty$ to a unit step input is 1, so as to ensure a zero steady state error to a step input. Using equation (2.23), λ is set as

$$\lambda = \frac{A_m(1)}{B^-(1)} = 0.2. \quad (2.37)$$

2.3.7 Incorporation of Integral Action

Using integral action yields a zero steady-state tracking error $e(t)$[2] despite inaccuracies in the model that the controller is based on. This is realised in discrete time by including a $\frac{1}{1-q^{-1}}$ term in series with the $\frac{1}{R}$ block as shown in figure 2.8.

The characteristic equation is thus augmented to become

$$R(1 - q^{-1})A + q^{-k}BS = A_m A_o. \quad (2.38)$$

Using the final value theorem, the steady state value of y(t) as $t \to \infty$ for a step input r(t) of magnitude R_m is given by

$$\lim_{q^{-1}\to 1} \left(\frac{1 - q^{-1}}{q^{-1}}\right) \cdot \left(\frac{R_m}{1 - q^{-1}}\right) \cdot \left(\frac{q^{-k}BT}{(1 - q^{-1})RA + q^{-k}BS}\right) \quad (2.39)$$

$$= R_m \frac{T(1)}{S(1)} = R_m. \quad (2.40)$$

[2]The tracking error $e(t)$ is defined as: $e(t) = r(t) - y(t)$.

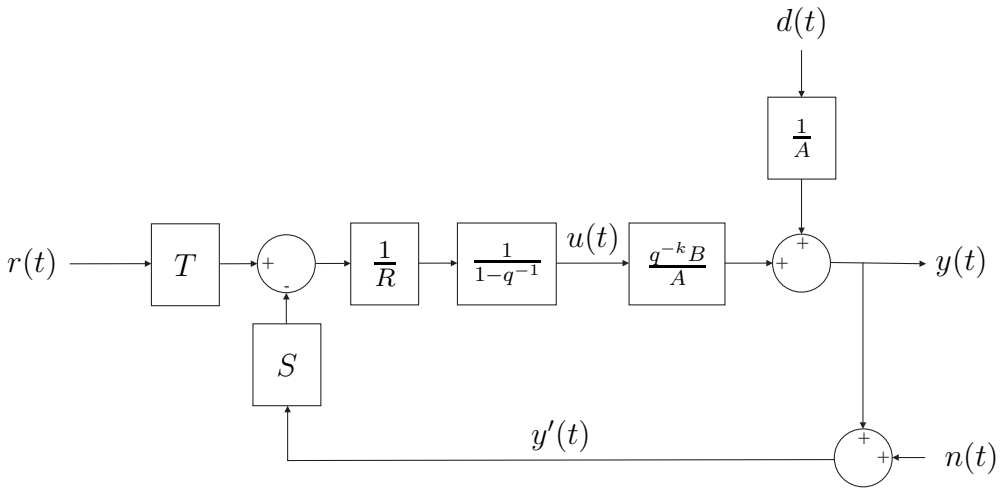

Figure 2.8: Incorporation of integral action. The control structure is augmented with a $\frac{1}{1-q^{-1}}$ term to ensure zero steady state error to a step input.

The last equality follows from the fact that zero steady state error is guaranteed for the nominal system through the use of equation (2.23). The final value is governed by $\frac{T(1)}{S(1)}$ and thus is not a function of the polynomials A and B which represent the model/plant. Therefore, zero state error is achieved through the integral action even where there are modelling errors.

2.3.8 Antiwindup Implementation

The input to the plant may be constrained using the saturation structure of figure 2.9. When the upper or lower limit is reached, a condition of saturation ensues and this can pose difficulties resulting from the use of integral action. During saturation, the feedback loop is effectively cut, and large values of the signal $v(t)$ can develop from the integration. This scenario is often called a windup condition and it can cause undesirable transient behaviour since the system will take time to recover from the windup as $v(t)$ returns to normal values [34].

For brevity, the substitution $R_i = R(1 - q^{-1})$ is made so that the new R_i polynomial includes the integral action. The antiwindup scheme in figure

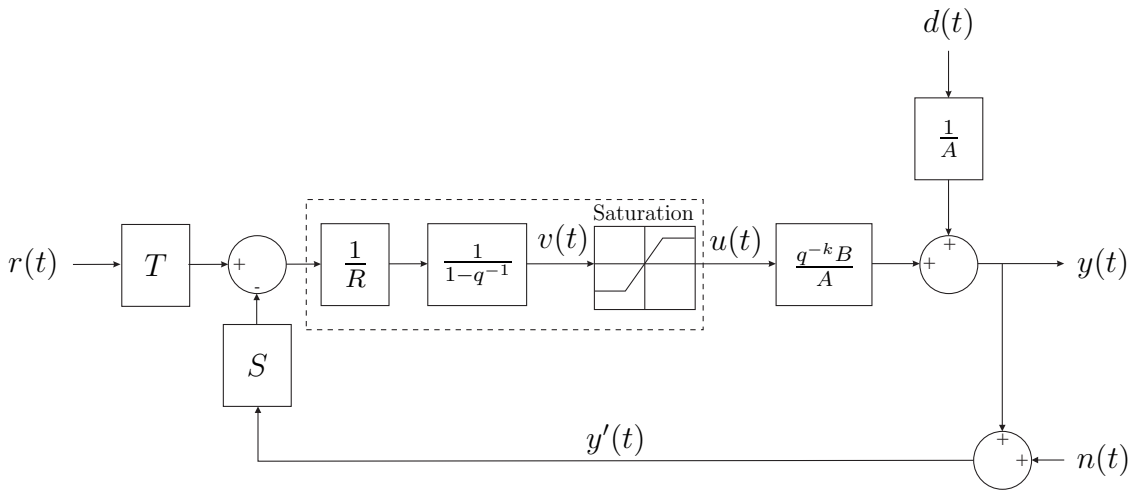

Figure 2.9: The control output $u(t)$ that the plant is exposed to can be limited using a saturation block.

2.10 is used to replace the subsystem enclosed in the dashed box of figure 2.9. A new polynomial R_0 is set up as a function of the observer polynomial A_o and R_i such that

$$R_o = A_o - R_i. \tag{2.41}$$

The antiwindup scheme includes a feedback loop from the control output $u(t)$ which effectively provides 'information' about whether or not the system is in saturation. Mathematically, the observer polynomial A_o does not contain the integrating term $[1 - q^{-1}]$ as a factor, and therefore it follows from equation (2.41) that R_o also cannot contain this factor. Therefore, during saturation conditions, $v(t)$ is governed by a sum of responses involving A_o and R_o, neither of which contains an integrating term and therefore, a steady state value is reached as $t \to \infty$ as opposed to the steady accumulation that would otherwise occur if the simple structure of figure 2.9 were used.

However, during normal operations, the transfer function representing the antiwindup system is given by

$$\frac{\frac{1}{A_o}}{1 - R_o\frac{1}{A_o}} = \frac{1}{A_o - R_o} = \frac{1}{R_i}. \tag{2.42}$$

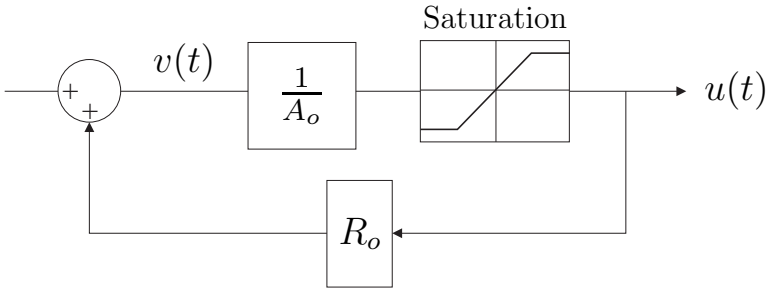

Figure 2.10: Antiwindup Scheme. Under conditions of saturation, the output $v(t)$ is determined by a summation of terms in $\frac{1}{A_o}$ and R_o, neither of which contain integral action. Under non-saturation conditions, the subsystem behaves as $\frac{1}{R_i}$.

Therefore, under non-saturation conditions, the system behaves simply as $\frac{1}{R_i}$ and is therefore equivalent to the nominal system of figure 2.8.

2.3.9 Direct Specification of Closed Loop Properties

The desired closed loop properties may be specified in terms of the rise times and damping factors of the control and observer components. These properties give rise to continuous time polynomials for the control and observer polynomials of the form

$$H(s) = \frac{\omega_n^2}{s^2 + 2\omega_n \xi s + \omega_n^2} \tag{2.43}$$

where the natural frequency is calculated from the specified rise time t_r and damping factor using equation (2.44).

$$\omega_n = \frac{1}{t_r\sqrt{1-\xi^2}} tan^{-1}\left(\frac{\sqrt{1-\xi^2}}{\xi}\right) \tag{2.44}$$

The next stage is to convert the above continuous time system into an equivalent discrete time transfer function. This can be performed numerically using MATLAB, and there are several methods available. The function 'c2d' was used and incorporates a zero order hold to keep the control signal $u(t)$

constant between sampling instants. This routine is equivalent to the system of figure 2.11.

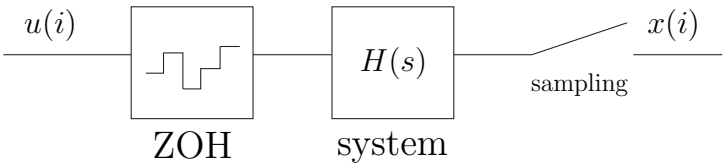

Figure 2.11: Discrete time realisation of the continuous time system $H(s)$ using a zero order hold (ZOH) and sampling. The input to the continuous time system $H(s)$ is thus held constant between sampling instants.

2.3.10 Further Decoupling: Incorporating a Pre-filter

Equation (2.18) reveals that the control polynomial A_m influences the responses to both the reference and disturbance signals. A prefilter positioned in series with the T block as shown in figure 2.12 can provide a means to decouple these responses such that different polynomials dictate the responses to the reference and disturbance signals. This is again achieved via pole-zero cancellation.

With R, S and T as previously defined and the filter block as

$$F = \frac{\lambda_f A_m}{A_f}, \tag{2.45}$$

the transfer function from the reference signal to the output is simply

$$\frac{q^{-k}\lambda_f A_m(1)B^-}{B^-(1)A_f} \tag{2.46}$$

and thus the response to $r(t)$ is no longer governed by A_m, but instead by the filter polynomial, A_f. λ_f is set as $\frac{A_f(1)}{A_m(1)}$ to ensure a unity steady state gain from reference to output.

2.3.11 Analysis of Robustness of Stability

Having determined the parameters of the polynomials, it is important to examine the robustness of the system against inaccuracies in the model.

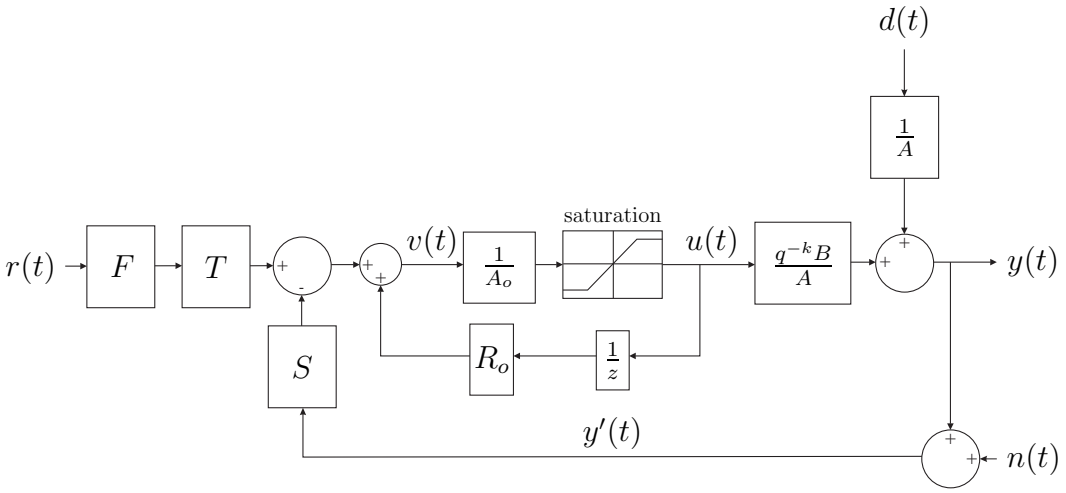

Figure 2.12: Positioning of pre-filter block, F.

Nominal stability of the system is guaranteed since the roots of the characteristic equation (2.19) are specified during the pole placement procedure. However, the real system will differ from this nominal, model closed loop and such variation has the potential to cause instability. In this thesis, the Nyquist plot is used to determine the robustness of stability of the systems in question.

The Nyquist test follows from Cauchy's principle of the argument [34]. A closed contour in the z-plane can be mapped by a function $F(z)$ to give a new, mapped contour as shown in figure 2.13.

Denoting the number of poles and zeros of $F(z)$ contained within the original contour as P and Z respectively, and N as the number of times that the mapped contour $F(z)$ encircles the origin in an anticlockwise direction, the principle of the argument states that

$$N = Z - P. \tag{2.47}$$

The discrete time closed loop system is stable provided that all the poles of the closed loop system lie within the unit circle. Therefore, a contour in the z-plane which encloses the unstable region such as that shown in figure 2.14 is used to check for the presence of unstable poles.

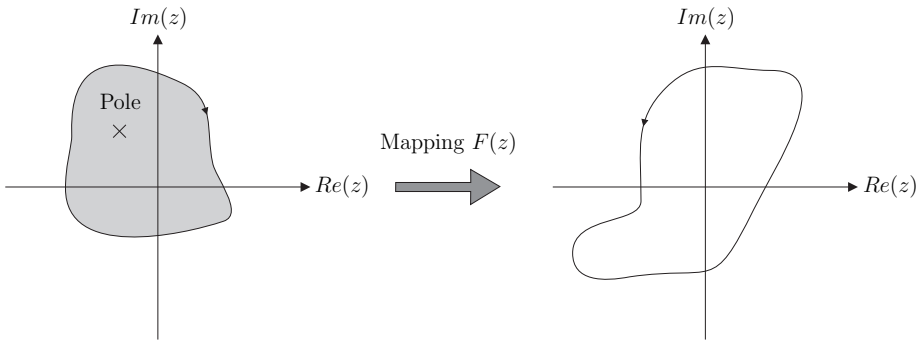

Figure 2.13: Principle of the argument. The number of encirclements by the mapped contour (right) is equal to the number of poles and zeros enclosed by the original contour (left) in the z-plane, which is 1 in this case.

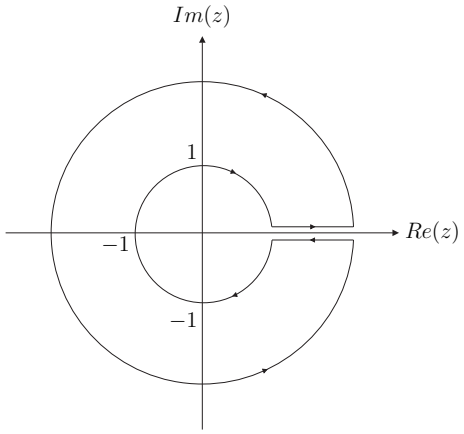

Figure 2.14: Contour on the z-plane for the Nyquist test. A closed contour encompassing all the points outwith the unit circle is used; note that the outer circular region of the contour thus theoretically has an infinite radius.

A closed loop transfer function can be expressed as $\frac{H_1(z)}{1+H_2(z)}$, where $H_2(z)$ is the loop transfer function. The stability is therefore governed by the zeros of $1 + H_2(z)$. Given that the number of poles of $1 + H_2(z)$ outside the unit circle is P, equation (2.47) shows that the Nyquist plot of $1 + H_2(z)$ must encircle the origin N times in the clockwise direction, or equivalently, $H_2(z)$ must make N clockwise encirclements of the $(-1, 0)$ point. Thus if there are no unstable poles of $1 + H_2(z)$, the Nyquist plot of $H_2(z)$ must not encircle the critical $(-1, 0)$ point for nominal closed loop stability.

Although the nominal system will be stable owing to the pole placement procedure, the contour of the actual system will differ from that of the nominal closed loop as shown in figure 2.15. The degree of uncertainty in the model that can occur without closed loop instability ensuing is reflected by the minimum distance from the Nyquist contour to the critical $(-1, 0)$ point. This distance is called the vector margin (V_m) and is shown in figure 2.15. If the plot of the actual system plant were to pass through the critical point, the value of N and therefore the number of unstable poles would change. The greater the vector margin, the greater the modelling error/uncertainty which can be tolerated. A practical design specification is that the vector margin be greater than 0.5 [9].

2.4 Summary

Linear discrete time models of various orders may be determined using input-output data taken when the system is in operation. Following the selection of a particular model, a closed loop system is synthesised based on a number of design criteria by pole placement. The additional elements of integral action, antiwindup implementation and pre-filter can be included as desired, and the robustness of the system to perturbations and errors in the plant can be assessed by means of Nyquist plots and the vector margin.

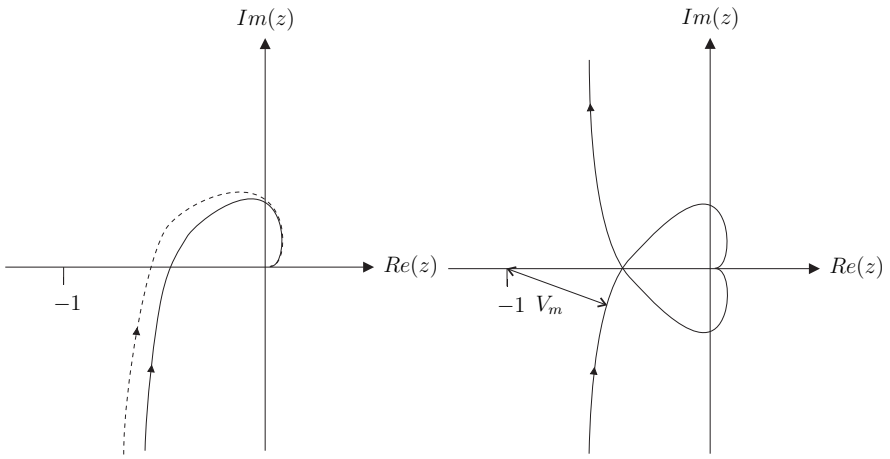

(a) Deviation from nominal system (b) Definition of vector margin

Figure 2.15: The real system will generally differ from its nominal counterpart due to modelling errors. Therefore, the point at which the contour comes closest to the $(-1, 0)$ point is important, since it shows the amount of deviation which may occur without instability ensuing. The minimum distance from the contour to the critical point is called the vector margin, V_m.

Chapter 3

Cadence Controller for Paediatric FES Cycling System

3.1 Introduction

Functional electrical stimulation (FES) cycling is a novel exercise method which has thus far mainly been applied to adults with a spinal cord injury. However, preliminary results have demonstrated the possibility of its application within the paediatric spinal cord injured population.

Due to the relative weakness of this population, it is useful to have some form of physical assistance that can be applied during exercise of this group. One option is to use an electric motor to provide additional torque where necessary.

After reviewing FES techniques and paediatric spinal cord injury, this chapter describes the development of a system for feedback control of an electric motor with the aim of regulating the angular velocity to desired levels during FES cycling exercise.

The work of this chapter has been submitted for publication:

- A. Pennycott and K.J. Hunt, 'Cadence Control System for Paediatric Functional Electrical Stimulation Cycling', submitted to *Control Engineering Practice*.

3.2 Background

3.2.1 Functional Electrical Stimulation

Several exercise applications for the SCI population utilise a technique called functional electrical stimulation. This is the application of timed electrical pulses via either transcutaneous means where electrodes are placed on the skin, or by implanted devices. The established electric field triggers neural signals called action potentials which are responsible for activating the muscles. During an action potential, an electrical stimulus causes ion channels in the cellular membrane to open, allowing movement of sodium ions into the cell; the latter has a slightly negative charge in the resting state which favours

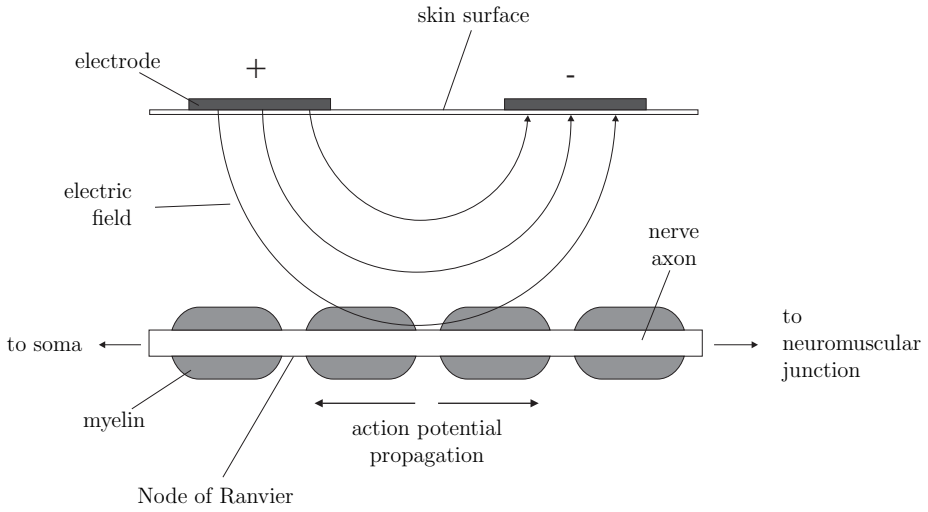

Figure 3.1: Application of FES. An electric field is established which triggers action potentials along the nerve. These elicit muscular contractions after the signal is chemically passed through the neuromuscular junction.

such movement. This influx yields a positive charge in a process called depolarisation. Restoration of the original negative charge occurs when different channels open to allow an outflux of potassium ions during repolarisation [111]. The action potential propagates along the neuron in a chain reaction. FES can be used to provide the initial stimulus for depolarisation so that muscles with no supraspinal input due to the SCI can nonetheless be activated artificially. The application of transcutaneous FES is depicted in figure 3.1.

FES can potentially enhance existing exercise methods in the SCI population by providing a greater muscle mass with which to stress the cardiovascular system and also by activating the 'muscle pump' of the lower limbs, increasing the venous return to the heart and thereby augmenting cardiac output. This may in turn promote a greater degree of development in the central support systems to be trained.

FES application is limited to individuals with damage to only their upper motor neurons because its application relies on the lower motor neurons

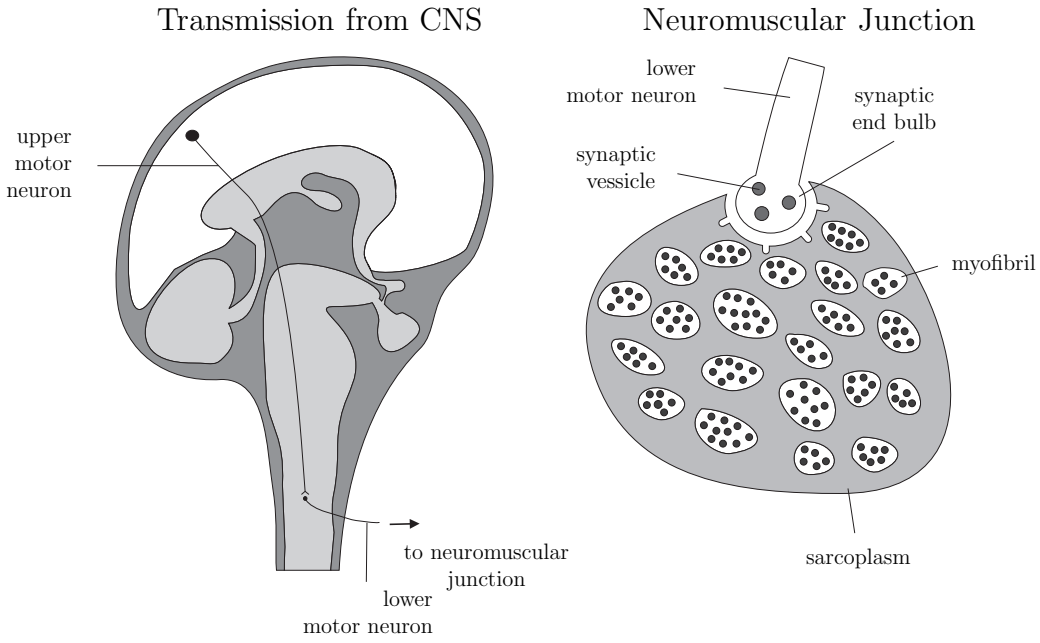

Figure 3.2: Transmission of neural signals from the CNS to the muscle. The signal passes in action potential form through the upper and motor neurons, and is then transferred chemically through the neuromuscular junction. FES application relies on the lower motor neuron being intact.

being intact as it is in these neurons that the initial action potentials are generated. Normal neural transmission from the higher centres to the muscles is illustrated in figure 3.2: electrical signals pass from the brain to the muscles via the upper and then lower motor neurons and are subsequently transmitted chemically through the neuromuscular junction. If the lower neurons are impaired, the peripheral neural pathways required for FES stimulation will not be functional, which is often the case for a person with an injury below the level T10 [56].

The electrical pulses of FES can be characterised in terms of period (and thus frequency), pulsewidth and current as shown in figure 3.3.

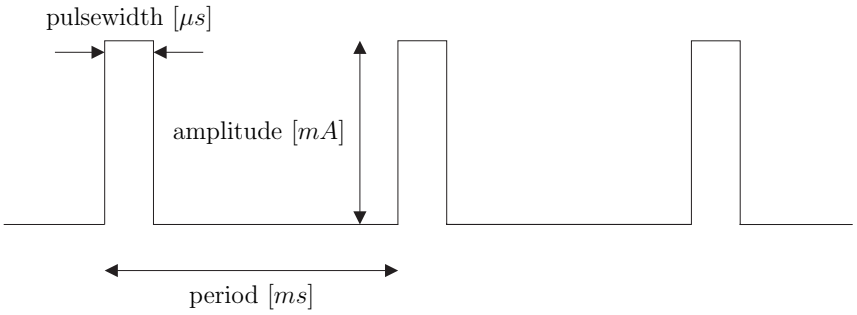

Figure 3.3: Stimulation parameters.

3.2.2 FES Cycling

FES has been applied to facilitate cycling in SCI persons. The basic trike technology used is illustrated in figure 3.4. The technology employs orthoses to secure the subject's feet and to ensure that the legs move in the appropriate plane, throttles to vary the level of stimulation and possibly the level of motor support, a magnetic brake (trainer) to vary the resistive torque and therefore the work rate, and often an electric motor to provide torque assistance. Torque and angular position are measured at the crank. In addition to this set-up, stimulation hardware must be incorporated for application of FES to the muscles.

During FES cycling, electrical stimulation is applied sequentially to different muscle groups - most commonly, the quadriceps, hamstrings and gluteals. The activation of the different groups in each leg is based on the angle measured at the crank as this uniquely determines the current position within the cycling kinematics and is realised by a muscle selection algorithm (see figure 3.5). For each muscle group, there is an angle range at which that group is active. These angle ranges are determined such that a given activated muscle group produces a positive moment at the crank arm. Care must be taken to prevent wasteful antagonistic muscle action which, aside from depleting limited energetic substrates required for exercise, also places the bones and joints under unnecessary stress. The system for application of stimulation

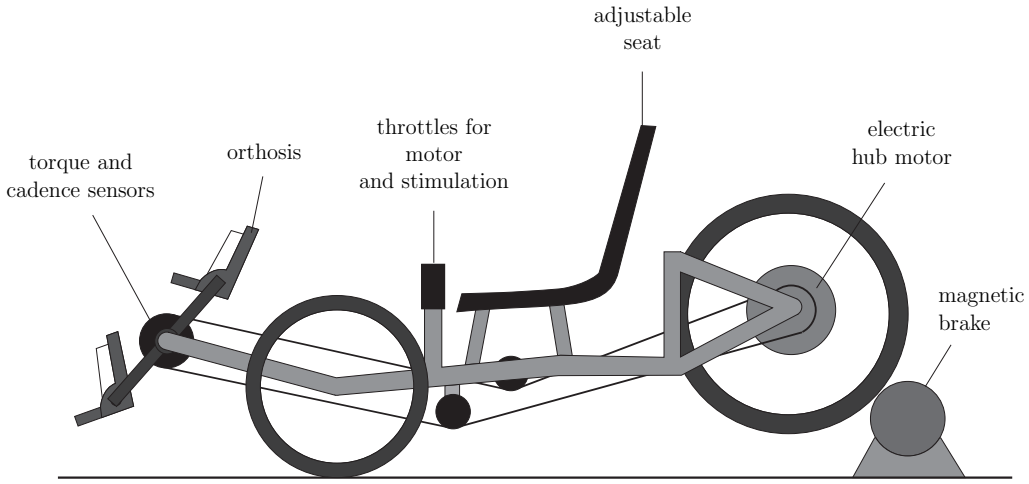

Figure 3.4: FES cycling hardware. The basic elements include orthoses, torque and cadence sensors, a magnetic brake (often called the trainer) and a stimulator (not shown).

during FES cycling is shown schematically in figure 3.5. In this arrangement, the stimulation is being applied in an open loop set-up since the intensity is manually set by the throttle.

FES cycling can be mechanically assisted through the use of an electric motor. FES cycling is very inefficient compared with volitional cycling and fatigue can rapidly develop, limiting the duration of the training [39]. Motor assistance is also important for mobile cycling where the torques required for propulsion are generally higher due to the added component of the cyclist's own inertia. Additionally, the work rate required for propulsion during mobile cycling can vary due to gradients and wind, and a motor can help to maintain a steady cadence in the face of these disturbances. Moreover, the use of such a motor can allow the cycling cadence to be more accurately controlled to desired levels which can be useful during application in an exercise testing setting. This chapter focuses on the latter benefit; however, similar feedback control schemes may be developed for mobile cycling using the same principles.

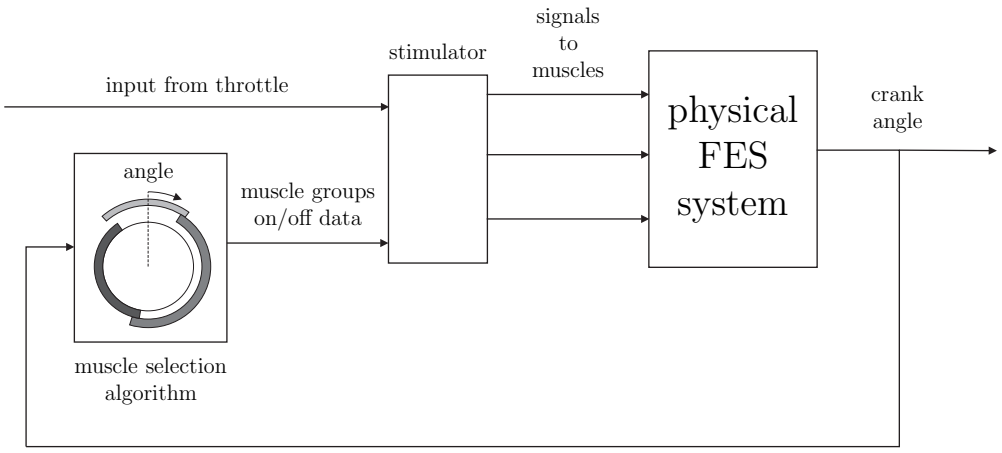

Figure 3.5: Open loop application of stimulation during FES cycling. The various muscle groups - the quadriceps, hamstrings and gluteals - are activated in sequence and are switched on or off by the muscle selection algorithm depending on the angle measured at the crank. The intensity of the stimulation can be varied using a throttle.

FES Cycling in the Literature

FES cycling was realised by using implanted electrodes in the 1980's by Kern [88]. In a later study by Perkins [87], intradural nerve roots were used as the site of electrode attachment due to the protection afforded to the electrodes by the spine in this position. This type of implanted application normally requires an empirical approach to determine the angle-dependent pattern for activation of the muscle groups (i.e. the muscle activation algorithm of figure 3.5).

Various groups have analysed the influence of different physical parameters of the apparatus and participant on the cycling motion. For example, Gföhler and colleagues investigated the effects of several parameters including the inclination angle of the backrest and horizontal distance between hip and pedal using a simulation approach [38].

Aside from the benefits already noted regarding the inclusion of an electric motor, its incorporation can also allow the training to occur at lower cadences. Cycling becomes difficult to control at low angular velocities if the

cycling is being controlled with only a braked flywheel. This obstacle may be overcome using an integrated electric motor. Cycling at low cadences may be important since force-velocity relationships suggest that higher forces are produced at lower cadences, and thus perhaps provide a more powerful stimulus for physical adaptation through the training [32].

Static ergometer devices have also been employed, with some having the facility of cadence control via an electric motor and feedback of the subject's torque contribution [32].

Several investigations have used electromyography (EMG) measurements during able bodied cycling in order to determine suitable/optimal intervals of application for the different muscle groups e.g. [61]. It was thought that the EMG results would indicate the angle ranges at which each muscle group was active and contributed to the cycling propulsion, thus yielding angle range data for the muscle selection algorithm (see figure 3.5) for stimulation during FES cycling. However, the data produced from these approaches have not yet been translated into optimal patterns for actual FES cycling. Therefore, various research groups have conducted investigations in physical test-beds in which the effects of the angle ranges, stimulation patterns and other factors were investigated and optimised [37].

Stone [108] and Schauer [101] focused on the control of cadence and work rate during FES cycling of adult SCI subjects. The former has additionally developed a method by which the oxygen uptake rate can be controlled during cycling.

Davis has reported that in conditions of constant oxygen uptake, metabolic rate and power output conditions, there was a significantly increased cardiac output and stroke volume when FES stimulation of the lower limbs was applied in conjunction with upper-body exercise, compared with upper-body exercise alone [19]. This implies that the loading of the cardiovascular system could be increased with simultaneous FES application.

The efficacy of FES in promoting beneficial change in SCI persons has been demonstrated using various indices. There have been improvements

reported in cycling endurance [89, 105] power output [30], benefits to the cardiovascular [30, 90] and respiratory [90] systems, and improved range of joint motion [86]. Other studies investigating the effects of FES on the skeletal system have also been conducted [6, 27, 28, 80] but further investigation is required to fully substantiate the benefits of FES with regard to reducing osteoporotic effects in SCI persons.

3.2.3 Paediatric Spinal Cord Injury

Paediatric spinal cord injury is fortunately a relatively rare event, partly owing to the greater plasticity of the spine of children compared with adults [115]. Children account for only around 5% of spinal cord injury cases [42]. As in adults, common causes of injury include motor accidents, sports (most commonly diving) and falls [16, 115, 117].

The epidemiology and mechanisms of spinal cord injury are slightly different for the child. Children have a head that is larger relative to the body than adults and have greater spinal mobility. The larger head leads to a fulcrum that is located higher in the spine, leading to an elevated incidence of cervical injury amongst SCI children [16, 75, 115]. Moreover, because of the plasticity that arises due to the generally weaker ligamentous support, injury without fracture or dislocation - termed spinal cord injury without radiological abnormality (SCIWORA) - is more common in children.

Furthermore, the immobilisation process and injury diagnosis by imaging are made more difficult in the paediatric case due to the distress and anxiety of the child [75].

Children with SCI suffer from similar secondary complications to those of adults: for example, Moynahan *et al* found a lower bone mineral density in SCI children than their age-matched counterparts [82]. Urologic infection [92] and pressure ulcers [131] are also common ailments of these patients. Joint contractures, often caused by the filling of joint spaces by fibrofatty material and changes in ligament properties, can limit joint movement and passive placement of the patient which may itself lead to pressure sores [113].

Furthermore, since the children are still developing, some secondary complications are more prevalent in paediatric SCI patients than in adults. For example, children with SCI are susceptible to spinal deformity as growth continues, caused by muscle imbalance or bony abnormality/deformity resulting from surgical intervention or from the injury itself [70]. Hip joint instability may lead to dislocation and is caused by positional irregularity from contractures and also arises because the weak muscular support allows gradual stretching of the joint structures over time [77]. The presence of contractures, hip instability and spinal deformity can pose an obstacle to the fitting of equipment for exercise training such as FES cycling and can necessitate specialised technological adaptations [76].

3.2.4 FES Application in Children with SCI

The feasibility of FES cycling application in the paediatric SCI population has been demonstrated by McRae [76]. Using the hardware as in this thesis and presented in section 3.3.1, a brief period of FES cycling was performed by a child with a complete spinal cord injury. This research provides the motivation for the current work on cadence control presented here.

Whilst there is only limited data on FES cycling in this subject group, research has been conducted on a number of alternative FES applications for the paediatric SCI population. For example, Johnston and colleagues demonstrated that participants performed activities such as reaching and wheelchair transfer with greater rapidity and more independently using implanted FES than with leg braces [66].

Percutaneous stimulation has been shown to facilitate grasping and release tasks in tetraplegic children [83]. The participants were able to perform the tasks unilaterally with the aid of FES so that the other limb could be used for balance and other functions.

Following strength training and standing work employing surface-applied FES, paediatric subjects demonstrated increases in muscle mass, strength and resistance to fatigue in the study by Popovic [94]. Though the bone

density data showed a large variance, there appeared to be an increasing trend.

Robinson *et al* investigated the use of FES stimulation of the lower extremities in combination with conventional arm cranking ergometry (ACE) work, arguing that the latter alone is limited due to the low active muscle mass [100]. The hybrid exercise where both ACE and FES were used showed a greater physiological response than the exercise form employing FES alone. The FES exercise nevertheless provoked a significant cardiopulmonary response, indicating the potential value of FES in exercise training in this group.

Triolo and colleagues found that 50% of evaluated candidates were suitable for participation in FES even without preparatory intervention such as transfer of excitable muscle in the group of tetraplegic subjects studied [112]. Common causes for exclusion from testing included peripheral denervation and psychological problems.

It is suggested that encouraging a child with a spinal cord injury to lead an active lifestyle through exercise may lead to such a lifestyle being continued throughout later life, thereby reducing the risk of cardiovascular disease. Moreover, it has been observed that exercise participation can improve self image, though it may cause a negative psychological effect in some participants due to unrealistic expectations such as the belief that the training will lead to neurologic improvement [116].

3.2.5 Cadence Control During FES Cycling

The ability to regulate cadence during cycling is important both in training and exercise testing. In training, close regulation of cadence can prevent erratic, uncontrolled movements of the limbs which can lead to spasticity and unnecessary stress on the joints. Such undesirable motions could also have negative psychological effects. In exercise testing, it is important to control all the parameters of exercise which are not being investigated as closely as possible because these can have a confounding effect on the results.

For example, cadence (velocity) affects the rate of muscle contraction and therefore has an effect on the overall efficiency of the exercise [95]. The statistical power of a test designed, for instance, to contrast the efficiency of exercise produced by different patterns of FES stimulation would be seriously weakened if the cadence were allowed to vary within tests.

3.2.6 Summary

FES artificially induces muscular contraction which can be harnessed to produce cycling motion. Preliminary results demonstrate the feasibility of FES cycling for children with an SCI. Furthermore, FES cycling can be enhanced by the addition of an electric motor to provide torque assistance where required.

3.3 Methods

The techniques of system identification and control design as outlined in Chapter 2 were applied to produce a closed loop control system to regulate the level of cadence during FES cycling by varying the torque contribution of the motor.

3.3.1 Apparatus

The hardware employed for the tests consisted of a child's trike (KMX Karts, UK), a magnetic braking device/trainer (Tacx, Netherlands), and a shaft encoder plus interface box (Hasomed GmbH, Germany). A 24V, 200W electric hub motor (Heinzmann GmbH, Germany) was used for torque assistance. The motor torque produced can be adjusted by varying a potentiometer voltage signal via a throttle when the system is run in open loop, whilst the stimulation intensity can be set using another throttle. In the first feedback control tests of this thesis, the torque was set in a closed loop system, and the

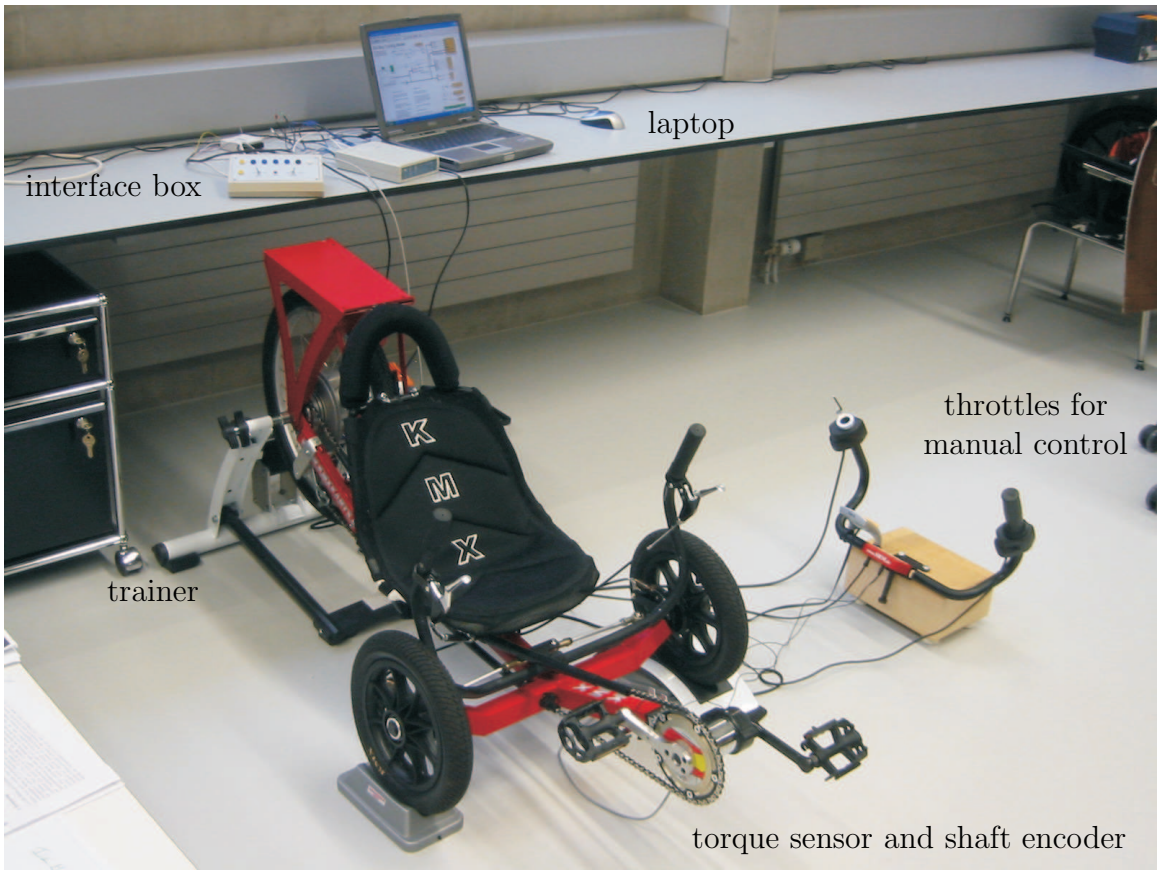

Figure 3.6: Paediatric FES cycling hardware. An interface box provides the link between the electronics of the cycling hardware and the laptop computer.

throttles were therefore not used. However, in the clinical trial in Philadelphia (see section 3.4.4), one throttle was used to set the level of reference cadence. The various elements of the hardware can be seen in figure 3.6.

The initial control tests were undertaken with no subject in the apparatus. In view of this, the controller had to be made sufficiently robust so as to maintain stability in the face of changes in the plant dynamics; i.e. if a cyclist were included in the apparatus, the closed loop properties would differ from the nominal version developed here. However, sample data from an actual FES cycling trial with a paediatric SCI subject are also included in this

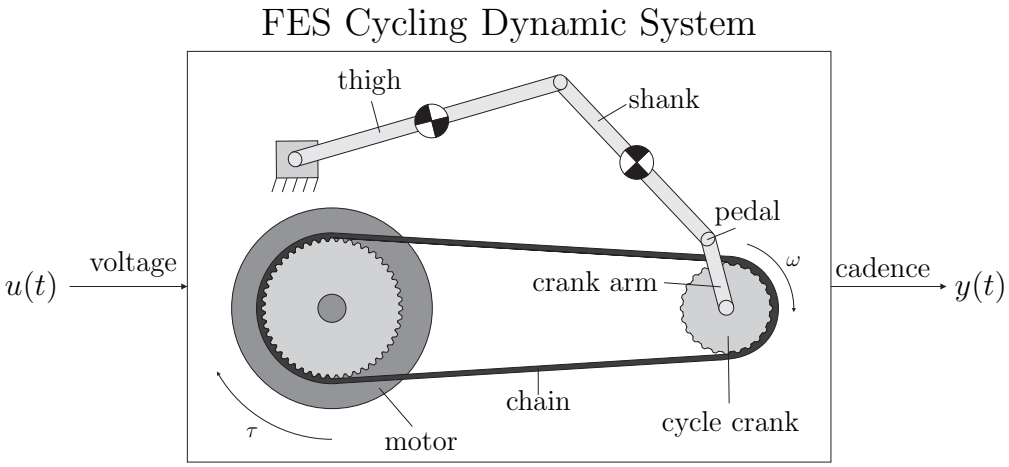

Figure 3.7: FES cycling dynamics. The system includes the dynamics of both the motor, responsible for producing the torque τ, and the mechanical linkage system of the cyclist's limbs. During the system identification and initial feedback control tests, the linkage element of the dynamics was absent as no subject was included.

chapter.

3.3.2 System Identification

The dynamic system in the FES cycling set-up relates the voltage input signal supplied to the motor with the resulting cadence (angular velocity) output signal as illustrated in figure 3.7.

The dynamics therefore encapsulate both the mechanical aspects of the trike including inertia, friction and gearing system, and also the elements of the electric motor. When a subject is included, there is the additional element of the effective mechanical linkage system of the cyclist's lower limbs.

By applying a PRBS as a voltage input, a cadence response was elicited from the plant (figure 3.7) to be identified. Using these two signals, ARX models of various orders were determined using the Ident tool of MATLAB. These were evaluated and assessed in terms of the fit variable as described in section 2.2.3 and defined in equation (2.15).

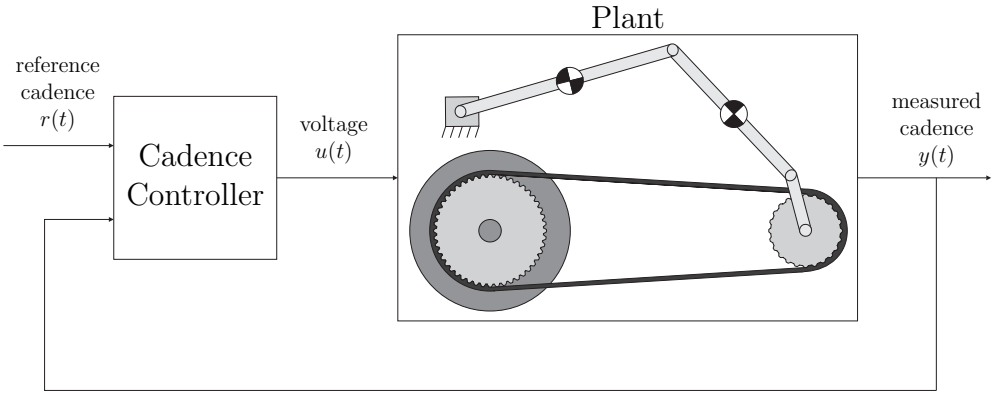

Figure 3.8: Closed loop cadence control. The voltage signal required to elicit the reference cadence is calculated and delivered to the motor based on a feedback measurement of the actual cadence.

3.3.3 Control Design

The motor trike system was controlled in a closed loop configuration as shown in figure 3.8. The controller adjusts the voltage signal online so that the actual cadence follows reference values.

Using the model developed as described in section 3.3.2, the control polynomials R, S and T were determined for the chosen design specifications. The control polynomial A_m was set to have a rise time of 2s and damping factor of 0.99, whilst the observer polynomial A_o was assigned a rise time of 0.5s and damping factor of 0.99. A sample time of 0.2s was used for all the tests of this chapter.

Integral action with antiwindup was implemented and the control input $u(t)$ was constrained to be between 0 and 5V. The vector margin was used as the criterion for assessing the robustness of stability of the resulting closed loop system.

3.3.4 Experimental Structure

The input-output data required for the determination of the empirical models were obtained from a PRBS system identification test. Following this, the

parameters of the discrete time models could be calculated and the control polynomials synthesised.

In order to assess the behaviour of the real closed loop system, the tracking ability of the system was tested using reference signals of square wave, sinusoid and ramp formats. The latter test also demonstrated the behaviour of the system during saturation conditions. The response of the system to disturbances was tested by manually applying a torque to the crank in order to ensure that the system did not become unstable in the face of such disturbances.

The system identification and initial control testing were carried out in the Guido A. Zäch Institut of Swiss Paraplegic Research, Nottwil, Switzerland. The motor trike system was also tested during actual FES cycling with a child with a spinal cord injury in Shriners Hospital for Children, Philadelphia, USA.

3.4 Results

3.4.1 System Identification

Figure 3.9 shows the identification data obtained for the FES motor trike system. The estimation and validation data sets are displayed separately and in the latter case, the system output as simulated by model arx112 (see table 3.1 and equation (3.1) for definition) is included as a dashed line. Measured data are plotted as solid lines.

Table 3.1 displays the levels of fit yielded by the various orders of the calculated ARX models. In general, increasing the order of the model increased the fit values. As a compromise between the fit achieved and model order, the arx112 model given in equation (3.1) was selected for control design. This model has a rise time of approximately 2 seconds.

$$y(t) = \frac{213.4q^{-2}}{1 - 0.7456q^{-1}}u(t) + \frac{1}{1 - 0.7456q^{-1}}d(t) \tag{3.1}$$

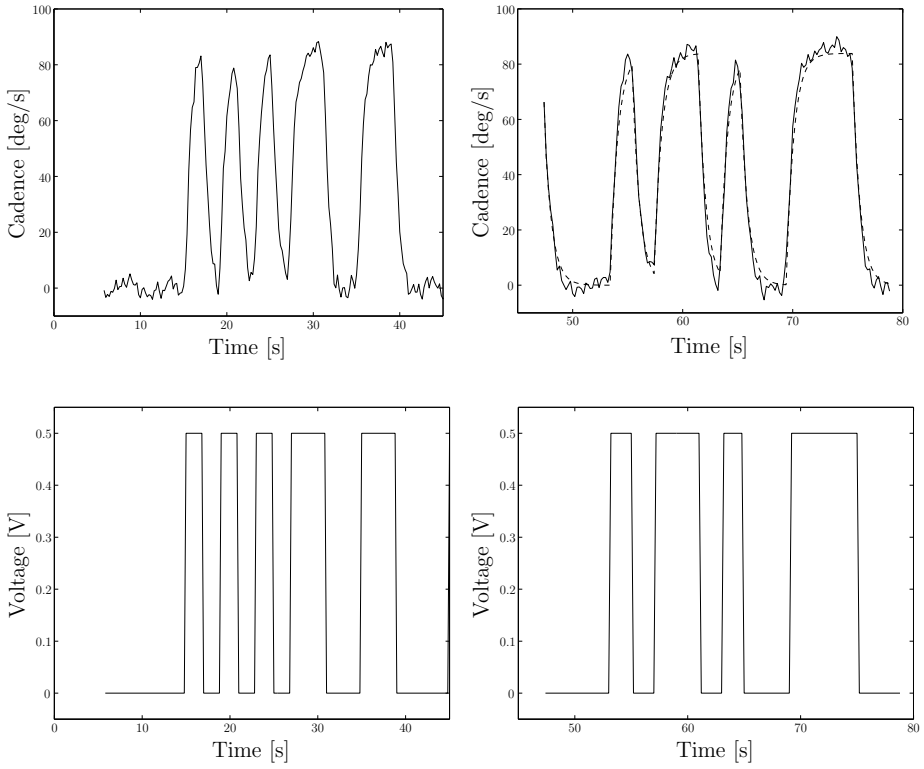

(a) Estimation Data (b) Validation Data

Figure 3.9: Motor identification results. The input and output signals of the working and validation data sets are displayed here; for the validation data, the output response as simulated by model arx112 is also depicted as a dashed line.

model	fit (%)
arx111	81.0
arx112	89.0
arx113	78.0
arx211	90.6
arx212	89.5
arx213	63.7
arx311	91.0
arx312	89.5
arx313	70.8
arx411	91.5
arx412	89.3
arx413	70.1

Table 3.1: Values of fit achieved using different orders of model for the motor trike identification. The model structures are indexed according to the number of coefficients of A and B - respectively n_a and n_b+1 - and the value of the delay, k. Therefore arxABC is an ARX model with $(n_a, n_b+1, k) = (A, B, C)$.

3.4.2 Control Polynomials

With the rise time and damping factors of the control and observer elements as set in section 3.3.3, the resulting control (A_m) and observer polynomials (A_o) were

$$A_m(q^{-1}) = 1 - 1.4526q^{-1} + 0.5276q^{-2} \quad (3.2)$$

$$A_o(q^{-1}) = 1 - 0.5559q^{-1} + 0.0775q^{-2}. \quad (3.3)$$

Using the arx112 model and the polynomials above, the control polynomials were calculated to be

$$R(q^{-1}) = 1 - 1.2629q^{-1} + 0.3178q^{-2} - 0.0548q^{-3} \quad (3.4)$$

$$S(q^{-1}) = \left(0.7181 - 0.5347q^{-1}\right) \times 10^{-3} \quad (3.5)$$

$$T(q^{-1}) = \left(0.3515 - 0.1954q^{-1} + 0.0272q^{-2}\right) \times 10^{-3}. \quad (3.6)$$

The vector margin was computed to be 1.00.

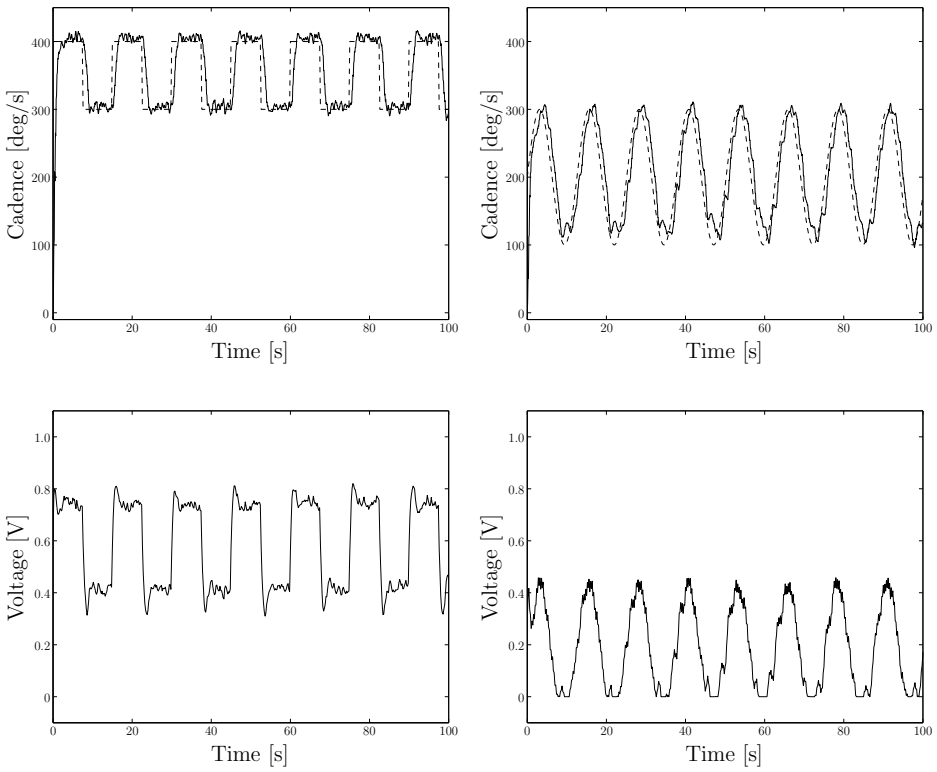

(a) Square wave reference (b) Sinusoidal Reference

Figure 3.10: Control test results part I. The cadence outputs are shown as solid lines, whilst the reference inputs are displayed as dashed lines. The corresponding voltage inputs are also displayed in the lower row.

3.4.3 Feedback Control Tests

The results of the closed loop control tests are shown in figures 3.10 and 3.11. The measured cadence outputs are shown as solid lines along with the corresponding reference signals (dashed lines). Furthermore, the control signals $u(t)$ (i.e. voltages delivered to the motor) are shown below each cadence plot.

The graphs show that the system produced a cadence output in close agreement to the reference signal for each type of input signal and did not display wind-up behaviour when saturated. During the test where an accelerative torque was manually applied to the crank, the closed loop system

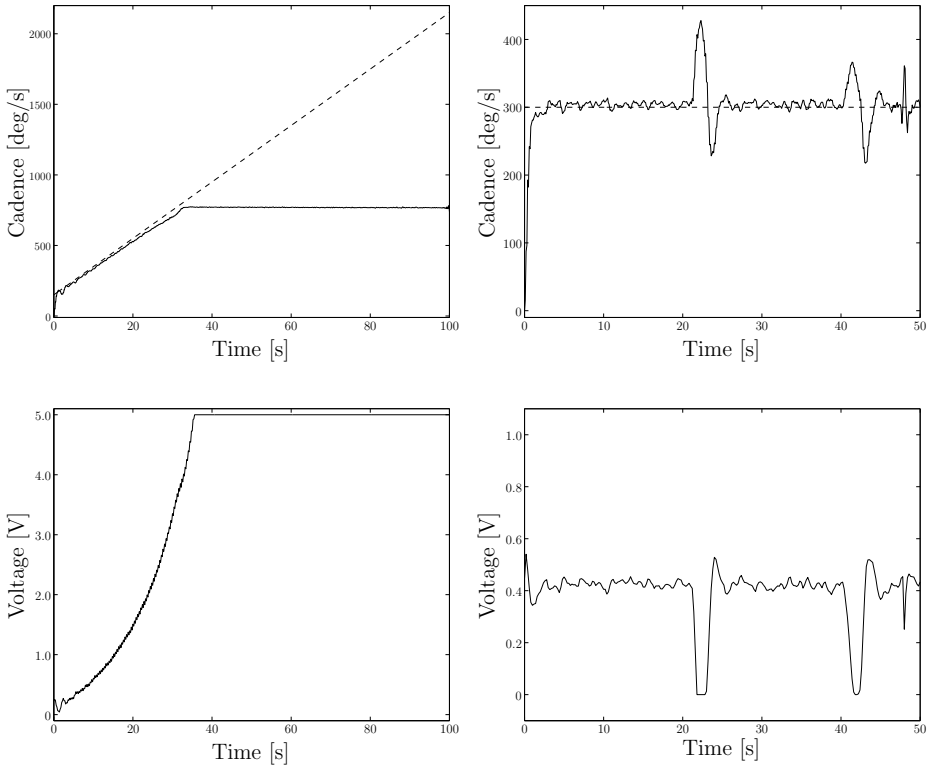

(a) Ramp reference (b) Disturbance Test

Figure 3.11: Control test results part II. The cadence outputs are shown as solid lines, whilst the reference inputs are displayed as dashed lines. The corresponding voltage inputs are displayed in the lower row of the figure. An accelerative torque was manually applied at the crank arm at 20s and 40s in the disturbance test.

reacted so as to return the cadence output towards the reference level.

3.4.4 Clinical Tests

The following results were taken from a trial forming part of a collaboration project at Shriners Hospital for Children in Philadelphia, USA. The data were collected by researcher Calum McRae, and show the application of the FES cadence control system in an FES cycling trial with a spinal cord injured child as the subject. Stimulation was manually applied in an open loop configuration, and the reference cadence was also varied manually using a throttle. The cadence, torque and voltage applied to the motor during this testing session are shown in figure 3.12.

Baseline $\dot{V}_{O_2}$ data were collected in the initial rest phase. The next portion of the test is a passive phase where the torque required to overcome friction and inertia to produce motion is provided entirely by the electric motor. There is no stimulation applied during these first two phases. During the '0 Watt' phase ('0W' in figure 3.12) , the subject exerts just enough torque via the stimulation to sustain the motion in the absence of an external load from the trainer. This is reflected in the zero torque observed during this phase. During the last phase, the subject cycles against an external resistive torque from the magnetically-braked trainer, and is said to be producing a positive work rate.

The plots show that as fatigue develops, the subject's torque contribution diminishes and the assistive torque from the motor must consequently grow in magnitude in order to maintain the constant cadence. This is reflected by the increasing motor voltage seen during the final, active portion of the test. The small offset between the actual and reference cadences may be due to the torque produced by the cyclist which is acting as a disturbance to the system; the motor can only accelerate the motion, and is unable to produce a braking torque to compensate for such disturbances.

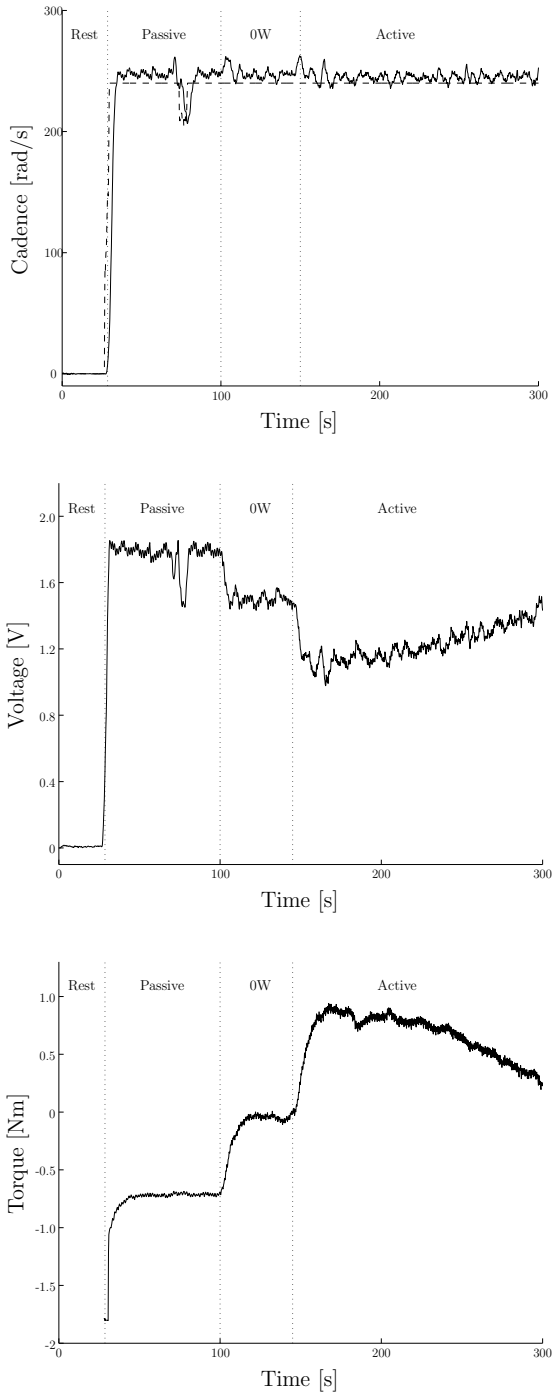

Figure 3.12: Results a from clinical trial at Shriners Hospital for Children, Philadelphia. Here the subject is a child with SCI. The top plot shows the reference and measured cadence, the middle plot the voltage signal to the motor, and the lower graph plots the torque contributed by the cyclist via stimulation.

3.5 Discussion

The resulting closed loop system produced a cadence output that closely followed the reference signal and demonstrated acceptable behaviour during saturation and disturbance scenarios.

Greater levels of fit were sometimes achieved using higher orders of model e.g. model 411; however, the magnitudes of these increases were small and therefore, the lower order model with good fit (arx112) was selected.

The vector margin of 1.00 is above the recommended value of 0.5 [9], indicating that the control system has good robustness of stability. This is important: even though the model demonstrated a good fit to the experimental data, the physical system was identified in the absence of a cyclist in the apparatus. The addition of a subject changes the physical properties of the system - principally the inertia - and the subject's torque contributions will also play the role of a disturbance. Therefore, the underlying dynamics will change with the inclusion of a subject and a large vector margin is necessary in order to prevent instability resulting from the consequent deviation from the nominal model. The preliminary results from the testing at Shriners Hospital for Children presented here demonstrate that the system has a stable response when a subject is included in the dynamics. However, further testing is required to quantify the effect on the performance in terms of the closed loop properties (e.g. rise time) of different subjects in the apparatus.

The cadence controller presented here may be combined with an additional power controller whose objective is to regulate the work rate produced by a subject by varying the stimulation intensity. An approach to combining the two control loops is presented by Hunt *et al* [54]. The power/stimulation system of figure 3.5 is subject to a high uncertainty since the dynamics are very sensitive to several factors such as electrode positioning and the physical condition of a subject, both of which can vary between and within tests. Moreover, the system can change in the course of a single test as a result of fatigue. Consequently, the model underlying the cadence control system,

although different across subjects, has a lower uncertainty and for this reason is normally set to be the faster of the two systems and assigned a higher closed-loop bandwidth when the two systems are to run in parallel.

3.6 Conclusions

The proposed closed loop system provides an effective means of eliciting a desired cadence response from the FES cycling system. The system can now be utilised in further exercise testing and training of paediatric FES cycling where a fixed level of cadence is required, perhaps in combination with a power controller.

Chapter 4

Estimation and Control of Work Rate During Robot-Assisted Ambulation

4.1 Introduction

Robot-assisted body weight supported treadmill technology is normally used in gait rehabilitation but also has potential use as an exercise tool for training and testing protocols for neurologically impaired subjects. The Lokomat is a specific model of robot-assisted hardware and is used in conjunction with a treadmill. The device supports a portion of a subject's bodyweight whilst mechanically assisting the walking motion by applying torques about the exerciser's limbs.

It would be useful in the application of the Lokomat to have a real-time estimate of the work rate being produced by the exercising subject and also to be able to control this level of power. This chapter outlines a method of estimating the active work rate of a subject during Lokomat walking, and then proposes a means by which this can be used in a feedback control loop in order to elicit a pre-determined, desirable level of power from a subject. The estimation and control scheme is then validated using 3 spinal cord injured subjects.

The work of this chapter has been submitted for publication:

- A. Pennycott, K.J. Hunt, L.P. Jack, C. Perret and T.H. Kakebeeke, 'Estimation and volitional feedback control of active work during robotic-assisted gait', submitted to *IEEE Transactions on Control Systems Technology*.

- K.J. Hunt, L.P. Jack, A. Pennycott, C. Perret, M. Baumberger and T.H. Kakebeeke, 'Control of work rate-driven exercise facilitates cardiopulmonary training and assessment during robot-assisted gait in incomplete spinal cord injury', *Biomedical Signal Processing and Control*, to appear.

- K.J. Hunt, L.P. Jack, A. Pennycott, T.H. Kakebeeke, C. Perret and M. Baumberger, 'Cardiopulmonary assessment protocols for robot-assisted gait in incomplete spinal cord injury', *Robotics in Rehabilitation Symposium*, Zürich, Switzerland, 2006.

4.2 Background

4.2.1 General Treadmill Training

Treadmill training and overground walking are common forms of rehabilitation employed for neurologically impaired people such as spinal cord injured or stroke patients. The mechanics of walking may be aided by physiotherapists and often also by walking aids. A proportion of the body weight of a subject can be supported in some cases by a harness for subjects who cannot bear the entirety of their weight unaided.

Treadmill walking assisted by physiotherapists has demonstrated improvements in terms of the participating subjects' walking distance, speed, balance and ASIA motor scores [7, 46]. The degree of body weight support required by the subjects also decreased in these studies. It can be argued that conventional rehabilitation alone, aimed at endurance development of surviving motor units and using assistive devices for functionality, may not be able to elicit such improvements since it will not provide the necessary sensory inputs for re-learning. Therefore, separate, more specific treadmill training is required.

In addition to SCI patients, treadmill training for stroke patients has also been investigated. For instance, Macko *et al* found that treadmill ambulation training was more effective than conventional stroke therapy in improving cardiovascular fitness (e.g. $\dot{V}_{O_2}$ peak) and walking ability, the latter being assessed by timed walks and a questionnaire style approach [74].

Improvements in walking are in general not well correlated with improvements in voluntary muscle contraction, indicating that there are factors other than gross muscular strength involved [120, 121, 129]. The improvements must arise from a learning mechanism, e.g. learning to activate new units, or to use the existing units more effectively, rather from changes in the muscle actuators themselves. Similarly, improvements in treadmill-based walking may not be well correlated to progress in overground walking, a finding that reflects the task-specificity of the training [23, 31, 46].

Studies investigating the more general effects of the training have thus far not demonstrated a link between ambulation ability and psychological well-being e.g. [46].

Although locomotor training appears to be of benefit in the short term, the question of the longevity of the training is important: i.e. what happens once the training ceases. Research has demonstrated that the effects of the training can decline following cessation of training, indicating that the other side of the neural plasticity coin can include detrimental, 'unlearning' effects [128]. Other studies showed no decrease in walking ability, but that an increase in the necessary body weight support was required [46]. Data from other research reflected no losses in ability over shorter periods following termination of the training [31].

The main idea of any gait training is to provide sensory data to the central nervous system. With this positional and loading data, the spinal cord may be able to adapt the patterns of muscle activation in a learning process. The three main mechanisms are to replace cells, regrow neural axons and to retrain (reprogram or 'rewire') the neural circuits - the '3 Rs of Rehabilitation' [24]. Higher neural centres and central pattern generators[1] may also play a role [7, 24, 126, 128].

The potential of treadmill work for cardiovascular training is important because some forms of exercise are impractical for certain groups, e.g. FES may be too painful for incomplete SCI patients. Cardiovascular effects have been demonstrated e.g. on heart rate variability [23], a factor which has implications for cardiovascular disease [67]. Cardiovascular responses to treadmill training have been noted for tetraplegic subjects in the literature [85], as well as improvements in the indices of the cardiovascular system [20].

[1]Neural circuitry that allows movement generation even in the absence of cortical drive and sensory input.

4.2.2 Robot-Assisted Systems

Robot-assisted technology provides assistance towards the work done required for gait propulsion in addition to supporting a proportion of the body weight of the subject. The Lokomat and its accompanying device called the Lokolift are described in section 4.3.1.

The advantages of robot-assisted training over the previously discussed manual treadmill rehabilitation techniques include economy of labour and consistency. Regarding the first point, manual treadmill techniques can demand the attention of up to three therapists for successful operation. Moreover, the duration of training is limited by the endurance of the trainers/therapists as a result of the labour-intensive nature of this therapy. Furthermore, since the trajectory of the walking gait can be largely dictated by the device, one can produce a more consistent, repeatable movement pattern compared to the corresponding manual treadmill techniques [36].

The main therapeutic value of the technology is thought to be in the rehabilitation of locomotor movement in neurologically impaired persons, as is the case with manual treadmill work. The main target groups for this type of therapy are spinal cord injured and stroke patients. It is clear that the strategies and gait patterns are likely to be different across these groups as stroke victims are often impaired in only one side of their body, a phenomenon which is not generally seen in SCI patients.

An assessment of the efficacy of the Lokomat and a comparison with other available types of training was undertaken by Hornby [49]. A multicentre study using the Lokomat to train the subjects and concurrently assess their progress was carried out where clinical assessments to evaluate the subjects' walking ability were used. The tests included the 10 metre and 6 minute walking tests; spasticity and muscle strength were also assessed. The results demonstrated that the various components of walking showed statistically significant differences (improvements) as time passed, demonstrating the effectiveness of the training. In order to compare the Lokomat

with other training modes, improvements noted in subjects using the Lokomat were compared with those undergoing therapist-assisted training and 'overground ambulation' training using 3 separate subject groups. Again, clinical assessments were taken every few weeks to evaluate the subjects' progress. Whilst within each group the mean values of the walking characteristics significantly improved, no differences were noted across the groups with respect to the extent of motor recovery, in spite of large differences in total distance covered by the various groups. One could take the perspective that the robotic training provided an equally effective method but required less assistance and therefore less time and labour from therapists than the other training forms.

Wirz and co-researchers addressed the question of whether Lokomat training could promote changes in walking ability and also reduce spasticity levels [129]. Following an 8-week training programme, subjects demonstrated improvements in walking speed and endurance, but did not generally improve walking with respect to the level of help needed from therapists or assistive devices required. No definitive patterns regarding spasticity reduction were apparent. Other studies have nevertheless found a positive effect on spasticity levels [79]. Robot-assisted systems may also be used to estimate spasticity, and these estimates have correlated well with more conventional tests [71].

The technology has been used as a validation tool in research into modelling FES applications and also for research concerning models of spinal locomotor circuitry [64, 65].

Limitations

Despite the advantages offered as described above, robot-assisted devices have a number of drawbacks. One concern of Galvez and co-authors was that the degrees of freedom currently available in the robotic various devices may not allow for a natural, physiological gait [36]. The possibility of inappropriate degrees of freedom in the current technology is suggested to be one

cause of the differences in EMG found between therapist-aided and robotic treadmill walking found in certain studies [49, 118]. For example, the foot-straps used to prevent toe clipping unnaturally flex the foot during walking, altering the neurological behaviour.

Controlling the Gait Pattern

A number of control strategies for the torque assist of the robotic devices have been developed to maintain the subject's gait in a fixed trajectory. The quality of this control will have a significant impact on the consistency of the sensory inputs to the subjects and therefore on the overall efficacy of the training. A central concept lies in the use of 'patient-cooperative strategies'. The underlying idea is that the machine recognises the intention of movement of a subject and accordingly adapts the reference trajectory of the gait. This prevents the patient from being completely passive in the therapy. Riener and colleagues list three fundamental ideas that are relevant to the control of the Lokomat: adaptivity, flexibility and online feedback to the patient regarding their performance. In addition to the previously discussed method of biofeedback, three separate control strategies are discussed [98].

In the strategy termed impedance control, an approach frequently utilised in the field of robotics, a deviation from the reference trajectory is permitted rather than rigidly imposing a set gait. In order to achieve an acceptable deviation, a torque must be applied to the limb to confine its movement appropriately. The relationship between this torque and the allowable deviation is called the impedance. The active torques being provided by the subject are estimated from an inverse dynamics approach using force measurements from the Lokomat. These torques are subtracted from the required impedance, so that the machine has to provide, via a separate torque controller, the required additional supporting torque so as to yield the correct impedance torque. A correction for friction and gravitational effects is also included. Other applicable control strategies include admittance [98] and adaptive control [63].

4.2.3 Robot-Assisted Devices in Exercise Applications

The main focus hitherto has thus been on rehabilitating the gait pattern through repetition of appropriate sensory input. However, preliminary data suggest that the robot-assisted training can also elicit a significant cardiopulmonary response [49, 55, 85]. Therefore, the use of robot-assisted body weight supported treadmill training (BWSTT) as a tool in cardiopulmonary training and testing has potential as a complementary rehabilitation application, aimed at reducing the impact of the secondary health conditions discussed in Chapter 1. Furthermore, the technology may also find application in assessing the levels of fitness and physical capacities of subjects undergoing an exercise programme.

The use of the technology in such a setting requires an estimate of the instantaneous work rate of the subject. However, a direct calculation is not possible due to the assistive nature of the apparatus: a proportion of the mechanical work done that drives the motion comes from the device itself in addition to that provided by the subject. Moreover, the mechanical assistance may even discourage active subject contribution so that the metabolic response to robotic-assisted gait may be smaller in magnitude than the response to manual treadmill work [49, 55].

It is therefore desirable to have an estimate of the magnitude of effort contributed by the exercising person as opposed to that of the machine, and also to have a means of encouraging the active participation of the subject. Riener, Lünenburger and colleagues used a weighted average of measured forces as biofeedback to the subject so as to encourage active subject contribution towards the gait [73, 98]. The elements responsible for weighting the output were heuristic functions based on whether a certain subject action was appropriate (close to normal walking behaviour) to the walking mechanics during the various phases of the gait, and 4 'biofeedback' variables of arbitrary unit were displayed to the subject.

Following on from this work, the remainder of this chapter is concerned

with the development and testing of a method aimed at estimating and controlling the rate of work done produced by an exercising subject, based on force and angular position measurements from the robotic device.

4.3 Methods

4.3.1 Apparatus

The research employed a driven-gait orthosis device called the Lokomat (Hocoma AG, Volketswil, Switzerland) shown in figure 4.1, in combination with a treadmill (Woodway GmbH, Weil am Rhein, Germany). The subject is fitted to robotically driven orthotic limbs via adjustable straps, and a portion of body weight is supported via a harness using a specialised, feedback controlled lift device called the Lokolift illustrated in figure 4.2 (Hocoma AG, Volketswil, Switzerland).

The Lokomat can support a subject whilst providing assistance towards the work done required to sustain the gait. It is designed as a parallelogram structure, allowing movement of the limbs in a desirable trajectory that resembles walking, but precluding lateral stability problems of the patient. The active support of the device is provided by four linear drives powered by DC motors that effectively apply torques around the knee and hip joints. 4 sensors provide measurements of the positions of the limbs throughout the trajectory. The Lokomat has an optical light sensor that monitors the movement of the feet and the device is halted should a 'trip' event be encountered. Furthermore, the subject is free to halt the ambulation at any time using the accessible emergency stop buttons.

Working alongside the Lokomat is the Lokolift as depicted in figure 4.2 and described by Frey *et al* [35]. The main force for body weight support is provided by the springs which can be pre-stressed by the electric spring drive. The electric winch can be used to vertically move the subject and also to keep the system in the optimal position range for operation of the dynamic drive. The latter element is responsible for making smaller adjustments in

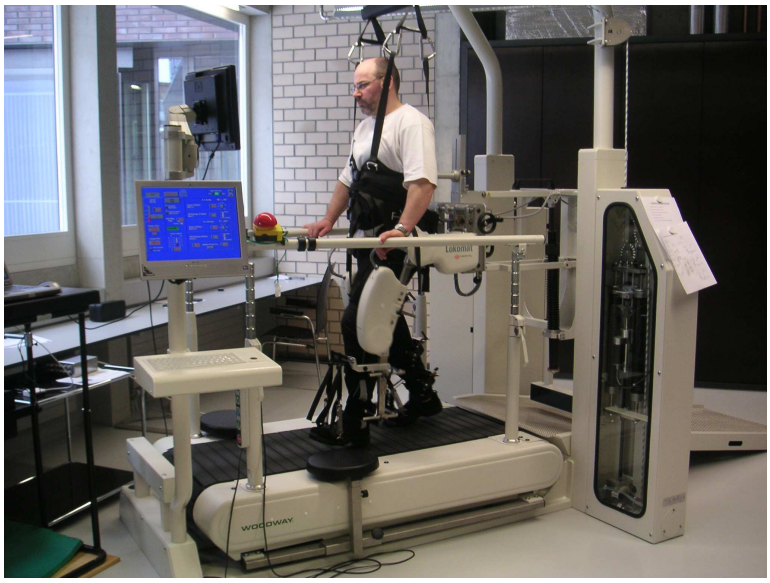

(a) The Lokomat in action.

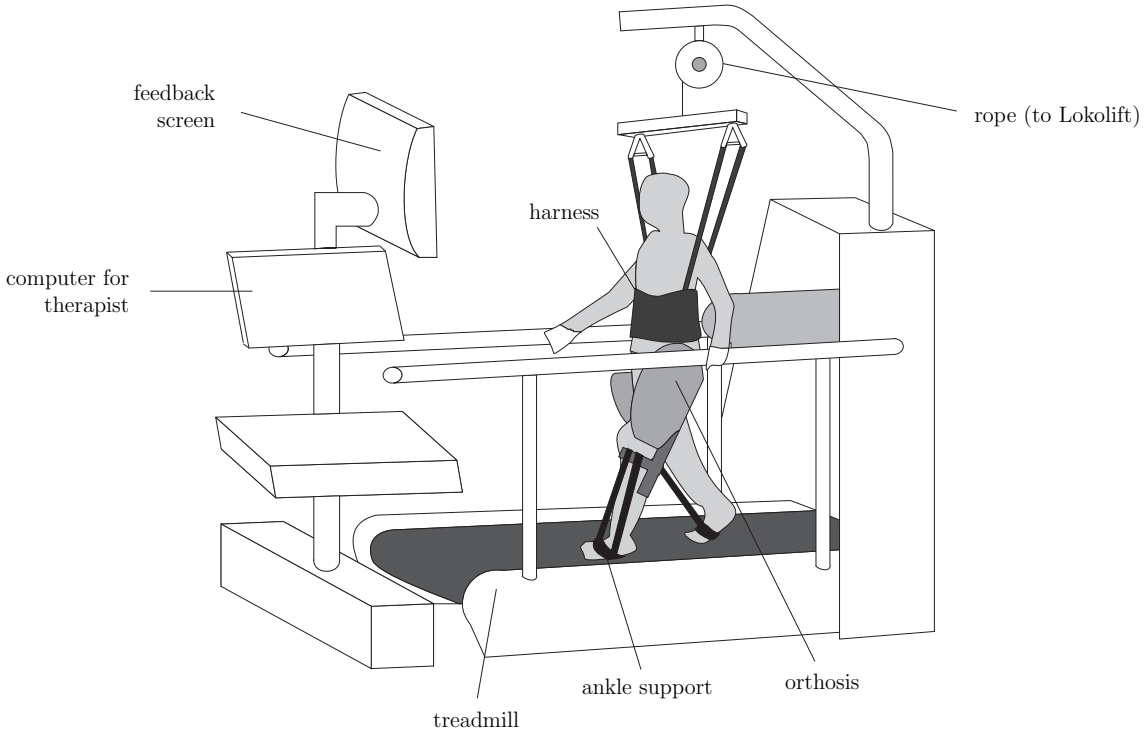

(b) Schematic of the Lokomat.

Figure 4.1: Photo and schematic of the Lokomat.

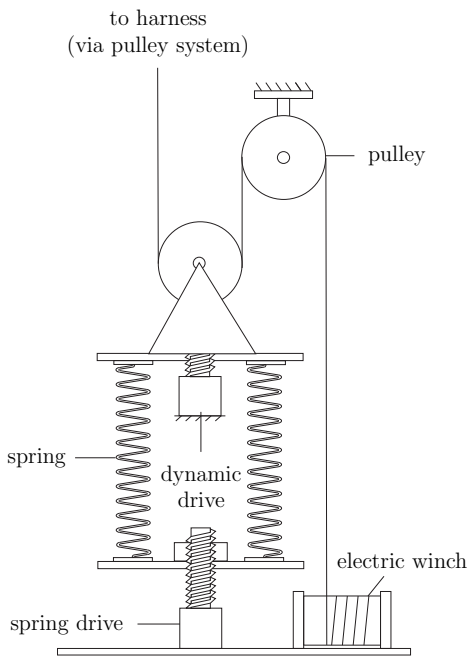

Figure 4.2: Diagram of the Lokolift System.

the force in an attempt to keep the vertical force ('unloading') on the subject constant, with the additional goal of minimising the required electrical power so that the risk of thermal overload is reduced. Simpler, static weight support systems can employ, for example, a counterweight to apply a force to a subject; however, these systems have the disadvantage of variations in the supporting force due to inertial components resulting from the movement of the counterweight [35].

Measurements of force and angular position at each joint of the orthoses were sampled at 5Hz and read into a Latitute D610 laptop computer (Dell, Austin, USA) using a USB-6009 DAQ card (National instruments, Austin, USA). MATLAB (Mathworks, Natick, USA) was the software package used for real time calculation and display.

4.3.2 Subjects

Three subjects with an incomplete spinal cord lesion were recruited. The subjects provided informed written consent prior to experimental participation. The study was approved by the Ethics Committee of Canton Luzern, Switzerland. The physical characteristics of the subjects are summarised in table 4.1.

Subject	Age (yr)	Sex	Mass (kg)	BWS (kg)	Lesion level	ASIA
S_1	41	m	102	40	T6	C
S_2	32	m	112	45	T11/12	C
S_3	42	f	70	35	T9	D

Table 4.1: Subject Details. The physical characteristics of the subject are noted along with the degree of body weight support (BWS) provided, the neurological level of the spinal cord injury and the classification of injury according to the American Spinal Cord Injury Association (ASIA) impairment scale.

4.3.3 Calculation Methods

The power contribution of the subject was derived from online measurements of force and position from the Lokomat apparatus. Figure 4.3 depicts the overall arrangement of the limb segments. Note that a limb segment discussed here refers to a combination of the robotic and human limb. These are bound to one another and have concentric joints, effectively making them a single body in the dynamics, e.g. the 'upper limb segment' refers to the combination of the subject's upper leg and the machine's upper segment. From the figure, one can see that the positions of the Lokomat's limbs are governed by the angles θ_1 and θ_2.

For the following discussion, let the length of and force developed within actuator 1 be denoted respectively as x_1 and F_1 and analogous variables be defined for actuator 2. Moreover, during the following discussion, the superscript P indicates a scenario in which the subject is passive and superscript A

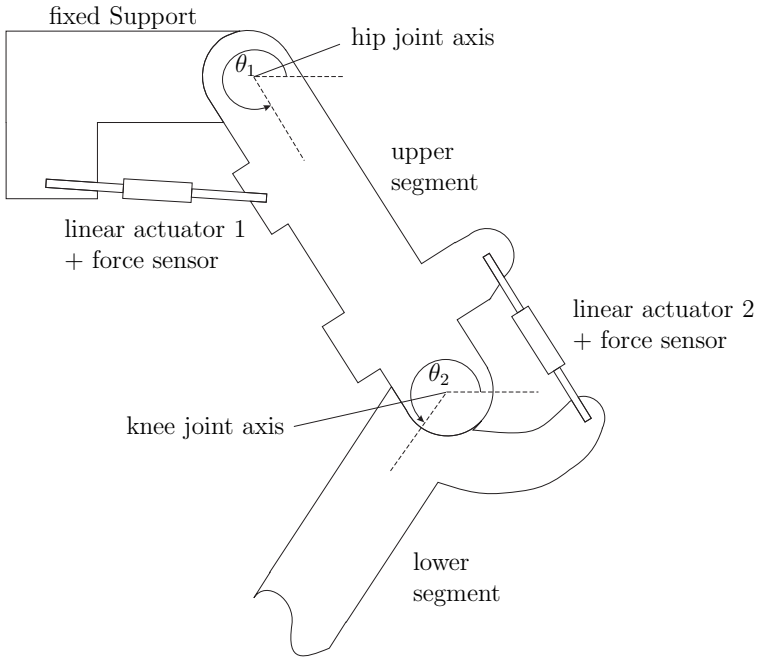

Figure 4.3: Overview of Lokomat limb geometry and placement of actuators and sensors.

refers to one in which the subject is actively contributing to the gait. During passive walking, the work done for motion is provided entirely by the linear actuators of the machine. The terms passive and active refer to idealised scenarios. In passive walking, the subject exerts as little effort towards the ambulation as possible (in the horizontal direction). Nevertheless, some level of support for the body weight in the vertical direction must be contributed by the subject in order to maintain an acceptable posture. In active walking, the subject exerts volitional forces so as to provide propulsion in the horizontal direction and in doing so effectively attempts to accelerate and decelerate the gait.

It is firstly necessary to determine the rate of supportive work done by the machine itself, W_L. The work done by each actuator for a given movement is given simply by the product of the force exerted and the change in length of the relevant actuator. This means that the total work done for infinitesimal

changes (represented by 'Δ' notation) in actuator length is, for each leg

$$\Delta W_L = F_1 \Delta x_1 + F_2 \Delta x_2. \tag{4.1}$$

These actuator lengths are dependent on the angles of the joints and therefore, using the total derivative [59]:

$$\Delta W_L = F_1 \left(\frac{\partial x_1}{\partial \theta_1} \Delta\theta_1 + \frac{\partial x_1}{\partial \theta_2} \Delta\theta_2 \right) + F_2 \left(\frac{\partial x_2}{\partial \theta_1} \Delta\theta_1 + \frac{\partial x_2}{\partial \theta_2} \Delta\theta_2 \right) \tag{4.2}$$

The work done can be partitioned into that performed on upper and lower segments to give

$$\Delta W_{L,upper} = \left(F_1 \frac{\partial x_1}{\partial \theta_1} + F_2 \frac{\partial x_2}{\partial \theta_1} \right) \Delta\theta_1 \tag{4.3}$$

$$\Delta W_{L,lower} = \left(F_1 \frac{\partial x_1}{\partial \theta_2} + F_2 \frac{\partial x_2}{\partial \theta_2} \right) \Delta\theta_2. \tag{4.4}$$

When the equations are each divided by Δt and the limit $\Delta t \to 0$ taken, the variables are transformed into work rates (i.e. power).

$$\dot{W}_{L,upper} = \left(F_1 \frac{\partial x_1}{\partial \theta_1} + F_2 \frac{\partial x_2}{\partial \theta_1} \right) \dot{\theta}_1 \tag{4.5}$$

$$\dot{W}_{L,lower} = \left(F_1 \frac{\partial x_1}{\partial \theta_2} + F_2 \frac{\partial x_2}{\partial \theta_2} \right) \dot{\theta}_2 \tag{4.6}$$

The Lokomat's trajectory is feedback controlled to follow a preset reference trajectory by the activity of the actuators. This means that irrespective of the magnitude of the subject's contribution, the net work rate during the passive and active cases is the same, i.e. the level of net work rate at a given position in the gait (given by θ_1 and θ_2) is approximately constant. Denoting the work rate of the subject during active walking as W_S^A and the work rates of the machine during passive and active walking as W_L^P and W_L^A respectively, the net work rate during passive walking is simply given by W_L^P whilst that during active walking is $W_L^A + W_S^A$.

Suppose that the muscles of the subject are now active and exert torques and forces on the upper and lower limb segments and thus do work. These work rates of the subject may be denoted $\dot{W}^A_{S,upper}$ and $\dot{W}^A_{S,lower}$ corresponding to work done on the upper and lower limb segments, respectively. However, the net rate of work done (the resultant of machine and subject work, $\dot{W}_L + \dot{W}_S$) on each segment is the same, since the motion is dynamically controlled. Using the aforementioned superscript notation, the following equations may be written for any position within the gait. The variables below all have angular positions (θ_1, θ_2) as arguments, but these are omitted for brevity.

$$\left(F_1^P \frac{\partial x_1}{\partial \theta_1} + F_2^P \frac{\partial x_2}{\partial \theta_1}\right)\dot{\theta}_1 = \left(F_1^A \frac{\partial x_1}{\partial \theta_1} + F_2^A \frac{\partial x_2}{\partial \theta_1}\right)\dot{\theta}_1 + \dot{W}^A_{S,upper} \quad (4.7)$$

$$\left(F_1^P \frac{\partial x_1}{\partial \theta_2} + F_2^P \frac{\partial x_2}{\partial \theta_2}\right)\dot{\theta}_2 = \left(F_1^A \frac{\partial x_1}{\partial \theta_2} + F_2^A \frac{\partial x_2}{\partial \theta_2}\right)\dot{\theta}_2 + \dot{W}^A_{S,lower} \quad (4.8)$$

Hence, if the forces in the actuators in the passive and active cases are known, the active work rates contributed by the subject can be determined by subtraction, i.e

$$\dot{W}^A_{S,upper} = \left(F_1^P \frac{\partial x_1}{\partial \theta_1} + F_2^P \frac{\partial x_2}{\partial \theta_1}\right)\dot{\theta}_1 - \left(F_1^A \frac{\partial x_1}{\partial \theta_1} + F_2^A \frac{\partial x_2}{\partial \theta_1}\right)\dot{\theta}_1 \quad (4.9)$$

$$\dot{W}^A_{S,lower} = \left(F_1^P \frac{\partial x_1}{\partial \theta_2} + F_2^P \frac{\partial x_2}{\partial \theta_2}\right)\dot{\theta}_2 - \left(F_1^A \frac{\partial x_1}{\partial \theta_2} + F_2^A \frac{\partial x_2}{\partial \theta_2}\right)\dot{\theta}_2. \quad (4.10)$$

These equations state that the work rates produced by the subject are given by the differences in powers contributed by the machine between passive and active cases, which is intuitively expected.

Notice that $\frac{\partial x_1}{\partial \theta_1}$ etc. correspond to moment arm definitions. The equations governing the moment arms are determined from the system geometry as depicted in figure 4.4.

Using the geometry as depicted as well as the angles θ_1 and θ_2 shown in figure 4.3, the moment arm equations can be derived:

$$\frac{\partial x_1}{\partial \theta_1} = \frac{-l_1 l_2 \sin\left(\theta_1 - \beta_1 - \beta_2\right)}{\left(l_1^2 + l_2^2 + 2 l_1 l_2 \cos\left(\theta_1 - \beta_1 - \beta_2\right)\right)^{0.5}} \quad (4.11)$$

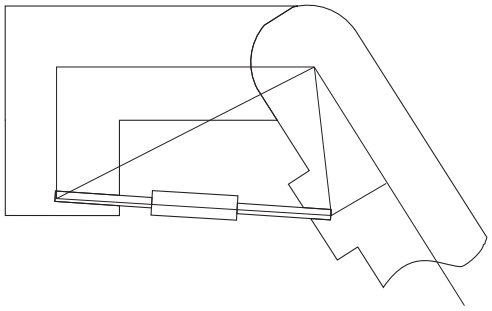

(a) Section of upper Lokomat geometry.

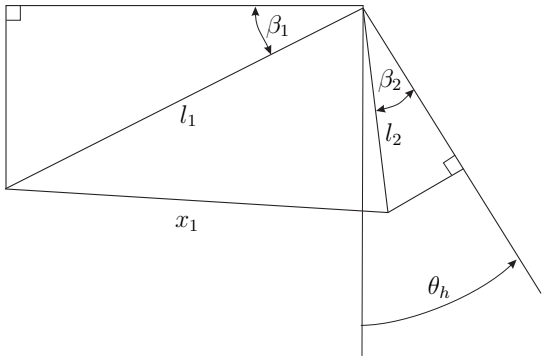

(b) Enlarged section of upper Lokomat geometry, showing trigonometric relationships and variable definition.

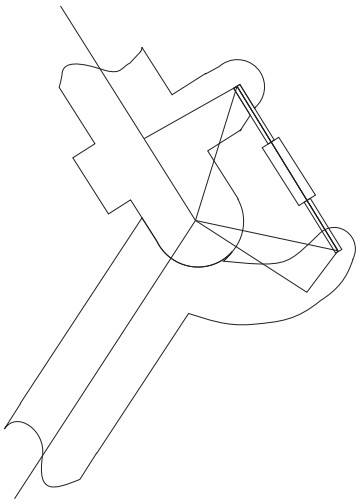

(c) Section of lower Lokomat geometry.

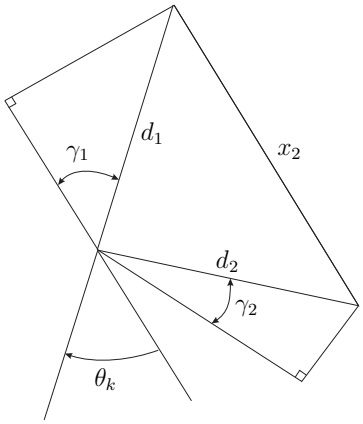

(d) Enlarged section of lower Lokomat geometry, showing trigonometric relationships and variable definition.

Figure 4.4: Diagrams for Lokomat geometry.

$$\frac{\partial x_1}{\partial \theta_2} = 0 \tag{4.12}$$

$$\frac{\partial x_2}{\partial \theta_1} = \frac{d_1 d_2 \cos(\theta_1 - \theta_2 - \gamma_1 - \gamma_2)}{(d_1^2 + d_2^2 + 2 d_1 d_2 \sin(\theta_1 - \theta_2 - \gamma_1 - \gamma_2))^{0.5}} \tag{4.13}$$

$$\frac{\partial x_2}{\partial \theta_2} = \frac{-d_1 d_2 \cos(\theta_1 - \theta_2 - \gamma_1 - \gamma_2)}{(d_1^2 + d_2^2 + 2 d_1 d_2 \sin(\theta_1 - \theta_2 - \gamma_1 - \gamma_2))^{0.5}} \tag{4.14}$$

The quantity $\frac{\partial x_1}{\partial \theta_2}$ is identically zero because F_1 from the upper actuator exerts no direct moment on the lower limb segment.

4.3.4 Angular Measurement Transformation

The quantities actually measured by the Lokomat are θ_h and θ_k which are the hip and knee joints of the Lokomat as displayed in figure 4.4. However, the angles used for the derivations here are the conventional anticlockwise angles measured from the x-axis to the limb as shown in figure 4.3.

The different angular definitions are related by

$$\theta_1 = \frac{3\pi}{2} + \theta_h \tag{4.15}$$

$$\theta_2 = \theta_1 - \theta_k \tag{4.16}$$

and the angular velocities are thus given by

$$\dot{\theta}_1 = \dot{\theta}_h \tag{4.17}$$

$$\dot{\theta}_2 = \dot{\theta}_1 - \dot{\theta}_k. \tag{4.18}$$

4.3.5 Passive Force Modelling by Fourier Series

Application of equations (4.9) and (4.10) to determine the active exercise work rates $\dot{W}_{S,upper}$ and $\dot{W}_{S,lower}$ requires knowledge of the passive forces F_1^P and F_2^P. During passive ambulation, forces are provided by the machine's actuators in order to overcome inertial and frictional effects to drive the motion in the absence of any human effort. These forces are dependent on the position within the gait cycle, and are thus functions of the angles θ_h and θ_k.

Forces from the 4 actuators of the Lokomat were recorded throughout the gait in a separate test phase in which the subjects were passively ambulated. Functions were determined that predicted the passive forces at all positions within the gait. In the discussion which follows, a real (measured) force output is denoted as F whilst a modelled force output is written as $\hat{F}$.

The form of the functions selected was the Fourier series which can be used to model periodic functions [59]. A periodic function $g(\theta)$ has repeated image values at regular intervals and therefore has the property

$$g(\theta) = g(\theta + 2\pi m). \tag{4.19}$$

Figure 4.5 provides an example of a periodic function.

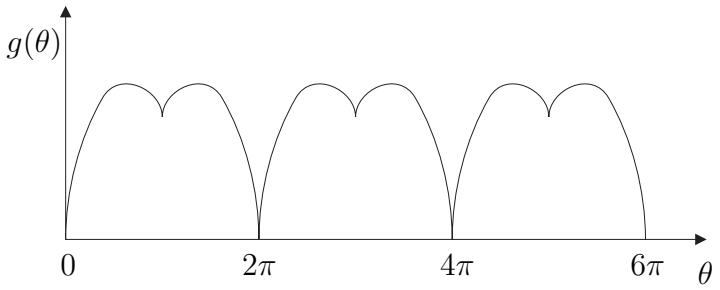

Figure 4.5: Example of a periodic function.

The Fourier series expansion of F is given by

$$\hat{F}(\theta) = \frac{1}{2}a_0 + \sum_{k=1}^{\infty} \left[a_k \cos(k\theta) + b_k \sin(k\theta)\right], \tag{4.20}$$

where, in general

$$a_k = \frac{1}{\pi}\int_0^{2\pi} F(\theta)\cos(k\theta)\, d\theta \tag{4.21}$$

$$b_k = \frac{1}{\pi}\int_0^{2\pi} F(\theta)\sin(k\theta)\, d\theta. \tag{4.22}$$

In a real approximation, a finite number of terms - giving the order n - must be used and the Fourier series approximation reduces to

$$\hat{F}(\theta, n) = \frac{1}{2}a_0 + \sum_{k=1}^{n} \left[a_k \cos(k\theta) + b_k \sin(k\theta)\right]. \tag{4.23}$$

The Fourier Series has the property that it will converge to any periodic function which satisfies a number of criteria called Dirichlet's conditions [58]. Briefly, these are that the function be bounded, and have a finite number of maxima/minima and discontinuities. Convergence implies that

$$\lim_{n\to\infty} \int_0^{2\pi} \left| F(\theta) - \hat{F}(\theta, n) \right| dt = 0. \tag{4.24}$$

An example of the convergence property is given in figure 4.6, where different orders of Fourier series are used to approximate a sawtooth function.

It is assumed that the force developed at each actuator can be represented by a linear summation of 2 Fourier series which have hip and knee angles as arguments. These Fourier series are only valid for the limited range of angles which are encountered during walking. The hip angles have a range of 0.68 radians (40 degrees) and knee angles a range of 1.07 radians (61 degrees). The form of the function for the approximation can be thus be rewritten as

$$\begin{aligned} \hat{F}^P(\theta_h, \theta_k) \;=\; & \frac{1}{2}a_0 + a_1\cos(\theta_h) + b_1\sin(\theta_h) + c_1\cos(\theta_k) + d_1\sin(\theta_k) \\ & + a_2\cos(2\theta_h) + b_2\sin(2\theta_h) + c_2\cos(2\theta_k) + d_2\sin(2\theta_k) \\ & \vdots \\ & + a_n\cos(n\theta_h) + b_n\sin(n\theta_h) + c_n\cos(n\theta_k) + d_n\sin(n\theta_k). \end{aligned} \tag{4.25}$$

The parameters a_1, b_1 etc. were optimised from experimental data by a least squares method where the term e_{LS} in equation (4.26) is minimised.

$$e_{LS} = \sum_{k=1}^{N} \left(F^P(k) - \hat{F}^P(k) \right)^2 \tag{4.26}$$

This can be solved using equation (2.14) by firstly defining the following matrices:

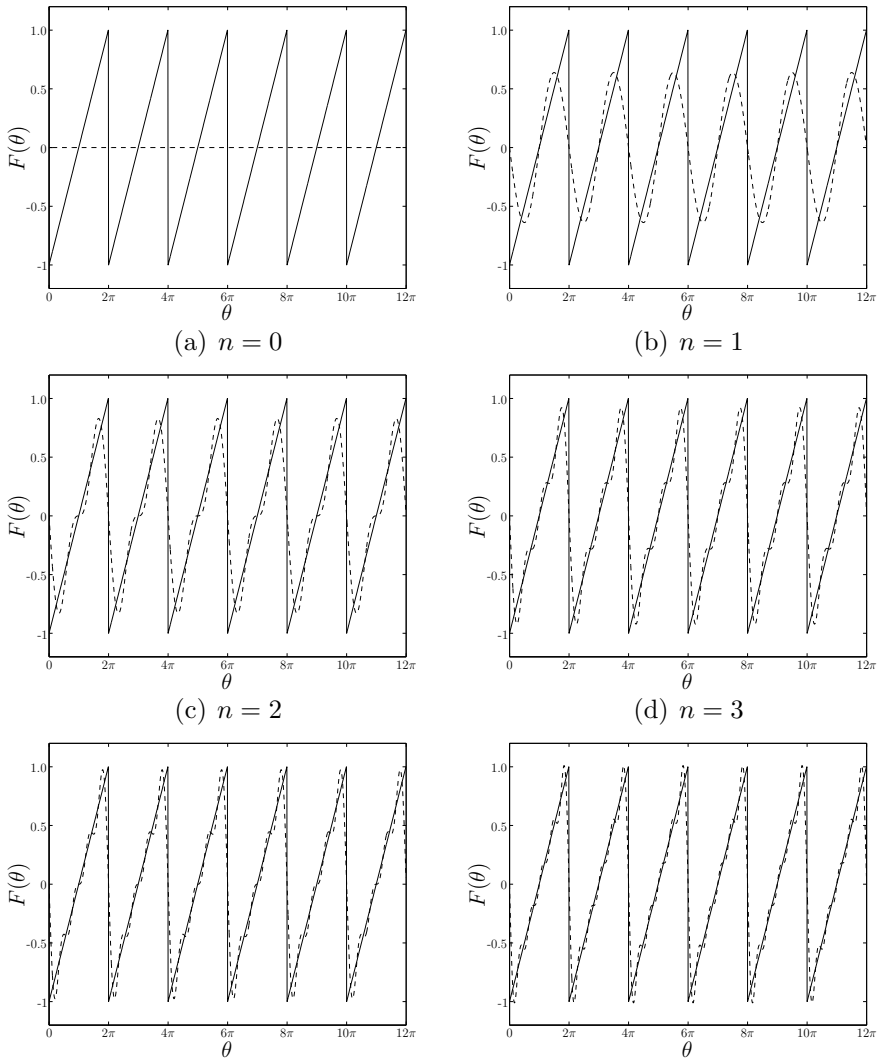

(a) $n = 0$ (b) $n = 1$

(c) $n = 2$ (d) $n = 3$

(e) $n = 4$ (f) $n = 5$

Figure 4.6: Convergence of a Fourier series approximation (dashed line) to a sawtooth function (solid line). The degree of fit increases with the order of the series, n.

$$\theta = \begin{bmatrix} a_0 \\ a_1 \\ b_1 \\ c_1 \\ d_1 \\ a_2 \\ b_2 \\ c_2 \\ d_2 \\ \vdots \\ a_n \\ b_n \\ c_n \\ d_n \end{bmatrix} \quad \varphi(i) = \begin{bmatrix} \frac{1}{2} \\ \cos(\theta_h(t_i)) \\ \sin(\theta_h(t_i)) \\ \cos(\theta_k(t_i)) \\ \sin(\theta_k(t_i)) \\ \cos(2\theta_h(t_i)) \\ \sin(2\theta_h(t_i)) \\ \cos(2\theta_k(t_i)) \\ \sin(2\theta_k(t_i)) \\ \vdots \\ \cos(n\theta_h(t_i)) \\ \sin(n\theta_h(t_i)) \\ \cos(n\theta_k(t_i)) \\ \sin(n\theta_k(t_i)) \end{bmatrix} \quad \Phi = \begin{bmatrix} \varphi(1)^T \\ \varphi(2)^T \\ \vdots \\ \varphi(N)^T \end{bmatrix} \tag{4.27}$$

A unique function was determined for each of the 4 actuator forces during passive motion.

The passive walking data was divided into two portions of equal size. The first of these was used to calculate the Fourier series functions, whilst the second was used to validate the resulting models using the fit variable of equation (2.15).

Limitations on the Fourier Series Order

The resulting functions consist of harmonic components of different frequencies. The maximal order of the Fourier series is limited by the sampling interval.

Consider a one-dimensional Fourier series problem. Again, one is interested in calculating the parameters of a function $\hat{F}$ from experimental data. Since it is necessary to take the inverse of $\phi^T\phi$, the possibility of solution depends on the rank of the matrix ϕ. The problem that arises when the order of the Fourier Series is too large for a given sampling rate is that the

columns of ϕ are not linearly independent, reducing the rank of ϕ and making $(\phi^T\phi)^{-1}$ singular, i.e. impossible to invert.

The matrix ϕ has the form:

$$\phi = \begin{bmatrix} 0.5 & \cos(x_1) & \sin(x_1) & \cos(2x_1) & \sin(2x_1) & \dots \\ 0.5 & \cos(x_2) & \sin(x_2) & \cos(2x_2) & \sin(2x_2) & \dots \\ 0.5 & \cos(x_3) & \sin(x_3) & \cos(2x_1) & \sin(2x_3) & \dots \\ \vdots & \vdots & \vdots & \vdots & \vdots & \ddots \end{bmatrix} \tag{4.28}$$

For a low sampling rate, the various columns may be identical. For example, with reference to figure 4.7, it is sometimes impossible to distinguish between different frequencies of sinusoid due to a limited sampling rate.

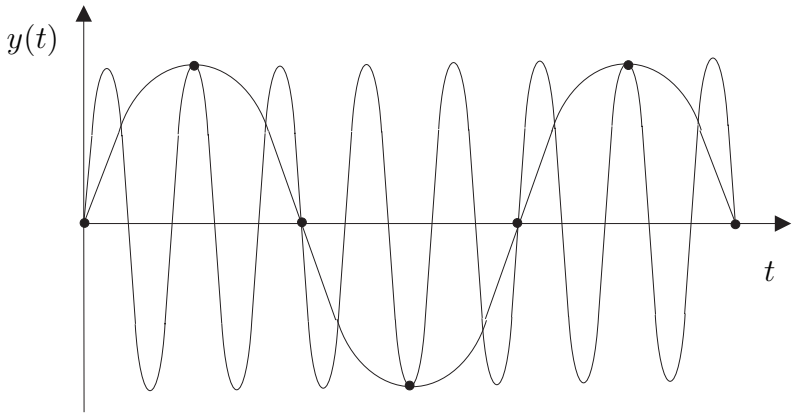

Figure 4.7: Aliasing problem. Due to an insufficient sampling rate, the sinusoids are indistinguishable from each other.

In the case of the experimental data, the matrix $\phi^T\phi$ does not actually become singular: the presence of 'noise' terms yields linear independence of the columns (so that the determinant never goes to zero) and hence a solution can be found. However, this solution is clearly nonsensical and large errors would be apparent during the validation phase.

4.3.6 Alternative Modelling Methods

The Fourier series was used to approximate the passive forces in all the Lokomat tests of this study, including the work on $\dot{V}_{O_2}$ control of Chapter 5. However, several alternative modelling methods are also possible. This section examines different possibilities for modelling the passive functions. It would be desirable to obtain functions that improve the degree of fit whilst reducing the computational demand during real time evaluation. The different methods can be contrasted by calculating the fits achieved for the various passive data sets using the different techniques.

The methods are outlined in 1-D for simplicity but the same principles may easily be extended to two dimensional models as is required for the passive force models. The various approaches are illustrated in figure 4.8.

Piecewise Linear Interpolation

An alternative to using continuous functions such as the Fourier series is to partition the data set into sub-domains and then use separate linear mappings to represent the passive forces.

The interpolation method has the following basic form:

$$\hat{F}(\theta) = \begin{cases} a_0 + b_0\theta & (\theta_0 < \theta \leq \theta_1) \\ a_1 + b_1\theta & (\theta_1 < \theta \leq \theta_2) \\ \vdots & \\ a_n + b_n\theta & (\theta_n < \theta \leq \theta_{n+1}). \end{cases} \tag{4.29}$$

Note that unlike the Fourier series, the function will generally be discontinuous at the boundaries of the various sub-domains as depicted in figure 4.8.

For each sub-domain, there is a linear function with two parameters which estimates the passive force for a given position within the gait. The method for determining the two parameters is the same least squares minimisation as used for the Fourier series and must be done for each sub-domain separately. Consequently, once the data have been obtained, they must be firstly divided

into the various sub-domains. During evaluation of the functions in real time to estimate the passive forces, the program must decide which sub-domain the angle pair belongs to, select the appropriate parameter set and then evaluate the function.

One option in linear interpolation is the way in which the data set is partitioned. It is possible to distribute the data into equal divisions, i.e. so that $(\theta_1 - \theta_0) = (\theta_2 - \theta_1) = (\theta_n - \theta_{n-1})$. This is referred to here as interpolation method I. This method has the advantage that a simple function can be used in real time to find the correct sub-domain, rather than having to 'search' through the data. For example, consider input data with a maximum value of θ_u and a minimum of θ_l with n partitions. The input θ_i will belong to the partition number equal to[2]

$$ceil\left(\frac{\theta_i}{\left\lceil\frac{\theta_u - \theta_l}{n}\right\rceil}\right). \tag{4.30}$$

Method I is disadvantageous in that the data are not evenly distributed spatially. This will lead to certain sub-domains having more data points than others during identification and therefore being more accurately represented than those with fewer points. It can also place a limit on the number of partitions since the even spacing can lead to sub-domains being created that have no data points at all within them.

One alternative - denoted here as interpolation method II - is to use an equal number of data points within each division. However, due to the uneven spatial distribution of the data, evaluation of the functions in real time can be sluggish due to the necessity of 'searching' through the data to decide on the appropriate sub-domain.

Polynomial Functions

A more simple method of representing the passive functions is to use polynomial functions. In common with the Fourier series, these have the advantage

[2] $ceil(\theta)$ is a function used in MATLAB which 'rounds the elements of θ to the nearest integers towards infinity.'

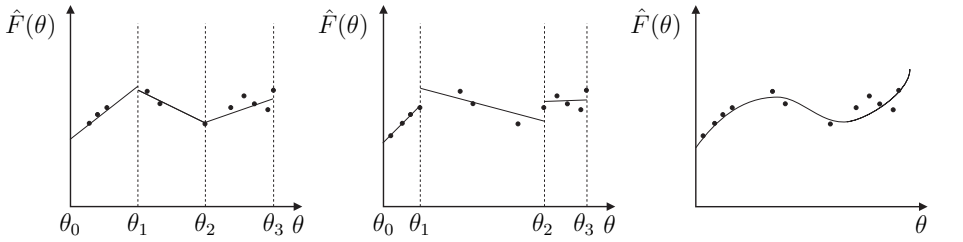

(a) Interpolation 1 (b) Interpolation II (c) Polynomial Modelling

Figure 4.8: Alternative methods of modelling the passive forces. Two methods of linear interpolation methods are illustrated along with a polynomial-based model.

that the data need not be partitioned and therefore there will not be issues with respect to accuracy across (or difficulty of solutions in) certain divisions. In one dimension, these functions are of the form

$$\hat{F}(\theta) = a_0 + a_1\theta + a_2\theta^2 + a_3\theta^3 + \ldots + a_n\theta^n \tag{4.31}$$

where n represents the order of the function.

4.3.7 Summation and Filtering

Following the approximation of the passive forces and the determination of the subject's 'active' work rates, the absolute values of the individual work rates of the four different limb segments (i.e. the upper and lower segments of the two legs) were summed together to obtain the total work rate of the subject, $\dot{W}_S$.

$$\dot{W}_S = \left|\dot{W}^A_{S,upper\ left}\right| + \left|\dot{W}^A_{S,lower\ left}\right| + \left|\dot{W}^A_{S,upper\ right}\right| + \left|\dot{W}^A_{S,lower\ right}\right| \tag{4.32}$$

Here, real time computations are performed using equations (4.9) and (4.10) in combination with moment arm equations (4.11)-(4.14), angle conversion equations (4.15)-(4.18) and the Fourier series approximation in equation (4.25).

The definition of equation (4.32) includes both positive and negative work arising respectively from concentric and eccentric muscular contractions, since both of these will cause a metabolic response and incur an energetic cost [127]. However, it is not a true measure of power in a mechanical sense.

Absolute values were used in the summation in order to avoid cancellation that could arise due to positive and negative[3] work being produced at the different limb segments. This would result in an effort on the part of the subject not being fully recognised in the work rate estimate.

Finally, the resulting summation was passed through a low-pass filter of bandwidth 1.2rad/s in order to smooth intra-gait-cycle variations. This filter has a rise time of 1.8s. Unlike the cadence variable that was controlled in the previous chapter, the (unfiltered) work rate is not a dynamic state - i.e. it is not produced by integration of the inputs to the system. As a result, the exerciser can vary his or her work rate almost instantaneously simply by producing larger forces. However, the ultimate objective of the work rate control is to influence the physiological variables such as heart rate and oxygen uptake in order to produce a training effect. These variables are not related to a power at any given instant, but rather a work rate sustained over a finite period of time i.e. an average power. It may be argued, furthermore, that it would be impossible to control an instantaneous power variable.

The filter, as the only dynamic element in the work rate estimate, effectively makes the work rate a moving average of the instantaneous power. In order to be able to influence and control the physiological variables as performed in the next chapter of this thesis, the bandwidth of the work rate control loop must be faster than the physiological response dynamics, and it is also essential that the rise time of the filter is such that the person is able to influence and regulate the filtered work rate that he is following on the screen in real time. The bandwidth of the filter was determined empirically using preliminary trials where subjects attempted to track a reference work

[3]Positive and negative work respectively correspond to actions which attempt to accelerate and decelerate the walking motion.

rate signal as done in the tests of this chapter; different parameters of filter were set between tests. Note that the properties of the filter do not affect the passive force modelling since the latter does not rely on feedback of the filtered work estimate (see figure 4.10), and consequently, the arguments of the Fourier series models are not passed through the filter.

Implications of the Use of Absolute Values

Using the modulus in the summation in equation (4.32) introduces inaccuracies into the estimate. Consider the free body diagrams of the system of figure 4.9. The system moves through infinitesmal angles $\delta\theta_1$ and $\delta\theta_2$ and during this transition work is done by the Lokomat and through the efforts of the subject. When considering each limb segment separately, work is also done by the internal forces F_r at the knee. Due to the equal and opposite nature of the forces, the net work done by this internal force to the overall multilink system is naturally zero. However, the use of the modulus causes this variable to corrupt the estimate, as demonstrated below.

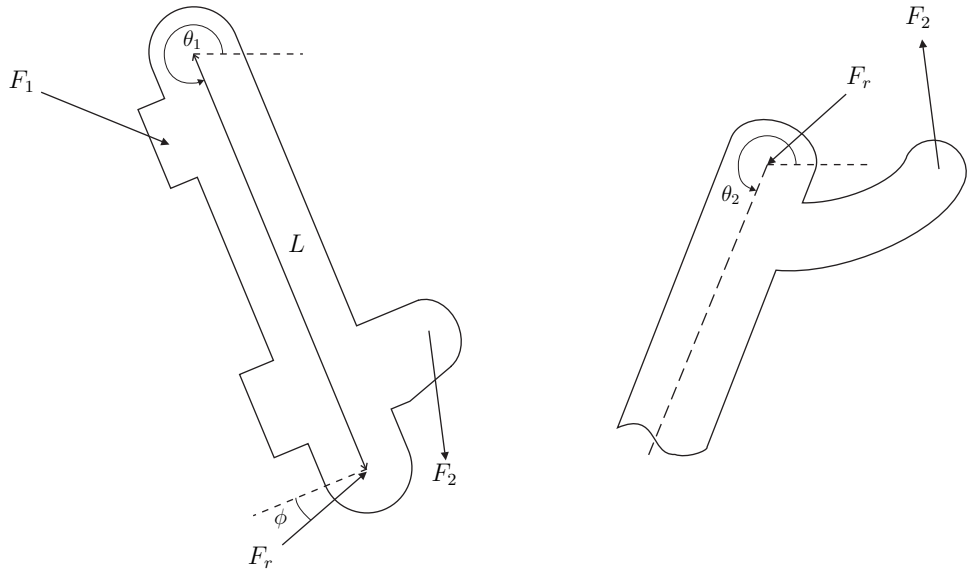

Figure 4.9: Individual free Body Diagrams of the upper and lower segments.

During passive walking, the net work rate on the upper segment is

$$\dot{W}^P_{net,upper} = F_1^P \frac{\partial x_1}{\partial \theta_1}\dot{\theta}_1 + F_2^P \frac{\partial x_2}{\partial \theta_1}\dot{\theta}_1 + F_r^P \dot{\theta}_1 L\cos\phi. \tag{4.33}$$

During active walking, the additional component of active subject work is present:

$$\dot{W}^A_{net,upper} = F_1^A \frac{\partial x_1}{\partial \theta_1}\dot{\theta}_1 + F_2^A \frac{\partial x_2}{\partial \theta_1}\dot{\theta}_1 + F_r^A \dot{\theta}_1 L\cos\phi + \dot{W}^A_{S,upper} \tag{4.34}$$

Since the trajectory of the Lokomat is controlled, the net work rate is the same between passive and active cases, and hence $\dot{W}^P_{net,upper} = \dot{W}^A_{net,upper}$.

$$\begin{aligned}\left(F_1^P \frac{\partial x_1}{\partial \theta_1} + F_2^P \frac{\partial x_2}{\partial \theta_1}\right)\dot{\theta}_1 - \left(F_1^A \frac{\partial x_1}{\partial \theta_1} + F_2^A \frac{\partial x_2}{\partial \theta_1}\right)\dot{\theta}_1 \\ = \left(F_r^A - F_r^P\right)\dot{\theta}_1 L\cos\phi + \dot{W}^A_{S,upper}\end{aligned} \tag{4.35}$$

Similarly, the equations for the lower limb are

$$\dot{W}^P_{net,lower} = F_1^P \frac{\partial x_1}{\partial \theta_2}\dot{\theta}_2 + F_2^P \frac{\partial x_2}{\partial \theta_2}\dot{\theta}_2 - F_r^P \dot{\theta}_1 L\cos\phi \tag{4.36}$$

$$\dot{W}^A_{net,lower} = F_1^A \frac{\partial x_1}{\partial \theta_2}\dot{\theta}_2 + F_2^A \frac{\partial x_2}{\partial \theta_2}\dot{\theta}_2 - F_r^A \dot{\theta}_1 L\cos\phi + \dot{W}^A_{S,lower} \tag{4.37}$$

and therefore

$$\begin{aligned}\left(F_1^P \frac{\partial x_1}{\partial \theta_2} + F_2^P \frac{\partial x_2}{\partial \theta_2}\right)\dot{\theta}_2 - \left(F_1^A \frac{\partial x_1}{\partial \theta_2} + F_2^A \frac{\partial x_2}{\partial \theta_2}\right)\dot{\theta}_2 \\ = -\left(F_r^A - F_r^P\right)\dot{\theta}_1 L\cos\phi + \dot{W}^A_{S,lower}.\end{aligned} \tag{4.38}$$

Using the work rate calculation scheme, the estimate for the total, active work rate for this leg is

$$\begin{aligned}&\left|\left(F_1^P \tfrac{\partial x_1}{\partial \theta_1} + F_2^P \tfrac{\partial x_2}{\partial \theta_1}\right)\dot{\theta}_1 - \left(F_1^A \tfrac{\partial x_1}{\partial \theta_1} + F_2^A \tfrac{\partial x_2}{\partial \theta_1}\right)\dot{\theta}_1\right| \\ + &\left|\left(F_1^P \tfrac{\partial x_1}{\partial \theta_2} + F_2^P \tfrac{\partial x_2}{\partial \theta_2}\right)\dot{\theta}_2 - \left(F_1^A \tfrac{\partial x_2}{\partial \theta_2} + F_2^A \tfrac{\partial x_2}{\partial \theta_2}\right)\dot{\theta}_2\right|\end{aligned} \tag{4.39}$$

which, according to equations (4.35) and (4.38) is equal to[4]

$$\left|\dot{W}^A_{S,upper} + \left(F_r^A - F_r^P\right) L\dot{\theta}_1\cos\phi\right| + \left|\dot{W}^A_{S,lower} - \left(F_r^A - F_r^P\right) L\dot{\theta}_1\cos\phi\right|. \tag{4.40}$$

[4]Notice that the terms involving F_r would cancel if absolute values were not taken.

In general, the internal forces F_r during passive and active walking will differ, and therefore $F_r^A - F_r^P \neq 0$. The estimate is therefore not equal to $|\dot{W}^A_{S,upper}| + |\dot{W}^A_{S,lower}|$ as would be desirable, but instead has been distorted by the use of absolute values and partitioning of work rates between the upper and lower segments.

4.3.8 Removing the Bias Term from the Work Rate

The use of absolute values also means that the estimate of the work rate is always positive. This gives a small bias/offset term during passive walking. In order to eliminate this term, the apparent work rate during passive walking $\hat{\dot{W}}^P_S$ is calculated using the estimation scheme from the N passive data samples. $\dot{W}_{offset}$ is then subtracted from the estimate when the calculation scheme is used in real time.

$$\dot{W}_{offset} = \frac{1}{N} \sum_{k=1}^{N} \hat{\dot{W}}^P_S(k) \tag{4.41}$$

4.3.9 Summary of Estimation Scheme

Figure 4.10 depicts the various stages of the active work rate estimate. The active forces of the subject are determined using the passive force approximations and used to determine the corresponding moment. These are multiplied by the angular velocities to give the work rates of the individual limbs which are then summed together using absolute values. Finally, a power offset term is removed from the estimate.

4.3.10 Feedback Control of Subject's Active Work Rate

In order to achieve the work rate profiles required for specific types of exercise test, it is necessary that the subject be able to produce a predetermined reference work rate.

The estimate of work rate as calculated by the scheme of figure 4.10 presents the opportunity of using a feedback control loop with the estimated

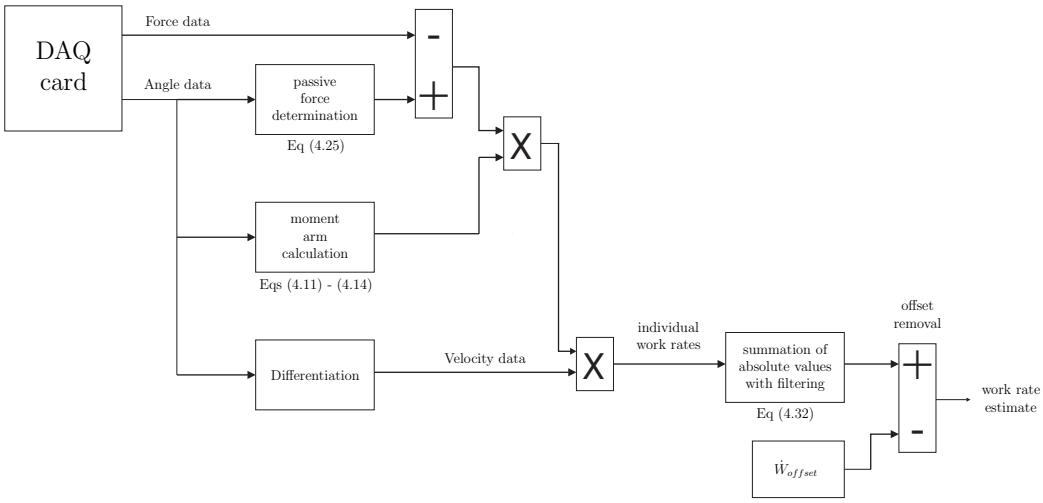

Figure 4.10: Block Diagram of overall estimation process with relevant equation numbers where appropriate.

work rate as the feedback variable. The use of feedback control enables the exercising subject to adjust their perceived level of effort so that their work rate is in accordance with a reference level. In this case, the plant to be controlled is a complex combination of the human subject and Lokomat machine. Changes in the system could arise in this case as a result of human fatigue.

The estimated work rate was displayed via computer screen to the subject along with the reference work rate signal. In this way, the person could adjust his or her perceived effort level in order to produce a work rate in accordance with a target, reference work rate. Therefore, the work rate calculation scheme played the role of an estimator in a feedback loop as depicted in figure 4.11.

Provided the target work rate is within the physical limits of the subject and that the estimation truly reflects the subject's work rate/effort, it will be possible to yield the reference power.

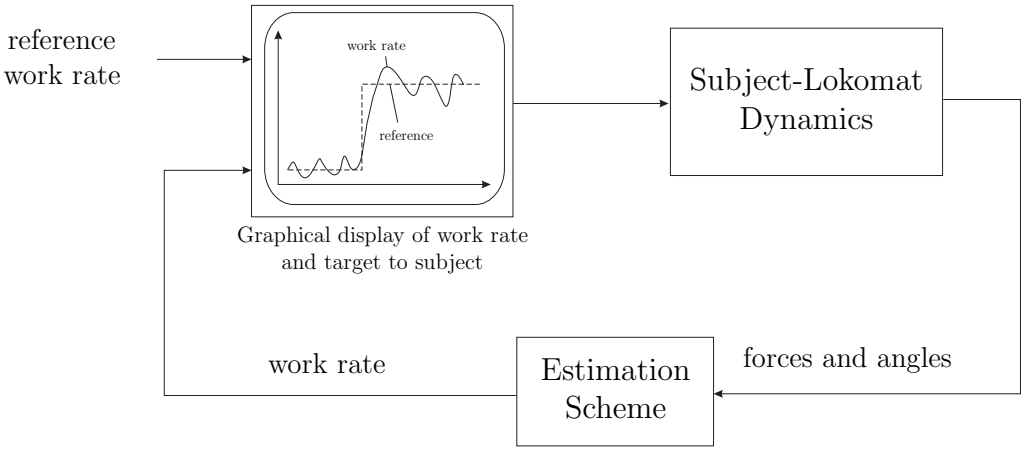

Figure 4.11: Proposed control loop for volitional control of exercise work rate, including visual feedback of estimated work rate.

4.3.11 Experimental Structure

The subjects performed two types of test in which they actively contributed: constant load tests (step exercise test, SET), and incremental load tests (incremental exercise test, IET). SETs consisted of a step transition from a work rate of zero to a pre-determined value, whilst the IETs imposed a work rate function that linearly increased with time. The two types of test yield different information about cardiopulmonary status and response as discussed in section 1.4.3. Here, the focus is on the work rate control results whilst cardiopulmonary outcomes are reported elsewhere [52, 60].

For both test types, the experimental sessions consisted of 4 distinct phases. These were, in chronological order: a rest phase where the subject simply stood in the Lokomat, a primary passive walking phase, an active walking phase, and a secondary passive walking phase. During the two passive phases, the subjects were instructed to exert effort only so as to maintain a good upright posture but not to contribute to the actual ambulation. The primary passive phase was used to calculate and assess the quality of the Fourier series functions as detailed in section 4.3.5.

The characteristics of the SETs and IETs were determined using data from maximal effort tests conducted during initial familiarisation sessions where the subjects performed brief periods of maximal volitional force production. Using this work rate data, the magnitude of the constant load during the SET was set at 40% of a given subject's maximal work rate. The gradient of the incremental work rate during the IETs was set such that the maximal work rate would be reached within approximately 10 minutes.

The experiments were conducted in the Guido A. Zäch Institut, Nottwil, Switzerland.

4.4 Results

4.4.1 Passive Function Fitting

Figure 4.12 shows an example of the accuracy achieved using different numbers of coefficients in the passive Fourier series approximations. Typically, the fit was maximised by using 4 Fourier terms in the functions. Ideally, the order of the functions would be adjusted to each individual data set. However, due to time constraints, the order of the Fourier series was set to 4, following initial testing sessions in which this was the optimal order.

In order to illustrate the quality of fit obtained for the passive force approximations, the functions from one test are presented in figure 4.13. The functions for all 4 limb segments are included, with measured and estimated forces being respectively shown as solid and dashed lines.

4.4.2 Cross Validation of Fourier Series Models

It is natural to ask whether the Fourier series parameters need be determined anew before each active testing session, since this adds to the total time required for each test and possibly also to subject discomfort. Table 4.2 shows, for each subject, the fit obtained for a particular set of passive data

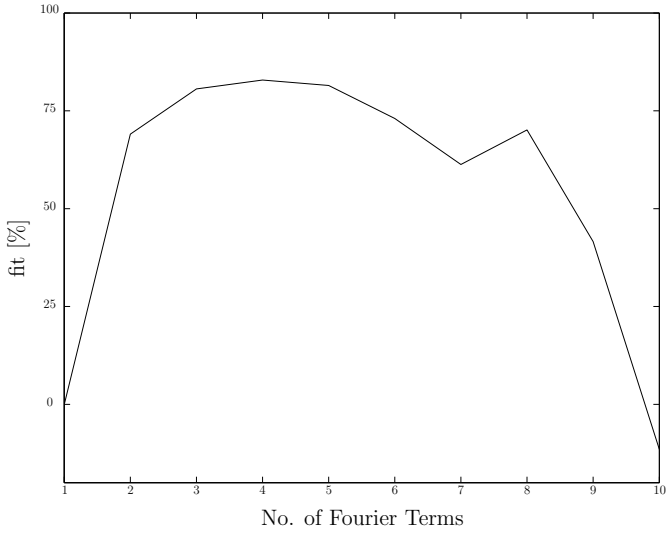

Figure 4.12: Values of fit obtained to passive data using different degrees of Fourier series. Data from the primary passive phase during the second IET of Subject S_2 were used.

using a Fourier series model (with $n = 4$) obtained from a different data set[5]. In this way, the validity of repetitively using the same model set throughout the tests could be assessed.

It is evident that using a model from a different test generally leads to a substantially lower fit than if the parameters from the same test day were used.

4.4.3 Comparison of Different Model Structures

Table 4.3 shows the degrees of fit yielded using different passive modelling structures. The maximum value of fit achieved by each is included for the various tests.

It is evident that the model structure used can have a large impact on

[5]The 'leading diagonal' elements of the tables correspond to a passive force model being used to predict the forces during passive walking of the same testing session. However, the off-diagonal fit values correspond to a particular model being used to predict the passive forces on a different day.

(a) Subject S_1.

	Model Used			
Data Set	SET 1	SET 2	IET 1	IET 2
SET 1	87.1	23.9	59.9	47.0
SET 2	7.0	52.6	43.4	59.8
IET 1	63.3	45.2	72.1	66.0
IET 2	31.5	55.0	62.8	73.4

(b) Subject S_2.

	Model Used			
Data Set	SET 1	SET 2	IET 1	IET 2
SET 1	84.3	62.3	58.9	50.3
SET 2	58.6	82.1	82.0	83.0
IET 1	56.7	77.6	77.8	77.6
IET 2	55.4	77.3	78.7	82.9

(c) Subject S_3.

	Model Used			
Data Set	SET 1	SET 2	IET 1	IET 2
SET 1	74.7	10.0	34.1	72.8
SET 2	-63.8	69.1	-80.3	-91.4
IET 1	12.0	49.7	66.4	4.4
IET 2	71.9	10.8	33.6	75.7

Table 4.2: Cross validation data. For each subject, the fit (%) values achieved using a model derived from a certain data set to approximate the passive forces in a different data set are shown. Data from the lower actuator of the left leg are used.

(a) Subject S_1.

	Model Type Used			
Data Set	Fourier	Interp. I	Interp. II	Polynomial
SET 1	87.3	79.2	87.5	87.8
SET 2	70.3	72.9	85.0	70.6
IET 1	79.7	73.4	80.4	80.0
IET 2	75.5	73.7	87.7	76.2
Average	78.2	74.8	85.2	78.7

(b) Subject S_2.

	Model Type Used			
Data Set	Fourier	Interp. I	Interp. II	Polynomial
SET 1	86.2	75.7	83.5	85.6
SET 2	82.1	79.3	86.3	82.8
IET 1	77.8	74.3	82.2	78.3
IET 2	82.9	84.0	88.9	83.2
Average	82.2	78.3	85.3	82.5

(c) Subject S_3.

	Model Type Used			
Data Set	Fourier	Interp. I	Interp. II	Polynomial
SET 1	76.1	67.0	86.8	79.7
SET 2	69.1	58.7	66.4	69.8
IET 1	66.4	62.2	52.8	67.9
IET 2	76.1	78.8	74.9	81.4
Average	71.9	66.7	70.2	74.7

Table 4.3: The maximal values of fit (%) achieved for the passive data using the different model structures are displayed. The orders of the various model types were varied and the maximum fit produced was selected from the data. Data from the upper actuator of the left leg are used.

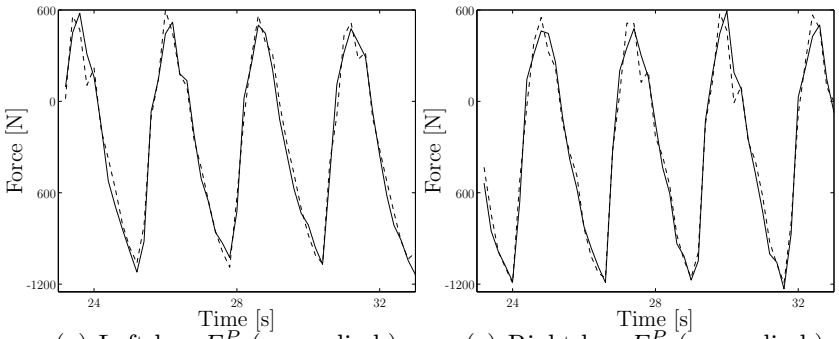

(a) Left leg, F_1^P (upper limb) (c) Right leg, F_1^P (upper limb)

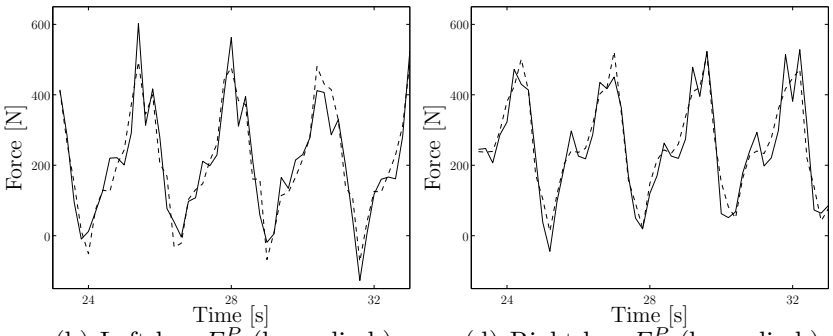

(b) Left leg, F_2^P (lower limb) (d) Right leg, F_2^P (lower limb)

Figure 4.13: Accuracy of passive force modelling for the same data as used in figure 4.12, with 4 Fourier coefficients. Each passive force recording, depicted as the solid line, is plotted with the Fourier series approximation, shown as the dashed line. A 10 second sample of the validation data for the 4 actuator forces during passive ambulation is displayed.

the level of fit attainable. Interpolation method II was optimal for subjects S_1 and S_2 but not for subject S_3 for whom the accuracies achieved by the models were generally lower.

4.4.4 Active Testing: Work Rate Results

Figure 4.14 depicts the active testing results for the 3 subjects, consisting of 2 step (SET) tests and two incremental (IET) tests for each. Measured and reference work rates are respectively included as solid and dashed lines.

It can be seen that the magnitude of the constant loads during the SETs

and gradients of reference power functions during the IETs are different between subjects. This reflects the fact that the various subjects had different combinations of physical and neurological ability. For instance, Subject S_3 performed the SET tests at a lower magnitude of active work rate than S_1 and S_2 due to relatively greater weakness.

The subjects achieved work rates close to reference values during the active phase of all the tests. However, in none of the tests does the work rate of the subject return to zero during the secondary passive phase, despite the corresponding work rates in the primary passive phase being close to zero.

4.5 Discussion

The passive functions accurately represented the forces encountered during passive walking, with the upper forces being reproduced better by the Fourier series than the lower forces. The measured lower forces demonstrated greater irregularity in form, perhaps because they are more sensitive to variations in the subject-treadmill interaction forces.

It is clear that the combination of work rate estimation and visual feedback control enabled the participants to produce effort levels close to the reference values. However, subject S_3 was not able to follow the reference work rate with as much accuracy as the other two subjects - a reflection of the relatively greater weakness of this subject and the greater levels of spasticity encountered during those tests. Moreover, the lower levels of fit achieved for the passive models of this subject resulted from the greater spasticity which increased the variance of the force measurements.

The passive power - that which the Lokomat must provide to sustain locomotion in the absence of human effort - was found to be in the region of 50W. For a reference power level of 5W, an error of 10% in the passive estimate would lead to a one hundred percent error in the apparent active power. This sensitivity to the passive calculation - resulting from the greater magnitude of machine contribution as compared to subject effort - illustrates

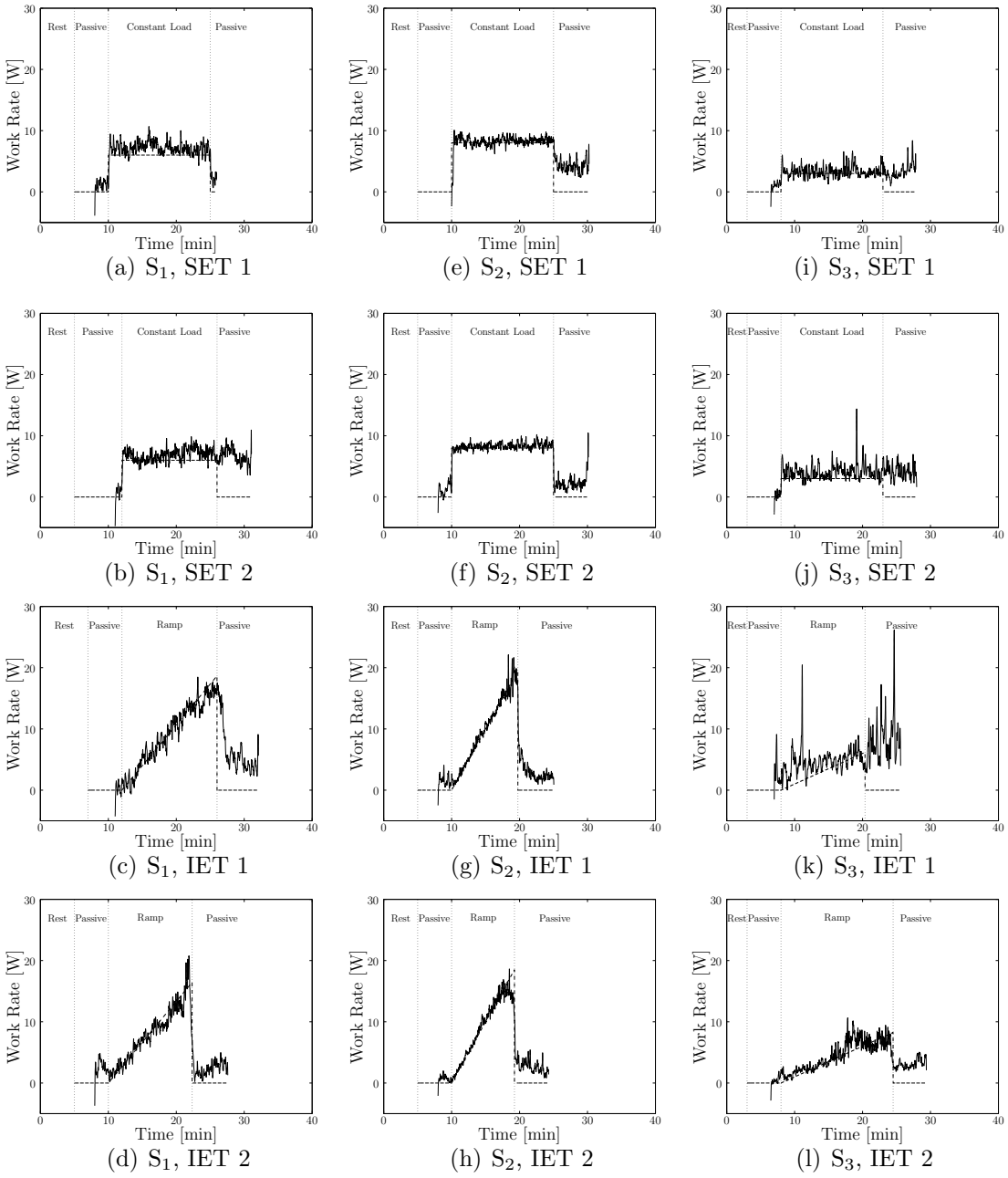

Figure 4.14: Volitional control test results: the results for each subject - 2 SET and 2 IET tests - are aligned in the 3 columns. Estimated and reference work rates are shown as solid and dashed lines, respectively.

the need for filtering or averaging in the output measurement, since small deviations and errors would otherwise lead to very large fluctuations in the reading.

As figure 4.14 shows, a common finding was that the reading of power did not return to zero in the transition from the active phase to the secondary passive walking phase at the end of the test. It is possible that this extra power arises from involuntary spasticity. Alternatively (or additionally), it may be difficult to consciously return to minimal effort compliance after such intense exercise. It could be that the subject, seeing the elevated reading, subconsciously attempted to return it to zero by resisting the motion. This would only serve to further increase the power variable resulting from the use of absolute values in equation (4.32). Therefore, it is recommended that the work rate estimate is not shown to subjects during the final passive walking phases in future tests.

The cross-validation results of figure 4.2 imply that the same passive model should not be repetitively used throughout the different tests for a subject and that a new passive model should be identified prior to each active test portion. In general, a given model will give lower values of fit when used to predict passive forces on a different test day. This results from the fact that the passive properties of the system such as the inertial elements are sensitive to the subject's exact positioning within the Lokomat which can vary slightly from test to test as the harness and straps are fitted and refitted.

The type of passive model used - i.e. Fourier series, interpolation or polynomial functions - can have a large effect on the value of fit achievable for the passive portion of walking. The fact that there is no structure giving the best fit throughout all the tests suggests that prior to active testing, the maximum values of fit achieved using each model type should be evaluated and the model yielding the best result be selected to give the best possible passive walking model.

The estimate of work rate does not take into account the work done performed in exchanges between treadmill and subject since the shear forces at the subjects' feet were not measured. The magnitude of the resulting work rates should be quantified through subsequent investigation and if necessary included in the calculation scheme. Similarly, although the body weight is partially supported, work will be done by the subject as the centre of mass moves through the vertical axis against gravity. This component of work done was also not included in the estimation method. Therefore, further investigation is required to quantify the magnitudes of these additional sources of work, and also the degree of distortion produced by using absolute values.

The power output estimate that a subject is provided with is not an instantaneous work rate but a filtered version and thus has a phase lag. The more severe the filtering, the less oscillatory the power output will appear, but this will generate a greater phase lag. This increased phase lag makes it more difficult for a subject to follow the reference since it takes longer for a given 'burst' of effort to become manifest in the reading. In an analogous feedback control scenario, a phase lag induced by a control algorithm can cause instability of the system [34]. It is clear that a compromise must be found between smoothness of signal and phase lag.

4.6 Conclusions

Through the combination of the work rate estimation algorithm, visual feedback and volitional control, the subjects produced work rates that were close to the target values.

This methodology may be used as a component in the application of robot-assisted body weight supported treadmill training in cardiopulmonary rehabilitation programmes and during assessment of cardiopulmonary parameters through exercise testing.

Chapter 5

Oxygen Uptake Rate Control During Robot-Assisted Ambulation

5.1 Introduction

Following the development of a method for work rate estimation and control during Lokomat exercise, a method for controlling the rate of oxygen uptake ($\dot{V}_{O_2}$) is developed in this chapter. A theoretical background of $\dot{V}_{O_2}$ is presented, then a feedback control system is devised and validated experimentally during ambulation of 5 able bodied subjects.

The work of this chapter has been submitted for publication:

- A. Pennycott, K.J. Hunt, S. Coupaud, D.A.B. Allan, T.H. Kakebeeke, 'Feedback control of oxygen uptake rate during robot-assisted gait', submitted to *Control Engineering Practice*.

5.2 Background

5.2.1 The Role of Oxygen in Exercise

The energy required for mechanical work during exercise comes from the chemical compound adenosine triphosate (ATP). This is synthesised from carbohydrate and fat substrates from food in a series of chemical reactions. If the exercise is aerobic[1], these ATP regeneration processses all use oxygen as a reactant, and therefore the rate of synthesis of ATP and in turn the exercise intensity may be inferred from the rate of oxygen utilisation [1].

The substrates fat and carbohydrates utilise oxygen and produce carbon dioxide in different relative quantities, and thus the ratio between them is required in addition to the rate of oxygen uptake to fully determine the rate of metabolic energy expenditure [1]. Nevertheless, $\dot{V}_{O_2}$ may be used as a guide to the physiological intensity of exercise.

[1]Aerobic and anaerobic chemical reactions are processes which respectively utilise or do not utilise oxygen as a substrate.

5.2.2 Motivation for Controlling $\dot{V}_{O_2}$

In addition to the control of mechanical variables, it is desirable to concurrently control physiological variables such as the oxygen uptake rate, $\dot{V}_{O_2}$. Such regulation would be useful both in exercise training and in exercise testing where a specific profile of oxygen uptake is normally required. Whilst $\dot{V}_{O_2}$ was chosen as the regulated variable in this work, other physiological variables are available for control such as heart rate (HR). The latter was not chosen because evidence in the literature suggests that the heart rate of complete SCI people can be blunted due to their impaired autonomic systems [3]. It is therefore possible that such a decoupled heart rate response would also be a feature of incomplete SCI subjects. Moreover, heart rate is influenced by several factors including emotional state and hydration level even amongst able-bodied people, making it difficult to use either in real-time control or as an index of exercise intensity. Therefore, it was elected to use $\dot{V}_{O_2}$ as the variable for control in this thesis.

5.2.3 Modelling of Gas Kinetics in the Literature

A substantial quantity of research has been conducted in order to determine the nature of the oxygen uptake response to exercise. The work has been mainly concerned with modelling the response to different intensities of work rate, the different phases intrinsic to the response and the presence of possible nonlinear features.

It is generally accepted that there are three separate phases of exercise; these are discussed below and depicted in figure 5.1. The first phase is often called the cardiodynamic response and is a mass effect due to the increased flow rate of pulmonary blood. A secondary cause for the change in measured uptake rate in this phase may be due to changes in the body's gas stores [122, 123].

The second phase reflects the increase in oxygen usage at the cellular level for ATP regeneration. It has been demonstrated that during the phase II

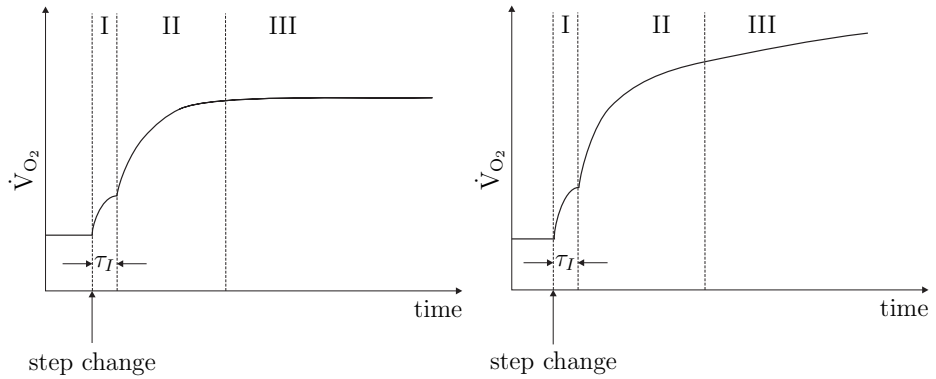

(a) Moderate Exercise (b) Heavy Exercise

Figure 5.1: Response of $\dot{V}_{O_2}$ to step changes of different intensities.

of aerobic exercise, the $\dot{V}_{O_2}$ response to a step change in work rate can be accurately represented by a decaying exponential function [1]. This phase corresponds to a change in composition of the venous blood due to increased oxygen extraction for energetic processes. Defining $\Delta\dot{V}_{O_2 ss}$ as the increase in uptake that occurs in the course of this phase and τ as a time constant, phase II has a time response of the form

$$\Delta\dot{V}_{O_2}(t) = \Delta\dot{V}_{O_2 ss}\left(1 - e^{-t/\tau}\right). \tag{5.1}$$

During phase III of aerobic exercise, a steady state level of oxygen uptake rate is reached whose value is equal to $\Delta\dot{V}_{O_2 ss}$ plus the value attained at the end of phase I. From this point onwards, the system is in equilibrium and the rate of oxygen utilisation at the cellular level for chemical reactions is equal to the rate of uptake at the lungs. In the non-steady-state condition, the rate of oxygen consumption at the cellular level cannot be determined from the rate of oxygen uptake at the nose or mouth due to transit delays between entry to the lungs and the chemical processes that follow, and also because the levels of oxygen storage in the blood are subject to change before the steady-state is established [123].

A steady state condition may not be reached in very intense exercise where

the $\dot{V}_{O_2}$ is above the anaerobic threshold, with the oxygen uptake continuing to slowly increase [122]. Some evidence points towards the presence of a second exponential term during more intense exercise [4]. Nevertheless, the characteristics of the primary, faster exponential component of equation (5.1) have been shown to be relatively independent of the work rate level, demonstrating the dynamic linearity of this component [124].

Whipp and colleagues performed step exercise tests at intensities below the anaerobic threshold in order to investigate the underlying dynamics [123]. Various structures of model were fitted to the data, incorporating elements such as separate phases and delays. The abrupt change in oxygen uptake rate during phase I as shown in figure 5.1 was more apparent in the transition from rest to sub-maximal exercise as compared to the transition from a lower intensity to the final level of the sub-maximal exercise. However, the fits achieved by the models were nevertheless improved when phase I was included in the model structure.

In addition to the effects on the $\dot{V}_{O_2}$ kinetics, the intensity of exercise also governs the production of lactate during exercise [122, 130]. Moderate exercise is characterised by the absence of a significant increase in blood lactate whilst heavy exercise produces oxygen uptake rates in excess of the lactate threshold but below the maximum lactate steady-state level (MLSS) [130]. Heavy exercise thus incurs a lactate concentration that steadily increases but eventually reaches a steady-state, in contrast to severe exercise which has a $\dot{V}_{O_2}$ above the MLSS. In this case, both oxygen uptake rate and lactate concentration levels progressively rise without reaching a steady-state condition.

The results of some studies suggest that the oxygen uptake response also has non-linear elements which would place limitations on the scope of empirical linear modelling techniques to represent the underlying dynamics. Hoffman *et al* investigated the possibility of non-linearity in the dynamics by applying work rate signals of PRBS and sinusoidal forms. Using the PRBS, the system's gains and phase shifts at various frequencies were determined

and compared to those produced by the sine-wave work rate forcing functions. If the system were linear, the gains yielded from the two tests at each frequency would be equal. The investigators found that this was the case only up to frequencies of 0.01Hz, implying that the system has non-linear elements at relatively higher frequencies of work rate. Similarly, other tests have shown that above a certain work rate, the actual oxygen uptake rate recorded exceeds that predicted from extrapolation from the relationship at moderate intensity which also suggests the presence of nonlinear elements [122, 130].

The mechanism behind the physiological regulation of $\dot{V}_{O_2}$ development remains controversial. Some research suggests that the kinetics are centrally governed by the ability of the body to deliver oxygen. For instance, links have been demonstrated between the speed of $\dot{V}_{O_2}$ response and the corresponding cardiac output response [50], providing support for the idea that the rate of mass delivery is at least partly responsible for the control mechanism. Conversely, other data suggest that the rate of utilisation in the muscles themselves is the key element of the control mechanism [130]. For example, it has been demonstrated that the dynamics of cardiac output are faster than those of $\dot{V}_{O_2}$, implying a utilisation-based control mechanism [132].

Different subjects with varying fitness will have different aerobic tolerances to exercise. Therefore, for a sufficiently high intensity of exercise, the less fit subject may require a greater length of time to reach a steady-state oxygen uptake level due to a higher prevalence of the slower exponential term [124]. Pathological conditions and age may also affect the form and parameters of the oxygen kinetics [130]. However, for exercise below the anaerobic threshold, the steady state gain in oxygen uptake during phase II, $\Delta\dot{V}_{O_2 ss}$, should be approximately constant across subjects [119].

As well as variation across subjects, the gas kinetics are also task specific meaning that the various characteristics including speed of response, limits (where the dynamics become saturated), and anaerobic threshold are dependent on the actual form of exercise used to elicit them [78, 122].

Carbon dioxide kinetics have a similar form to those of oxygen but are slower due to the larger capacitance of the blood and muscles for CO_2 storage [122].

5.3 Methods

The techniques of identification and control design to develop a $\dot{V}_{O_2}$ control system are discussed in the following sections. The basic methods described in Chapter 2 are applicable here.

5.3.1 Apparatus

The Lokomat and Lokolift as described in section 4.3.1 were again used for the tests. In addition, oxygen uptake was measured in real-time using the MetaMax 3B breath-by-breath measuring system (Cortex Biophysik GmbH, Germany). This system is comprised of a low dead-space mask, a gas analyser to measure gas composition and a turbine for measurement of volume flow rate. Prior to each test, the volume transducer was set up by means of a 3 litre syringe whilst the gas analyser was set up via 2 point calibration with atmospheric air and a reference gas of known (certified) composition.

5.3.2 Subjects

The $\dot{V}_{O_2}$ identification and control tests employed 5 able bodied subjects whose details are displayed in table 5.1. It was elected to use able bodied subjects for this initial feasibility study since the greater neurological control and physical strength of these subjects relative to incomplete spinal cord injured people would lead to more regular, predictable $\dot{V}_{O_2}$ responses and also closer following of reference work rate signals. As detailed in section 5.3.4, the volitional control aspect is critical to the overall control structure. These characteristics combined should facilitate the control of oxygen uptake rate. Success in able bodied subjects would lead the way to the more challenging

control task with incomplete spinal cord injured subjects.

Subject	Sex	Mass (kg)	BWS (kg)	Height (cm)
S_A	M	72	50	173
S_B	M	72	50	178
S_C	M	98	70	182
S_D	F	62	45	160
S_E	M	71	50	174

Table 5.1: Subject Details. The physical characteristics of the subjects are noted along with the degree of body weight support (BWS) provided.

Participants were students of the University of Glasgow and were required to have no outstanding health problems. The subjects gave their informed written consent prior to the experimentation. The study was approved by the South Glasgow and Clyde Research Ethics Committee.

5.3.3 Averaging the $\dot{V}_{O_2}$ Data

Each breath produces a $\dot{V}_{O_2}$ value and therefore the oxygen uptake data is not produced at regular intervals but rather at time instants corresponding to the end of each breath. In order to have a constant sampling rate for system identification and control, the $\dot{V}_{O_2}$ data were averaged over 20s periods such that a particular sample of the averaged data set consisted of the mean of the $\dot{V}_{O_2}$ samples of the previous 20s. Although this incurs a delay, this is short compared with the overall time scales of the underlying dynamics. The method used for real time averaging is shown in figure 5.2.

5.3.4 System Identification

The dynamic system is the same as in the previous chapter except that the $\dot{V}_{O_2}$ is now considered to be the overall output of the system. In the closed loop, the subject adjusts his level of work rate in accordance to a reference work rate signal and the varying magnitudes of work rate naturally

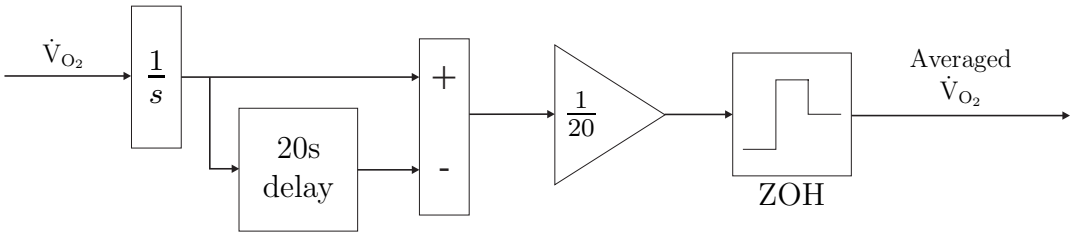

Figure 5.2: Realisation of $\dot{V}_{O_2}$ averaging in real time, incorporating integration $\left(\frac{1}{s}\right)$, a delay and a zero order hold (ZOH) block.

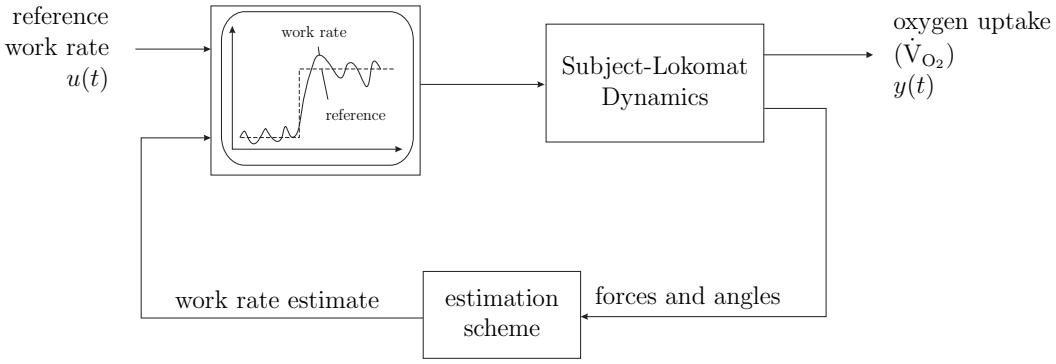

Figure 5.3: The underlying dynamic system (plant). The outputs of the system are the work rate and oxygen uptake rate ($\dot{V}_{O_2}$) both of which respond to the reference work rate input. The subject's volitional control efforts form an integral part of the plant.

also produce different levels of $\dot{V}_{O_2}$ as the exercise intensity changes. The volitional control aspect, where the subject takes on the role of the (inner loop) controller, is therefore an integral part of the system dynamics and successful $\dot{V}_{O_2}$ control relies on accurate volitional work rate regulation on the part of the subject. The resulting dynamic system which is effectively the plant of the $\dot{V}_{O_2}$ control loop is shown in figure 5.3.

A $\dot{V}_{O_2}$ response was elicited from the system using a PRBS reference work rate input signal. The PRBS was set such that the longest time between a change in work rate levels was approximately equal to the expected rise

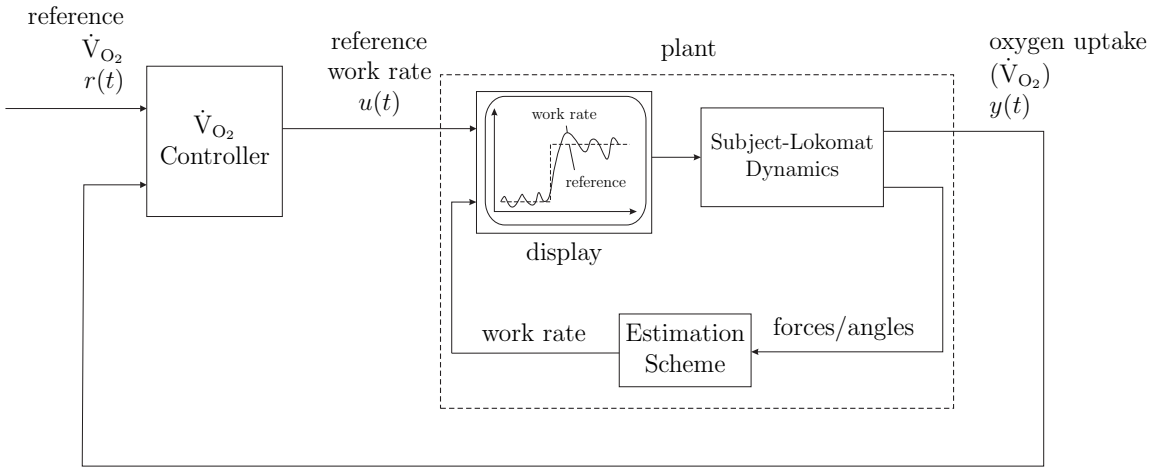

Figure 5.4: Proposed feedback system for control of $\dot{V}_{O_2}$. The system output of oxygen uptake rate ($\dot{V}_{O_2}$) responds to a given reference work rate. A controller is developed which adjusts the level of reference work rate and thereby yields the desired $\dot{V}_{O_2}$.

time of the underlying system. In this way, the input signal would contain frequency components close to the dominate modes of the system. Following data collection, ARX models of various orders were determined using the Ident tool of MATLAB and these were assessed using the fit criterion of equation (2.15).

5.3.5 Control Design

The overall control structure for $\dot{V}_{O_2}$ is shown in figure 5.4 whilst the nominal closed loop structure is that of figure 2.6. The controller varies the reference work rate such that the intensity of exercise yields the desired, reference $\dot{V}_{O_2}$. In the inner loop, the subject is constantly adjusting his level of effort so that the reference work rate is met. It is clear, therefore, that the success of the overall control loop depends on the ability of the subject to match the reference work rate via the volitional feedback control method described in the previous chapter.

The control polynomials were determined by pole placement as detailed

in chapter 2. The control polynomial A_m was assigned a rise time of 200s and damping factor of 0.9, whilst the observer polynomial A_o was set to have a rise time of 50s and damping factor of 0.9. The sampling time is set by the averaging period of 20s, giving 10 samples per closed loop rise time.

It was decided to use the same polynomials for all the tests across all subjects. Therefore, R, S and T were always the same polynomials based on a single model from one of the subjects' identification tests. The model with the best fit from all the tests was chosen. In this way, the robustness of performance and stability of the system could be experimentally verified. In addition, in the eventual application of the controller in exercise testing and training, it may not be practical to identify a separate model and synthesise new control polynomials for each subject due to time constraints and it is therefore useful to examine the feasibility of using a single controller for all subjects.

5.3.6 Experimental Structure

Each subject underwent 3 separate testing sessions. The first enabled the various straps and harness of the Lokomat to be fitted to the individual participants and also allowed the subjects to be familiarised with the Lokomat and experimental concepts. Each person performed Lokomat walking and practised following a reference work rate signal, and also performed brief periods of maximal exertion in the Lokomat so that their individual maximal work rates could be determined.

The second test was used to collect the system identification data and consisted of three distinct phases. The first two phases were respectively the rest and passive phases as described in section 4.3.11. The rest phase was used to collect baseline $\dot{\mathrm{V}}_{\mathrm{O}_2}$ data whilst the measurements from the passive phase were used to calculate the parameters of the work rate estimation algorithm (i.e. the coefficients of the Fourier series). During the final phase, the reference work rate was varied as a PRBS and the corresponding $\dot{\mathrm{V}}_{\mathrm{O}_2}$ was recorded. The levels of the PRBS corresponded to 25% and 50% of the

given subject's maximal work rate as noted from the first testing session.

Following the offline determination of the identified models and calculation of the control polynomials, the third experimental session was used to test the closed loop control system in real time. Again, the tests consisted of 3 phases, with the first 2 being the rest and passive phases as before. The controller was activated during the last portion of the passive phase where the reference $\dot{V}_{O_2}$ was set to the value of oxygen uptake measured during the passive phase of the identification test, and thus the reference work rate outputs of the controller were close to zero during initial controller activation. In the active walking portion, the reference $\dot{V}_{O_2}$ was set as a square-wave signal whose levels were selected such that the resulting reference work rates set by the controller would not exceed the levels encountered during the identification test of that subject. The reference work rate displayed and demanded of the subject was limited (using a saturation block as in figure 2.9) to be between 0 and 50% of a given subject's maximal work rate.

The various phases of the identification and control tests are shown in figure 5.5. All the tests of this chapter were conducted in the Spinal Injuries Unit of the Southern General Hospital, Glasgow, UK.

5.4 Results

5.4.1 Identification

The identification data for each subject are presented in figure 5.6. Measured data are shown as solid lines and the outputs as simulated by a first order model (arx111) are included as dashed lines for the validation data sets in order to illustrate the accuracy achieved by the modelling for the different subjects. The data are shown as deviations from steady state levels of $\dot{V}_{O_2}$ (see section 2.2.2).

The quality of fit achieved for subjects S_A, S_C and S_E using different model orders is shown in table 5.2. Settings of $k = 1$ or $k = 2$ led to a much greater fit than for $k = 3$ or $k = 4$. As the order of A increases

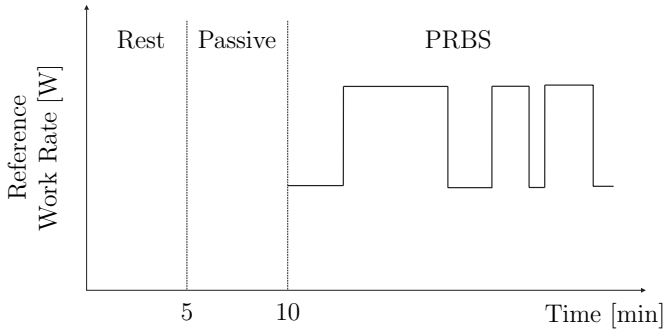

(a) Identification test structure

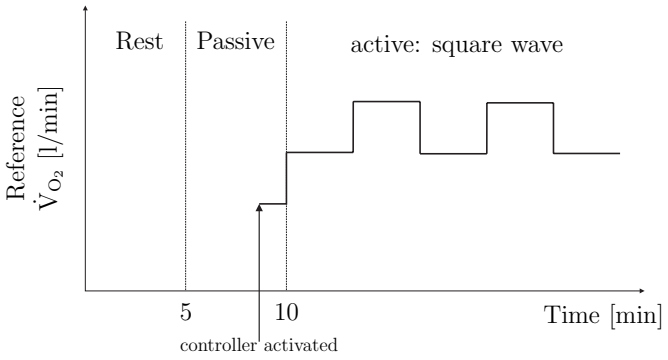

(b) Control test structure

Figure 5.5: Format of $\dot{V}_{O_2}$ identification and control tests.

from 1 to 2, the fit generally increased but the degrees of fit achieved for the different subjects varied considerably. The fit values for S_B and S_D were mostly negative and therefore the identified models for these subjects were very poor representations of the underlying dynamics of these subjects and their results are not included in the table. These poor fits can nonetheless be seen in the validation data sets of these two subjects in figure 5.6.

Since it is desirable to have a low order of model for control design, the arx111 model of subject S_A given by equation (5.2) was selected for control synthesis. The increase in fit yielded from using higher order models was small.

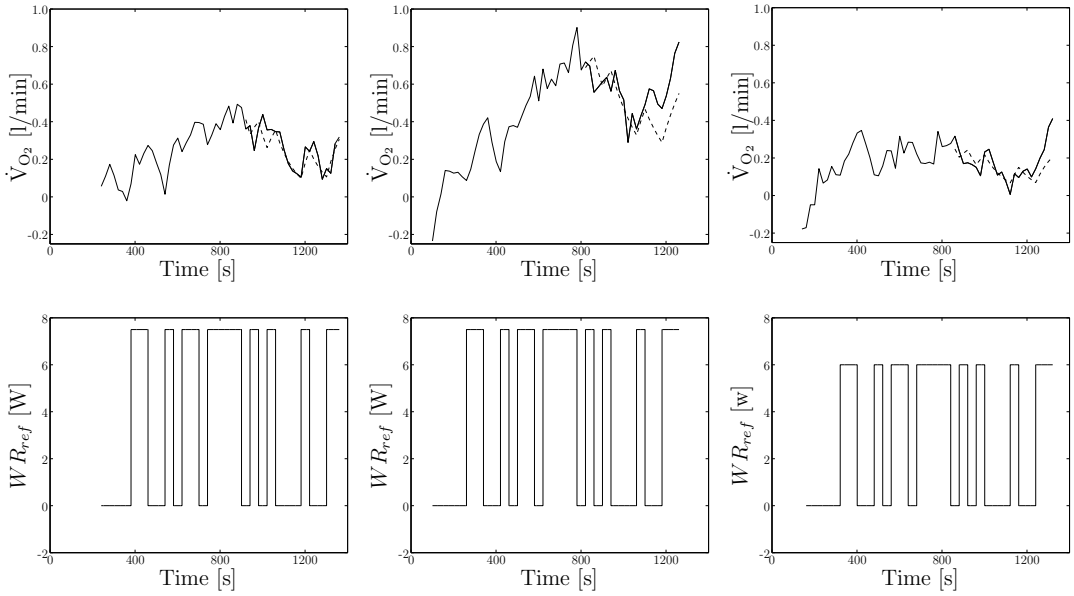

(a) Subject S_A (b) Subject S_B (c) Subject S_C

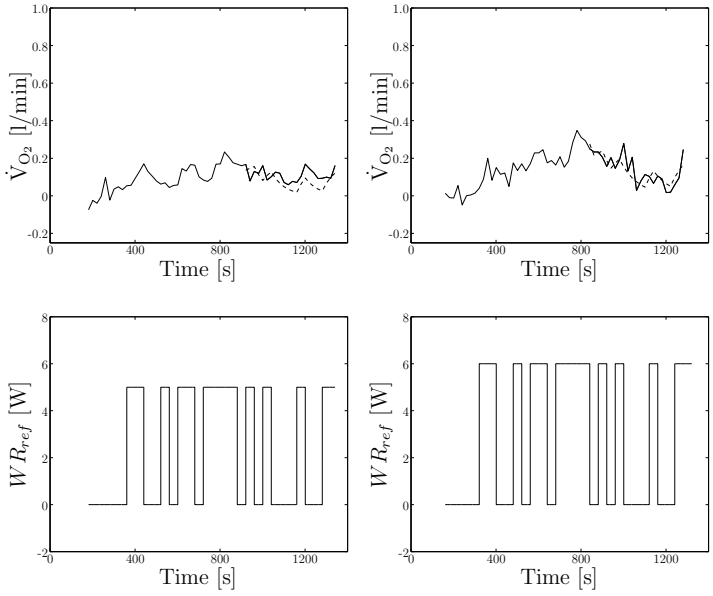

(d) Subject S_D (e) Subject S_E

Figure 5.6: Experimental identification test results. For each subject, the oxygen uptake rate ($\dot{V}_{O_2}$) outputs are shown along with the work rate inputs, with measured data being shown as solid lines. For the validation data, the simulated outputs of the arx111 models are included as dashed lines.

	Subject		
Model	S_A	S_C	S_E
arx111	42.5	16.5	35.1
arx112	33.2	16.4	35.1
arx113	11.6	-	27.8
arx114	6.1	-	21.7
arx211	44.2	16.9	26.4
arx212	40.3	19.0	34.4
arx213	11.8	-	8.7
arx214	3.8	-	1.1
arx311	45.1	17.1	26.2
arx312	45.8	17.5	30.1
arx313	11.7	-	9.5
arx314	-	-	3.3
arx411	52.5	16.2	19.2
arx412	46.8	17.0	18.6
arx413	7.6	-	-
arx414	-	-	-

Table 5.2: Values of fit (%) achieved using different model orders for subjects S_A, S_C and S_E. The model structures are indexed according to the number of coefficients of A and B - respectively n_a and $n_b + 1$ - and the value of the delay, k. Therefore arxABC is an ARX model with $(n_a, n_b{+}1, k) = (A, B, C)$.

$$y(t) = \frac{0.01127q^{-1}}{(1 - 0.8602q^{-1})}u(t) + \frac{1}{(1 - 0.8602q^{-1})}d(t) \tag{5.2}$$

5.4.2 Control Polynomials

The time domain design requirements yielded the following control (A_m) and observer (A_o) polynomials:

$$A_m(q^{-1}) = 1.0000 - 1.5283q^{-1} + 0.5933q^{-2} \tag{5.3}$$
$$A_o(q^{-1}) = 1.0000 - 0.6160q^{-1} + 0.1239q^{-2} \tag{5.4}$$

The control polynomials were calculated as:

$$R(q^{-1}) = 1.0000 - 1.4602q^{-1} + 0.5457q^{-2} - 0.0855q^{-3} \tag{5.5}$$
$$S(q^{-1}) = 15.6230 - 12.6916q^{-1} \tag{5.6}$$
$$T(q^{-1}) = 5.7711 - 3.5549q^{-1} + 0.7152q^{-2} \tag{5.7}$$

5.4.3 Nominal Stability and Robustness

The vector margin of the closed loop system for subject S_A was computed to be 0.84 which is above the recommended minimum value of 0.5 [9]. Nyquist plots of the nominal closed loop systems for subjects S_A, S_C and S_E are displayed in figure 5.7 Here, the control polynomials in equations (5.5)-(5.7) are used along with the models computed for each individual subject. The plots of S_B and S_D are not included because their low values of fit reveal that these models are not reliable representations of the subjects' $\dot{V}_{O_2}$ dynamics, and therefore their corresponding Nyquist plots would not be a useful guide to robustness. The Nyquist plots for the closed loop systems of subjects S_C and S_E reveal that these nominal systems are stable and indeed have even greater vector margins than the system of subject S_A.

Table 5.3 shows the vector margins of various nominal closed loop systems of subject S_A, where different orders of model are used as the plant and for

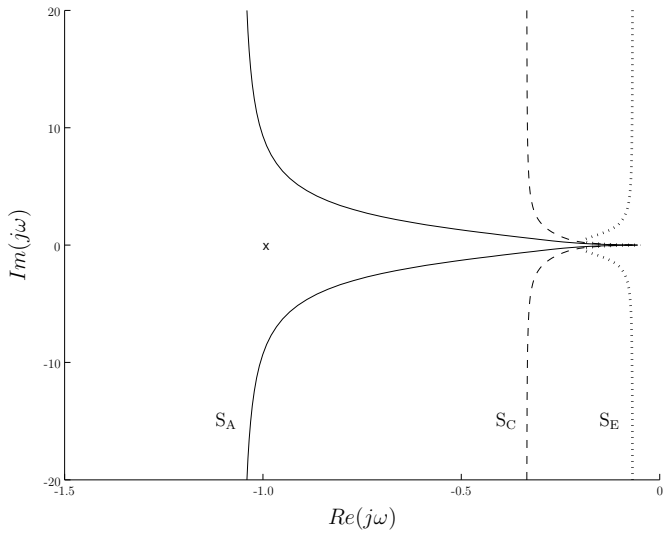

Figure 5.7: Nyquist plots for the closed loop systems using the control polynomials in equations (5.5)-(5.7) and the identified model for a given subject in order to illustrate the nominal stability and robustness yielded by using the same control polynomials (R, S and T) for each subject. The plots corresponding to the systems of subjects S_A, S_C and S_E are shown respectively as solid, dashed and dotted lines.

model	arx111	arx211	arx311	arx411
vector margin	0.80	0.29	0.47	0.46

Table 5.3: Vector margins for nominal closed loop systems of subject S_A, based on different orders of model. Each nominal system consists of the model combined with the control polynomials derived from it in the configuration of figure 2.6.

control polynomial calculation. The arx111-based system has an appreciably larger vector margin than the nominal closed loops based on higher orders of model.

5.4.4 Feedback Control Testing

Figure 5.8 shows the results of the closed loop control tests. The measured, reference and ideal $\dot{V}_{O_2}$ responses are respectively included as solid, dashed and dotted lines. The ideal response is that specified in terms of rise time and damping factor in the pole placement routine. In this case, the ideal response has a rise time of 200s, a damping factor of 0.9 and zero steady state error. Beneath each $\dot{V}_{O_2}$ plot, the corresponding work rate results are shown, with the estimated work rates plotted as solid lines and reference work rates as dashed lines. The $\dot{V}_{O_2}$ outputs tend towards the reference values and in each case closely follow the ideal responses as specified by the pole placement routine.

5.5 Discussion

The identification procedure yielded dynamic models of different orders for each subject, each representing the $\dot{V}_{O_2}$ response to a given reference work rate input for that participant. The quality of the fits achieved for the different subjects is highly variable. One possible reason for this is that subjects S_B and S_D - for whom relatively lower fits were achieved - were subject to

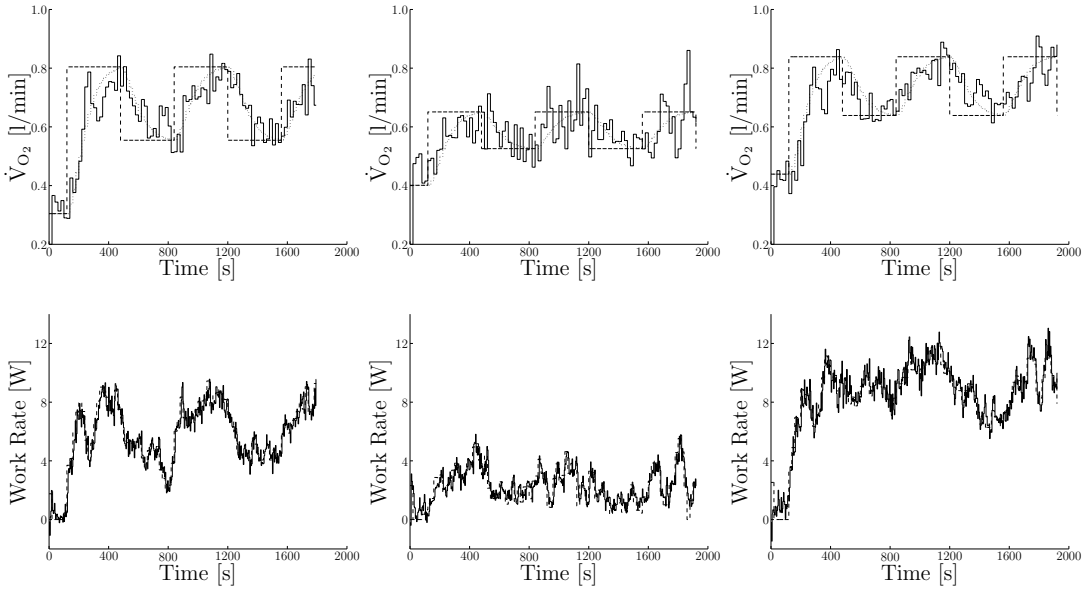

(a) Subject S_A (b) Subject S_B (c) Subject S_C

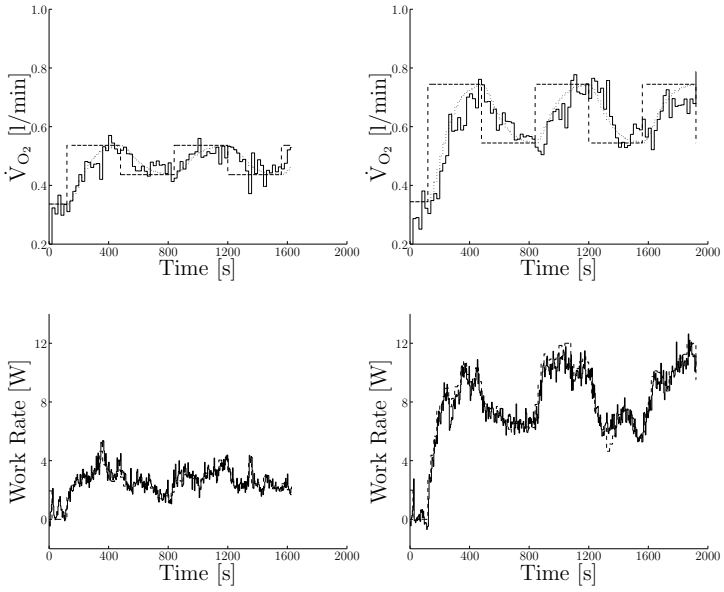

(d) Subject S_D (e) Subject S_E

Figure 5.8: Experimental control test results. For each subject, the oxygen uptake rate ($\dot{V}_{O_2}$) results are shown along with the work rate data. The measured, reference and ideal $\dot{V}_{O_2}$ responses are drawn as solid, dashed and dotted lines. The measured and reference work rates are shown as solid and dashed lines.

greater levels of discomfort during ambulation and this was reflected in the $\dot{V}_{O_2}$ measurement (i.e. due to hyperventilation).

The time period of approximately 200s to reach a steady state $\dot{V}_{O_2}$ found for the models of S_A, S_C and S_E is comparable to values reported in the literature for other modes of exercise [122].

The durations of the estimation and validation data sets are relatively short. Since the total time for each test can be limited by subject discomfort, it may be better in future to conduct several identification tests for each person and then use different combinations of these for parameter calculation and validation as performed in the identification procedure of Hunt [51], as opposed to partitioning the data from individual testing sessions as done here.

The proposed approach to real-time $\dot{V}_{O_2}$ control was demonstrated to be feasible, with the resulting closed loop structure showing acceptable robustness of performance and stability properties. A stable response was elicited from each subject using the same control polynomials. Moreover, the $\dot{V}_{O_2}$ output signal, although noisy, tends towards the desired reference values and follows the ideal response in each case.

It is clear that the robustness characteristics of the resulting closed-loop system are important due to uncertainty and errors in the models of the underlying dynamics. The fit achieved during the identification process was relatively low, indicating a high degree of uncertainty in the model. The Nyquist plots for the nominal systems suggest that the closed-loop structures corresponding to the various subjects are nominally stable with vector margins in excess of the recommended value of 0.5. Moreover, although the control polynomials were based on the dynamics of subject S_A, the quality of reference tracking is not discernably different across subjects, indicating a satisfactory robustness of performance of the system. The slightly lower fit of the arx111 structure used in control synthesis as compared to the higher order models is offset by the higher vector margin of the nominal closed loop

given by the lower order arx111 model. Moreover, it is normally considered advantageous to develop control polynomials of low order and this is facilitated by using a low order of model.

The work rate reference signals respond so as to give the desired $\dot{V}_{O_2}$ output in each case; however, the responses appear to be sensitive to the noise corruption $n(t)$. This sensitivity could be reduced by incorporating a pre-filter adjacent to the input $r(t)$ as described in section 2.3.10 and [51]. The decoupling can reduce the sensitivity of the control output $u(t)$ to the noise and thereby smooth its response.

The proposed control concept and structure are therefore feasible for use with able bodied subjects. However, control of $\dot{V}_{O_2}$ with neurologically impaired subjects gives rise to additional challenges due to the decreased capacity for control and range of work rates that may be produced. Moreover, as a result of their altered autonomic nervous system physiology, it can be seen that spinal cord injured subjects often produce complex $\dot{V}_{O_2}$ responses that may be difficult to model [52]. Indeed, it may be necessary to base the control polynomials for each subject on models of their individual $\dot{V}_{O_2}$ dynamics rather than use the same controller across subjects as done here.

5.6 Conclusions

The proposed identification and control methodology achieved $\dot{V}_{O_2}$ responses in close accordance with desired outputs and ideal responses, and produced closed loop systems with satisfactory robustness of stability and performance characteristics for each subject.

The feasibility of the approach has thus been demonstrated for able bodied subjects. Further testing is required to validate the approach with spinal cord injured participants, a task which will impose additional difficulties in both the identification and control design stages.

Chapter 6

Conclusions and Further Work

In this thesis, methods of estimation and control have been applied to two separate exercise applications: paediatric FES cycling and robot-assisted treadmill walking. These are designed for different groups of people, but have the common aim of improving the physical condition and reducing the severity of the secondary health complications faced by their potential users. The conclusions and outlook of each application are now presented separately.

6.1 Paediatric FES Cycling

An angular velocity controller has been developed which enables a predetermined cadence to be produced during paediatric FES cycling, even in the face of disturbances and system changes due to fatigue. The control structure is used in conjunction with cycling hardware especially adapted for children with an SCI, and can be used in a test bed and as a training apparatus for paediatric FES cycling. The controller meets the performance characteristics and has demonstrated satisfactory robustness properties.

In addition to this cadence control, it may be desirable to concurrently control the power (work rate) during cycling. This can be realised by varying the intensity of stimulation in a feedback loop. The problem then becomes one of multivariable control but has already been accomplished in adult FES cycling [108].

Following this additional technological implementation, the next step for paediatric FES cycling will be to verify its efficacy with respect to increasing the physical capacities of children with an SCI, and also its potential for reducing the severity of the secondary health conditions caused by long periods of immobilisation. To this end, a longitudinal study is currently being carried out at Shriners Hospital for Children in Philadelphia.

Methods for improving the efficiency of the cycling should also be developed. The low levels of efficiency during FES cycling lead to rapid fatigue which limits the duration of exercise and also poses difficulties for outdoor, mobile cycling where additional disturbances such as wind and gradients may

be present.

The transfer of FES cycling from the laboratory to the outdoor environment may be important since it can provide a more pleasant and interesting environment for the participants and thus help to maintain their motivation and enthusiasm for the training. The use of the electric motor will facilitate this transfer but a new controller must be synthesised for the outdoor application due to the considerable differences in the underlying dynamic systems inherent to stationary and mobile cycling.

One avenue of FES research has focused on exploiting a nonlinear property of muscle called the catch effect [125]. Under this principle, the force contribution from two pulses of FES in quick succession is greater than the force that would be produced by superposition of the force responses from the 2 individual pulses. Therefore, variations in the frequency of the pulse trains of FES can have an impact on the power output, and this may have potential in reducing the stimulation intensity required for a given force/torque output and therefore may help to reduce fatigue. However, only limited data is currently available for the application of the new pulse trains within the specific activity of FES cycling. Test protocols aimed at optimising the form of stimulation train used would therefore be helpful in improving efficiency, reducing fatigue and in the transfer from static to mobile cycling where higher forces are required.

6.2 Robot-Assisted Gait

A method for estimating, in real time, the level of work rate being produced by a subject during robot-assisted gait has been developed and incorporated into a feedback system which drives the subject's work rate to desired levels via biofeedback. The combined estimation and control approach enables the subject to produce work rate levels that closely follow predetermined reference levels which is essential for exercise testing applications and is also a useful way of ensuring a sufficient intensity of exercise during gait training.

However, the work rate estimate remains noisy and this can make the volitional control aspect more difficult. Rather than measure the forces and angular velocities at the actuators to calculate work done, it may be possible to reduce the noise by calculating the power contributions of the Lokomat machine in a more direct way, using the voltages and currents delivered to the electric motors of the Lokomat and calculating the power from these measurements.

The magnitude of the work done against/by the treadmill during active ambulation should be quantified. This will require additional hardware to measure the shear forces between the treadmill and the feet of the exercising subject. The work rate estimation algorithm must clearly be augmented to include this contribution to work done should its magnitude prove substantial.

Other forms of biofeedback implementation may be investigated. The current feedback is provided in the form of a graph; however, other forms of implementation such as an animation-based feedback display may be more effective, especially for children with an incomplete spinal cord injury.

The control of $\dot{V}_{O_2}$ during robot-assisted gait has been demonstrated to be feasible for able bodied subjects. This can be used in exercise testing to produce, for example, a $\dot{V}_{O_2}$ output of linear form in order to estimate the anaerobic threshold from breath-by-breath data. Moreover, the $\dot{V}_{O_2}$ control can be used to elicit a desired level of $\dot{V}_{O_2}$ during training programmes to ensure that the exercise intensity is of optimal level in order to yield cardiovascular improvements.

The ultimate use of the $\dot{V}_{O_2}$ control concept would be found in the cardiovascular rehabilitation of incomplete spinal cord injured people, and therefore the next step of research should be to test the control approach using subjects from this group. This may prove more difficult due to the more irregular $\dot{V}_{O_2}$ dynamic responses seen in this group and their generally poorer volitional control of work rate.

In common with FES cycling, the clinical benefits of the Lokomat with

respect to increasing physical status and improving fitness should also be investigated in detail. The capacity of the Lokomat as a training device and also as a tool for exercise testing should be assessed and compared with existing exercise platforms such as arm cranking ergometry. Various outcome measures are applicable to assess the efficacy of the technology as a training tool, including changes induced in the force-producing capacity (strength) of the lower limbs, peak oxygen uptakes of subjects and bone mineral density.

Bibliography

[1] P.O. Astrand, K. Rodahl, and H.A. Dahl. *Textbook of Work Physiology - Physiological Bases of Exercise*. McGraw-Hill, 1986.

[2] K. J. Åström and B. Wittenmark. *Computer-Controlled Systems: Theory for the User*. Prentice Hall, 2^{nd} edition, 1990.

[3] T. Barstow, E. Scremin, C.F. Mutton, and T. G. Kunkel. Gas exchange kinetics during functional electrical stimulation in subjects with spinal cord injury. *Medicine & Science in Sports & Exercise*, 27(9), 1995.

[4] T.J. Barstow and P.A. Molé. Linear and nonlinear characteristics of oxygen uptake kinetics during heavy exercise. *Journal of Applied Physiology*, 71(6):2099–2106, 1991.

[5] W.A. Bauman, R.H. Adkins, A.M. Spungen, R. Herbert, C. Schechter, D. Smith, B.J. Kemp, R. Gambino, P. Maloney, and R.L. Waters. Is immobilization associated with an abnormal lipoprotein profile? Observations from a diverse cohort. *Spinal Cord*, 37(7):485–493, 1999.

[6] K. BeDell, E. Scremin, K.L. Perell, and C.F. Kunkel. Effects of functional electrical stimulation-induced lower extremity cycling on bone density of spinal cord-injured patients. *American Journal of Physical Medicine and Rehabilitation*, 75(1):29–34, 1996.

[7] A. Behrman and S. Harkema. Locomotor training after human spinal cord injury: a series of case studies. *Physical Therapy*, 80(7):688–700, 2000.

[8] Y. Bhambhani. Physiology of wheelchair racing in athletes with spinal cord injury. *Sports Medicine*, 32(1):23–51, 2002.

[9] Kwakernaak H. Bosgra, O.H. *Notes for a course of the Dutch Institute of Systems and Control: winter term 1999-2000.*

[10] M.-P. Bougenot, N. Tordi, A.C. Betik, X. Martin, D. Le Foll, B. Parratte, J. Lonsdorfer, and J.D. Rouillon. Effects of a wheelchair ergometer training programme on spinal cord-injured persons. *Spinal Cord*, 41(8):451–456, 2003.

[11] L.N. Burkett, J. Chisum, W. Stone, and B. Fernhall. Exercise capacity of untrained spinal cord injury individuals and the relationship of peak oxygen uptake to level of injury. *Paraplegia*, 28(8):512–521, 1990.

[12] W.P. Castelli. Epidemiology of coronary heart disease: The Framingham study. *The American Journal of Medicine*, 76(2A):4–12, 1977.

[13] M. Castro, D. Apple, E. Hillegass, and G. Dudley. Influence of complete spinal cord injury on skeletal muscle cross-sectional area within the first 6 months of injury. *European Journal of Applied Physiology and Occupational Physiology*, 80:373–378, 1999.

[14] M.F. Cawley. *The Child With A Spinal Cord Injury*, chapter Incomplete Spinal Cord Injury. The American Academy of Orthopaedic Surgeons, 1996.

[15] J.J. Chen, N.Y. Yu, D.G. Huang, B.T. Ann, and G.C. Chang. Applying fuzzy logic to control cycling movement induced by functional electrical stimulation. *IEEE Transactions on Rehabilitation Engineering*, 5(2):158–169, 1997.

[16] B. Cirak, S. Ziegfeld, V.M. Knight, D. Chang, A.M. Avellino, and C.N. Paidas. Spinal injuries in children. *Journal of Pediatric Surgery*, 39(4):607–612, 1997.

[17] R.M. Crameri, A. Weston, M. Climstein, Davis. G.M., and J.R. Sutton. Effects of electrical stimulation-induced leg training on skeletal muscle adaptability in spinal cord injury. *Scandinavian Journal of Medicine and Science in Sports*, 12(5):316–322, 2002.

[18] M. Dalyan, D.D. Cardenas, and B. Gerard. Upper extremity pain after spinal cord injury. *Spinal Cord*, 37(3), 1999.

[19] G. Davis, F. Servedio, R. Glaser, S. Gupta, and A. Suryaprasad. Cardiovascular responses to arm cranking and FNS-induced leg exercise in paraplegics. *Journal of Applied Physiology*, 69(2):671–677, 1990.

[20] D.C.L. de Carvalho and A Cliquet. Energy expenditure during rest and treadmill gait training in quadriplegic subjects. *Spinal Cord*, 43:658–663, 2005.

[21] A.E. De Ruz, E.G. Leoni, R. Herruzo, and R.H. Cabrera. Epidemiology and risk factors for urinary tract infection in patients with spinal cord injury. *Journal of Urology*, 164(4):1285–1289, 2000.

[22] M.J. DeVivo. Causes and costs of spinal cord injury in the United States. *Spinal Cord*, 35(12):809–813, 1997.

[23] D. Ditor, M. Kamath, M. MacDonald, J. Bugaresti, N. McCartney, and A. Hicks. Effects of body-weight supported treadmill training on heart rate variability and blood pressure variability in individuals with spinal cord injury. *Journal of Applied Physiology*, 98(4):1519–1525, 2005.

[24] B. Dobkin. Functional rewiring of brain and spinal cord after injury: the three Rs of neural repair and neurological rehabilitation. *Current Opinion in Neurology*, 13(6):655–659, 2000.

[25] J. Doke, J.M. Donelan, and A.D. Kuo. Mechanics and energetics of swinging the human leg. *The Journal of Experimental Biology*, 208(3):439–455, 2005.

[26] S. Dorgan and M. O'Malley. A nonlinear mathematical model of electrically stimulated skeletal muscle. *IEEE Transactions on Rehabilitation Engineering*, 5(2):179–194, 1997.

[27] P. Eser, E.D. de Bruin, I. Telley, H.E. Lechner, H. Knecht, and E. Stüssi. Effect of electrical stimulation-induced cycling on bone mineral density in spinal-cord injured patients. *European Journal of Clinical Investigation*, 33(5):412–419, 2003.

[28] P. Eser, A. Frotzler, Y. Zehnder, L. Wick, H. Knecht, J. Denoth, and H. Schiessl. Relationship between the duration of paralysis and bone structure: a pQCT study of spinal cord injured individuals. *Bone*, 34(5):869–880, 2004.

[29] G. Exner and F.-W. Meinecke. Trends in the treatment of patients with spinal cord lesions seen within a period of 20 years in German centres. *Spinal Cord*, 35(7):415–419, 1997.

[30] P. Faghri, R. Glaser, and S. Figoni. Functional electrical stimulation leg cycle ergometer exercise: training effects on cardiorespiratory responses of spinal cord injured subjects at rest and during submaximal exercise. *Archives of Physical Medicine and Rehabilitation*, 73(11):1085–1093, 1992.

[31] E.C. Field-Fote. Combined use of body weight support, functional electric stimulation, and treadmill training to improve walking ability in individuals with chronic incomplete spinal cord injury. *Archives of Physical Medicine and Rehabilitation*, 82(6):818–824, 2001.

[32] C. Fornusek, G.M. Davis, P.J. Sinclair, and B. Milthorpe. Development of an isokinetic functional electrical stimulation cycle ergometer. *Neuromodulation*, 7(1):56–64, 2004.

[33] H.L. Frankel, J.R. Coll, S.W. Charlifue, G.G. Whiteneck, B.P. Gardner, M.A. Jamous, K.R. Krishnan, I. Nuseibeh, G. Savic, and P. Sett. Long-term survival in spinal cord injury: a five year investigation. *Spinal Cord*, 36(4):266–274, 1998.

[34] G.F. Franklin, J.D. Powell, and A. Emami-Naeini. *Feedback Control of Dynamic Systems*. Prentice Hall, 3^{rd} edition, 2002.

[35] M. Frey, G. Colombo, M. Vaglio, R. Bucher, M. Jörg, and R. Riener. A novel mechatronic body weight support system. *IEEE Transactions on Neural Systems and Rehabilitation Engineering*, 14(3):311–321, 2006.

[36] J. Galvez and D. Reinkensmeyer. Robotics for gait training after spinal cord injury. *Topics in Spinal Cord Injury Rehabilitation*, 11(2):18–33, 2005.

[37] M. Gföhler, T. Angeli, T. Eberharter, P. Lugner, W. Mayr, and C. Hofer. Test bed with force-measuring crank for static and dynamic investigations on cycling by the means of functional electrical stimulation. *IEEE Transactions on Neural Systems and Rehabilitation Engineering*, 9(2):169–179, 2001.

[38] M. Gföhler and P. Lugner. Dynamic simulation of FES-cycling: influence of individual parameters. *IEEE Transactions on Neural Systems and Rehabilitation Engineering*, 12(4):398–405, 2004.

[39] R. Glaser, S. Figoni, S. Hooker, M. Rodgers, A. Ezenwa, B. Suryaprasad, S. Gupta, and T. Mathews. Efficiency of FNS leg cycling ergometry. In *IEEE Engineering in Medicine and Biology Society* 11^{th} *Annual International Conference*, 1989.

[40] H. Gollee and K.J. Hunt. Nonlinear modelling and control of electrically stimulated muscle: a local model network approach. *International Journal of Control*, 68(6):1259–1288, 1997.

[41] G. Grimby, C. Broberg, I. Krotkiewska, and M. Krotkiewski. Muscle fibre composition in patients with traumatic cord lesion. *Scandinavian Journal of Rehabilitation Medicine*, 8:37–42, 1976.

[42] D. Grundy and A. Swain. *ABC of Spinal Cord Injury*. BMJ Publishing Group, 4^{th} edition, 2002.

[43] J.A. Haisma, L.H.V. van der Woude, H.J. Stam, M.P. Bergen, T.A.R. Sluis, and J.B.J. Bussmann. Physical capacity in wheelchair-dependent persons with a spinal cord injury: a critical review of the literature. *Spinal Cord*, 44:642–652, 2006.

[44] A. Hartkopp, H. Brønnum-Hansen, A.M. Seidenschnur, and F. Biering-Sørensen. Survival and cause of death after traumatic spinal cord injury: a long-term epidemiological survey from Denmark. *Spinal Cord*, 35(2):76–85, 1997.

[45] B.L. Hicken, J.D. Putzke, and J.S. Richards. Bladder management and quality of life after spinal cord injury. *American Journal of Physical Medicine and Rehabilitation*, 80(12):916–922, 2001.

[46] A.L. Hicks, M.M. Adams, K.M. Ginis, L. Giangregorio, A. Latimer, S.M. Phillips, and N. McCartney. Long-term body-weight-supported treadmill training and subsequent follow-up in persons with chronic SCI: effects on functional walking ability and measures of subjective well-being. *Spinal Cord*, 43:291–298, 2005.

[47] M.D. Hoffman. Cardiorespiratory fitness and training in quadriplegics and paraplegics. *Sports Medicine*, 3(5):312–330, 1986.

[48] M. Hopman, A. J. Dallmeijer, G. Snoek, and L.H.V. van der Woude. The effect of training on cardiovascular responses to arm exercise in individuals with tetraplegia. *European Journal of Applied Physiology*, 74(1-2):172–179, 1996.

[49] T. G. Hornby, D. Campbell, D. Zemon, and J. Kahn. Clinical and quantitative evaluation of robotic-assisted treadmill walking to retrain ambulation after spinal cord injury. *Topics in Spinal Cord Injury Rehabilitation*, 11(2):1–17, 2005.

[50] R.L. Hughson and M.A. Morrissey. Delayed kinetics of $\dot{V}o_2$ in the transition from prior exercising. Evidence for O_2 transport limitation of $\dot{V}o_2$ kinetics: a review. *International Journal of Sports Medicine*, 4(1):31–39, 1990.

[51] K. J. Hunt, O. Ajayi, H. Gollee, and L. Jamieson. Feedback control of oxygen uptake during treadmill exercise. *IEEE Transactions on Control Systems Technology*, 2007. In press.

[52] K. J. Hunt, L. P. Jack, A. Pennycott, C. Perret, M. Baumberger, and T. H. Kakebeeke. Control of work-rate-driven exercise facilitates cardiopulmonary training and assessment during robot-assisted gait in incomplete spinal cord injury. *Biomedical Signal Processing and Control*, 2007. To appear.

[53] K.J. Hunt, M. Rothe, T. Schauer, A. Ronchi, and N.O. Negaard. Automatic speed control in FES cycling. In *Proceedings of the* 6^{th} *Annual Conference of IFESS*, 2001.

[54] K.J. Hunt, B. Stone, N.O. Negard, T. Schauer, M.H. Fraser, A.J. Cathcart, C. Ferrario, S.A. Ward, and S. Grant. Control strategies for integration of electric motor assist and functional electrical stimulation in paraplegic cycling: utility for exercise testing and mobile cycling. *IEEE Transactions on Neural Systems and Rehabilitation Engineering*, 12(1):89–101, 2004.

[55] J. F. Israel, D. D. Campbell, J. H. Kahn, and T. G. Hornby. Metabolic costs and muscle activity patterns during robotic- and therapist-assisted treadmill walking in individuals with incomplete spinal cord injury. *Physical Therapy*, 86(11):1466–1478, 2006.

[56] P.L. Jacobs and M.S. Nash. Exercise recommendations for individuals with spinal cord injury. *Sports Medicine*, 34(11):727–751, 2004.

[57] R.P. Jaime, Z. Matjačć, and K.J. Hunt. Paraplegic standing supported by FES-controlled ankle stiffness. *IEEE Transactions on Neural Systems and Rehabilitation Engineering*, 10(4):239–248, 2002.

[58] G. James. *Advanced Modern Engineering Mathematics*. Addison-Wesley, 2^{nd} edition, 1999.

[59] G. James. *Engineering Mathematics*. Addison-Wesley, 3^{rd} edition, 2000.

[60] L.P. Jamieson. *Development and Assessment of Novel Methods of Exercise Testing During Treadmill Gait in Incomplete Spinal Cord Injury*. PhD thesis, University of Glasgow, 2007.

[61] G.C. Jang, J.J. Chen, C.T. Shih, and T.C. Huseh. Design of FES-cycling system and its stimulation patterns. *Chinese Journal of Medical Biological Engineering*, 13(4):305–316, 1993.

[62] T. Janssen, A.J. Dallmeijer, D. Veeger, and L.H.V. van der Woude. Normative values and determinants of physical capacity in individuals with spinal cord injury. *Journal of Rehabilitation Research & Development*, 39(1):29–39, 2002.

[63] S. Jezernik. Controlling the human-robot interaction for robotic rehabilitation of locomotion. In 7^{th} *International Workshop on Advanced Motion Control*, 2002.

[64] S. Jezernik, G. Colombo, T. Keller, H. Frueh, and M. Morari. Robotic Orthosis Lokomat: a rehabilitation and research tool. *Neuromodulation*, 6(2):108–115, 2003.

[65] S. Jezernik, R.G.V. Wassink, and T. Keller. Sliding mode closed-loop control of FES: controlling the shank movement. *IEEE Transactions on Biomedical Engineering*, 51(2):263–272, 2004.

[66] T.E. Johnston, R.R. Smith, B.T. an Betz, M.J. Mulcahey, and J.J. McCarthy. Implanted functional electrical stimulation for upright mobility in pediatric spinal cord injury: a follow-up report. In *Proceedings of the* 28^{th} *Annual Northeast Bioengineering Conference*, 2002.

[67] R.E. Kleiger, J.P. Miller, J.T. Bigger, and Moss A.J. Decreased heart rate variability and its association with increased mortality after acute myocardial infarction. *The American Journal of Cardiology*, 59(4):256–262, 1987.

[68] L. Ljung. *System Identification: Theory for the User*. Prentice Hall, 1987.

[69] L. Ljung and Söderström. *Theory and Practice of Recursive Identification*. The MIT Press, 1983.

[70] J.P. Lubicky and R.R. Betz. *The Child With A Spinal Cord Injury*, chapter Spinal Deformity in Children and Adolescents After Spinal Cord Injury. The American Academy of Orthopaedic Surgeons, 1996.

[71] L. Lünenburger, G. Colombo, Riener R., and V. Dietz. Clinical assessments performed during robotic rehabilitation by the gait training robot Lokomat. In *Proceedings of the 2005 IEEE* 9^{th} *International Conference on Rehabilitation Robotics*, 2005.

[72] L. Lünenburger, G. Colombo, and R. Riener. Biofeedback for robotic gait rehabilitation. *Journal of NeuroEngineering and Rehabilitation*, 4(1):1–11, 2007.

[73] L. Lünenburger, G. Colombo, R. Riener, and V. Dietz. Biofeedback in gait training with the robotic orthosis Lokomat. In *Proceedings of*

the 26^{th} *Annual Conference of the IEEE EMBS*, San Francisco, USA, 2004.

[74] R. Macko, L. Ivey, M. Forrester, D. Hanley, J. Sorkin, L. Katzel, K. Silver, and A. Goldberg. Treadmill exercise rehabilitation improves ambulatory function and cardiovascular fitness in patients with chronic stroke: a randomized, controlled trial. *Stroke*, 36(10):2206–2211, 2005.

[75] B. Martin. Paediatric cervical spine injuries. *Injury*, 36:14–20, 2005.

[76] C.G.A. McRae. *Approaches to Functional Electrical Stimulation Induced Cycling and Application for the Child with a Spinal Cord Injury.* PhD thesis, University of Glasgow, 2006.

[77] F. Miller and R.R. Betz. *The Child With A Spinal Cord Injury*, chapter Hip Joint Instablity. The American Academy of Orthopaedic Surgeons, 1996.

[78] G.P. Millet, S. Libicz, B. Roels, and M. Hill. $\dot{V}_{O_2}$ kinetics is slower in swimming than in arm cranking or cycling in trained triathletes. *Medicine & Science in Sports & Exercise*, 38(5):S237–S238, 2006.

[79] M.M. Mirbagheri, C. Tsao, E. Pelosin, and W.Z. Rymer. Therapeutic effects of robotic-assisted locomotor training on neuromuscular properties. In *Proceedings of the 2005 IEEE* 9^{th} *International Conference on Rehabilitation Robotics*, 2005.

[80] T. Mohr, J. Pødenphant, F. Biering-Sørensen, H. Galbo, G. Thamsborg, and M. Kjaer. Increased bone mineral density after prolonged electrically induced cycle training of paralysed limbs in spinal cord injured man. *Calcified Tissue International*, 61(1):22–25, 1997.

[81] J.Z. Montgomerie. Infections in patients with spinal cord injuries. *Clinical Infectious Diseases*, 25(4), 1997.

[82] M. Moynahan, R.R. Betz, R.J. Triolo, and A.H. Maurer. Characterization of the bone mineral density of children with spinal cord injury. *Journal of Spinal Cord Medicine*, 19(4):249–254, 1996.

[83] M.J. Mulcahey, B.T. Smith, R.R. Betz, R.J. Triolo, and P.H. Peckham. Functional neuromuscular stimulation: outcomes in young people with tetraplegia. *The Journal of the American Paraplegia Society*, 17(1):20–35, 1994.

[84] S. Muraki, N. Tsunawake, Y. Tahara, S. Hiramatsu, and M. Yamasaki. Multivariate analysis of factors influencing physical work capacity in wheelchair-dependent paraplegics with spinal cord injury. *Medicine & Science in Sports & Exercise*, 81(1-2):28–32, 2000.

[85] M. Nash, P. Jacobs, B. Johnson, and E. Field-Fote. Metabolic and cardiac responses to robotic-assisted locomotion in motor-complete tetraplegia: a case report. *The Journal of Spinal Cord Medicine*, 27(1):78–82, 2004.

[86] P. Palmer, K. Harris, and J. Palmer. *Spinal Cord Injury: A Guide for Living*. The John Hopkins University Press, 1999.

[87] T.A. Perkins, N. de N. Donaldson, N.A.C. Hatcher, I.D. Swain, and D.E. Wood. Control of leg powered paraplegic cycling using stimulation of the lumbosacral anterior spinal nerve roots. *IEEE Transactions on Neural Systems and Rehabilitation Engineering*, 10(3):158–164, 2002.

[88] J. Petrofsky, H. Heaton, and C.A. Phillips. Outdoor bicycle for exercise in paraplegics and quadriplegics. *Zeitung für Orthopadie und Ihre Grenzgebiete*, 123(1):1–12, 1985.

[89] J. Petrofsky and R. Stacy. The effect of training on endurance and the cardiovascular responses of individuals with paraplegia during dynamic exercise induced by functional electrical stimulation. *European Journal of Applied Physiology*, 64(6):487–492, 1992.

[90] C. Phillips, D. Danopulos, P. Kezdi, and D. Hendershot. Muscular, respiratory and cardiovascular responses of quadriplegic persons to an FES bicycle ergometer conditioning program. *International Journal of Rehabilitation Research*, 12(2):147–157, 1989.

[91] M. Pollock, G.A. Gaesser, J.D. Butcher, J.P. Despres, R.K. Dishman, B.A. Franklin, and C.E. Garber. The recommended quantity and quality of exercise for developing and maintaining cardiorespiratory and muscular fitness, and flexibility in healthy adults. *Medicine & Science in Sports & Exercise*, 30(6):975–991, 1998.

[92] M.A. Pontari and S.B. Bauer. *The Child With A Spinal Cord Injury*, chapter Urologic Issues in Spinal Cord Injury: Assessment, Management, Outcome, and Research Needs. The American Academy of Orthopaedic Surgeons, 1996.

[93] H. Pontzer. A new model predicting locomotor cost from limb length *via* force production. *The Journal of Experimental Biology*, 208(8):1513–1524, 2005.

[94] B.D. Popovic, J. Watt, R.B. Stein, J. Raso, and T. Overton. Functional electrical stimulation in the rehabilitation of the spinal cord injured child. In *Proceedings of the* 13^{th} *Annual International Conference of the IEEE Engineering in Medicine and Biology Society*, Orlando, USA, 1998.

[95] S. Powers, R. Beadle, and M. Mangum. Exercise efficiency during arm ergometry: effects of speed and work rate. *Journal of Applied Physiology*, 56(2):495–499, 1984.

[96] F. Previdi, T. Schauer, S.M. Savaresi, and K.J. Hunt. Data-driven control design for neuroprotheses: a virtual reference feedback tuning (VRFT) approach. *IEEE Transactions on Control Systems Technology*, 12(1):176–182, 2004.

[97] G.M. Reaven. Role of insulin resistance in human disease. *Nutrition*, 13(1):65–65(1), 1997.

[98] R. Riener, L. Lünenburger, S. Jezernik, M. Anderschitz, G. Colombo, and V. Dietz. Patient-cooperative strategies for robot-aided treadmill training: first experimental results. *IEEE Transactions on Neural Systems and Rehabilitation Engineering*, 13(3):380–393, 2005.

[99] R. Riener, J. Quintern, and G. Schmidt. Biomechanical model of the human knee evaluated by neuromuscular stimulation. *Journal of Biomechanics*, 29(9):1157–1167, 1996.

[100] D.E. Robinson, R.J. Triolo, and R.R. Betz. Physiological responses to FNS exercise in SCI children. In *Proceedings of the* 11^{th} *Annual International Conference of the IEEE Engineering in Medicine and Biology Society*, Seattle, USA, 1998.

[101] T. Schauer. *Feedback Control of Cycling in Spinal Cord Injury Using Functional Electrical Stimulation*. PhD thesis, University of Glasgow, 2005.

[102] T. Schauer and K.J. Hunt. Nonlinear predictive control of knee-joint angle using FES. In *Proceedings of the* 5^{th} *Annual Conference of IFESS*, 2000.

[103] L.M. Schutte, M.M. Rodgers, F.E. Zajac, and R.M. Glaser. Improving the efficacy of electrical stimulation-induced leg cycle ergometry: an analysis based on a dynamic musculoskeletal model. *IEEE Transactions on Rehabilitation Engineering*, 1(2):109–125, 1993.

[104] L.H.S. Sekhon and M.G. Fehlings. Epidemiology, demographics, and pathophysiology of acute spinal cord injury. *Spine*, 26(24S):S2–S12, 2001.

[105] K. Sloan, L. Bremner, J. Byrne, R. Day, and E. Scull. Musculoskeletal effects of cycling for the SC injured. *Paraplegia*, 32(6):407–415, 1994.

[106] R.J. Soden, J. Walsh, J.W. Middleton, M.L. Craven, S.B. Rutkowski, and J.D. Yeo. Causes of death after spinal cord injury. *Spinal Cord*, 38(10):604–610, 2000.

[107] R. Stengel. *Optimal Control and Estimation*. Dover Publications, 1986.

[108] B.A. Stone. *Control Strategies for Functional Electrical Stimulation Induced Cycling*. PhD thesis, University of Glasgow, 2005.

[109] S. Sutbeyaz, B. Koseoglu, and P. Fitzgerald. The combined effects of controlled breathing techniques and ventilatory and upper extremity muscle exercise on cardiopulmonary responses in patients with spinal cord injury. *International Journal of Rehabilitation Research*, 28:273–276, 2005.

[110] A. Taylor, E. McDonell, and L. Brassard. The effects of an arm ergometer training programme on wheelchair subjects. *Paraplegia*, 24:105–114, 1986.

[111] G. Tortora and S. Grabowski. *Principles of Anatomy and Physiology*. John Wiley & Sons, inc., 9^{th} edition, 2000.

[112] R.J. Triolo, R.R. Betz, M.J. Mulcahey, and E.R. Gardner. Application of functional neuromuscular stimulation to children with spinal cord injuries: candidate selection for upper and lower extremity research. *Paraplegia*, 32(12):824–843, 1994.

[113] M. Tynan. *The Child With A Spinal Cord Injury*, chapter Joint Contractures in Children With Spinal Cord Injuries. The American Academy of Orthopaedic Surgeons, 1996.

[114] L.H.V. van der Woude, C. Bouten, H.E.J. Veeger, and T. Gwinn. Aerobic work capacity in elite wheelchair athletes: a cross-sectional analysis. *American Journal of Physical Medicine and Rehabilitation*, 81(4):261–271, 2002.

[115] L.R. Vialle and E. Vialle. Pediatric spine injuries. *Injury*, 36(2):S104–S112, 2005.

[116] L.C. Vogel. *The Child With A Spinal Cord Injury*, chapter Long Term Prophylactic Medical Care. The American Academy of Orthopaedic Surgeons, 1996.

[117] L.C. Vogel, S.J. Klaas, J.P. Lubicky, and C.J. Anderson. Long-term outcomes and life satisfaction of adults who had pediatric spinal cord injuries. *Archives of Physical Medicine and Rehabilitation*, 79(12):1496–1503, 1998.

[118] A. Wall and J. Hidler. Alterations in EMG patterns during robotic assisted walking. In *Northeast Bioengineering Annual Conference*, 2004.

[119] K. Wasserman, J.H. Hansen, D.Y. Sue, W.W. Stringer, and B.J. Whipp. *Principles of Exercise Testing and Interpretation*. Lippincott Williams & Wilkins, 4^{th} edition, 2004.

[120] A. Wernig, S. Müller, A. Nanassy, and E. Cagol. Laufband therapy based on 'rules of spinal locomotion' is effective in spinal cord injured persons. *European Journal of Neuroscience*, 7(4):823–829, 1995.

[121] A. Wernig, A. Nanassy, and S. Müller. Maintenance of locomotor abilities following laufband (treadmill) therapy in para- and tetraplegic persons: follow-up studies. *Spinal Cord*, 36(11):744–749, 1998.

[122] B.J. Whipp. Dynamics of pulmonary gas exchange. *Circulation*, 76(VI):18–28, 1987.

[123] B.J. Whipp, S.A. Ward, N. Lamarra, J.A. Davis, and K. Wasserman. Parameters of ventilatory and gas exchange dynamics during exercise. *Journal of Applied Physiology*, 52(6):1506–1513, 1982.

[124] B.J. Whipp and K. Wasserman. Oxygen uptake kinetics for various intensities of constant-load work. *Journal of Applied Physiology*, 33(3):351–356, 1972.

[125] D. Wilson and J. Larimer. The catch property of ordinary muscle. *Proceedings of the National Academy of Sciences of the United States of America*, 61(3):909916, 1968.

[126] P. Winchester, R. McColl, R. Querry, N. Foreman, J. Mosby, K. Tansey, and J. Williamson. Changes in supraspinal activation patterns following robotic locomotor therapy in motor-incomplete spinal cord injury. *Neurorehabilitation and Neural Repair*, 19(4).

[127] D.A. Winter. A new definition of mechanical work done in human movement. *Journal of Applied Physiology*, 46(3):79–83, 1979.

[128] M. Wirz, G. Colombo, and V. Dietz. Long term effects of locomotor training in spinal humans. *Journal of Neurology, Neurosurgery & Psychiatry*, 71(1):93–96, 2001.

[129] M. Wirz, D. Zemon, R. Rupp, A. Scheel, G. Colombo, V. Dietz, and G. Hornby. Effectiveness of automated locomotor training in patients with chronic incomplete spinal cord injury: a multicenter trial. *Archives of Physical Medicine and Rehabilitation*, 86(4):672–680, 2005.

[130] F. Xu and E.C. Rhodes. Oxygen uptake kinetics during exercise. *Sports Medicine*, 27(5):313–327, 1999.

[131] G.M. Yarkony. *The Child With A Spinal Cord Injury*, chapter Pressure Ulcers: Classification and Overview. The American Academy of Orthopaedic Surgeons, 1996.

[132] T. Yoshida and B.J. Whipp. Dynamic asymmetries of cardiac output transients in response to muscular exercise in man. *Journal of Physiology*, 480:355–359, 1994.

[133] L.D. Zwiren and O. Bar-Or. Responses to exercise of paraplegics who differ in conditioning level. *Medicine and Science in Sports*, 7(2):94–98, 1975.